


January 2012

Volume-Phase Transitions in Responsive Photo-Cross-Linked Polymer Network Films

Leena Patra

University of South Florida, leena.patnaik@gmail.com

Follow this and additional works at: <http://scholarcommons.usf.edu/etd>

 Part of the [American Studies Commons](#), and the [Chemical Engineering Commons](#)

Scholar Commons Citation

Patra, Leena, "Volume-Phase Transitions in Responsive Photo-Cross-Linked Polymer Network Films" (2012). *Graduate Theses and Dissertations*.

<http://scholarcommons.usf.edu/etd/4197>

This Dissertation is brought to you for free and open access by the Graduate School at Scholar Commons. It has been accepted for inclusion in Graduate Theses and Dissertations by an authorized administrator of Scholar Commons. For more information, please contact scholarcommons@usf.edu.

Volume-Phase Transitions in Responsive Photo-Cross-Linked Polymer Network Films

by

Leena Patra

A dissertation submitted in partial fulfillment
of the requirements for the degree of
Doctor of Philosophy
Department of Chemical and Biomedical Engineering
College of Engineering
University of South Florida

Major Professor: Ryan G. Toomey, Ph.D.
Venkat Bhethanabotla, Ph.D.
Nathan Gallant, Ph.D.
Julianne Harmon, Ph.D.
Mark Jaroszeski, Ph.D.

Date of Approval:
March 22, 2012

Keywords: Poly(N-alkylacrylamides), QCM-D, ATR-FTIR, Critical temperature,
Hofmeister series, Ellipsometry

Copyright © 2012, Leena Patra

DEDICATION

I would like to dedicate this dissertation to my parents and sisters for their unconditional love and support. I would also like to dedicate this work to my husband, for being patient and understanding, and to our precious daughter, Prisha, who is the joy of our lives.

ACKNOWLEDGEMENT

First and foremost, I express my reverence and gratitude for my advisor and mentor, Dr. Ryan Toomey, for his constant encouragement, guidance and support throughout the course of this study. I am indebted towards him for shaping my research life. I would also like to extend my gratitude to my committee members: Dr. Venkat Bhethanbotla, Dr. Nathan Gallant, Dr. Julliane Harmon and Dr. Mark Jaroszowski for their intellectual support to make this dissertation possible. I would like to thank Dr. Norma Alcantar for letting me use her lab.

Life in graduate school would not have been good if not for the help and encouragement of fellow graduate students. I would like to express my thanks to my lab members: Ajay Vidyasagar, Ophir Ortiz, Carlos Bello, Ryan Cates, Samuel DuPont, Gulnur Efe, Maritza Muniz, Vinny and Kemi. I am also thankful to members from Dr. Alcantar group: Eva Williams, Audrey Buttice and Dawn Fox.

My deepest gratitude to my parents, my in-laws and my daughter Prisha whose unconditional love and support made it possible to achieve this milestone. Last, but certainly not least, I am forever indebted to my husband, Trailokya Patra, whose understanding, patience, unwavering support and constant encouragement have been pivotal in accomplishing this journey. Above all, I want to thank God for providing me with all that I could ask for and more.

TABLE OF CONTENTS

LIST OF TABLES	iv
LIST OF FIGURES	v
ABSTRACT	ix
CHAPTER 1: INTRODUCTION	1
CHAPTER 2: BACKGROUND AND MOTIVATION	5
2.1 Background	5
2.2 Unconstrained and Constrained Polymer Networks	9
2.3 Cross-linked Networks of Thermally Responsive Polymers	11
2.4 Forces Inducing Phase Transition in Gels	12
2.5 Fundamentals of Volume-Phase Transitions in Cross-linked Thermoresponsive Polymers	14
2.6 Benzophenone Chemistry for Fabricating Thin Films	17
2.7 Influence of Molecular Structure on the Volume Phase Transition	18
2.8 Applications	19
2.8.1 Microfluidic-Based Separations	20
2.8.2 Tissue Engineering	21
2.8.3 Drug Delivery	22
2.8.4 Cell Attachment and Detachment	23
2.9 Influence of Different Compounds on Transition Behavior of Thermoresponsive Polymers	24
2.9.1 Hofmeister Series Effect on Volume Phase Transition	24
CHAPTER 3: MATERIALS AND METHODS	26
3.1 Reagents	26
3.2 Synthesis	28
3.3 Formation of Surface-Attached Thin Films	29
3.4 Characterization Technique	30
3.4.1 Ellipsometry	30
3.4.1.1 Theory of Ellipsometry	30
3.4.1.2 Experimental Protocol	31
3.4.2 Attenuated Total Reflectance-Fourier Transform Infrared Spectroscopy (ATR-FTIR)	33
3.4.2.1 Principles of ATR-FTIR	33
3.4.2.1 Experimental Protocol	35

3.4.3 Quartz Crystal Microbalance with Dissipation Monitoring QCM-D	36
3.4.3.1 Principles of QCM-D	36
3.4.3.2 Experimental Protocol	38
CHAPTER 4: SYNTHESIS AND CHARACTERIZATION OF	
N-ALKYLACRYLAMIDE POLYMERS	40
4.1 Synthesis of Methacryloxybenzophenone (MaBP).....	40
4.2 Characterization of MaBP	41
4.3 Synthesis of Cyclopropylacrylamide (cPAAm).....	41
4.4 Characterization of cPAAm.....	43
4.5 Synthesis of NVIBAm	43
4.6 Co-polymer Synthesis of N-alkylacrylamides	45
4.6.1 Synthesis of Poly (NIPAAm-co-MaBP)	45
4.6.2 Synthesis of Poly (nPAAm-co-MaBP).....	46
4.6.3 Synthesis of Poly (cPAAm-co-MaBP).....	46
4.6.4 Synthesis of Poly (N, N-DEAAm-co-MaBP).....	47
4.6.5 Synthesis of Poly (N-EMAAm-co-MaBP)	47
4.6.6 Synthesis of Poly (NVCL-co-MaBP).....	47
4.6.7 Synthesis of Poly (NVP-co-MaBP).....	48
4.6.8 Synthesis of Poly (NVIBAm-co-MaBP).....	48
CHAPTER 5: VISCOELASTIC RESPONSE OF PHOTO-CROSS-LINKED	
POLY (N-ISOPROPYLACRYLAMIDE) COATINGS BY QCM-D	49
5.1 Introduction	49
5.2 Results and Discussion.....	51
5.3 Conclusion.....	68
CHAPTER 6: EFFECT OF HOFMEISTER SERIES ON THE TRANSITION	
BEHAVIOR OF POLY(NIPAAm) AND POLY(DEAAm).....	69
6.1 Introduction	69
6.2 Results and Discussion.....	71
6.3 Conclusion.....	86
CHAPTER 7: STUDIES OF THE POLYMER STRUCTURE ON THE	
PHASE TRANSITION IN PRESENCE OF SALTS	87
7.1 Introduction	87
7.2 Results and Discussion.....	89
7.3 Conclusion.....	102
CHAPTER 8: SWELLING BEHAVIOR OF BILAYER AND THIN FILMS	103
8.1 Introduction	103
8.2 Results and Discussion.....	104
8.3 Conclusion and Future Work.....	110
REFERENCES	111

APPENDICES	132
Appendix A: Publications.....	133

LIST OF TABLES

Table 2.1	LCST of aqueous solution of poly (N-alkylacryl)amides).....	19
Table 3.1	Role of the different reactants in polymerization.....	26

LIST OF FIGURES

Figure 1.1	Swelling and deswelling of surface attached polymer network	1
Figure 2.1	3D Swelling of hydrogel and 1D Swelling of surface attached gel	11
Figure 2.2	(a-d) Fundamental interactions for volume phase transition in hydrogels	12
Figure 2.3	Dependence of interaction parameter in bringing up phase transition	17
Figure 2.4	Opening and closing of a valve in the microfluidic device	21
Figure 2.5	Proliferation and migration of cells into the pores of tissue engineering scaffold	22
Figure 2.6	Drug delivery	23
Figure 2.7	Cell detachment and attachment	23
Figure 3.1	Copolymerization of MaBP and N-alkylacrylamides	28
Figure 3.2	Photochemical technique for the surface fabrication of thermoresponsive polymers	29
Figure 3.3	Schematic diagram of ellipsometry	31
Figure 3.4	(a, b) Ellipsometry data and fits	32
Figure 3.5	Schematic representation of ATR-FTIR	35
Figure 3.6	Schematic diagram of spring-dashpot model	37
Figure 3.7	Workflow for data fitting	39
Figure 4.1	Schematic of synthesis of MaBP	40
Figure 4.2	NMR spectrum of MaBP	41
Figure 4.3	Schematic of synthesis of cPAAm	42

Figure 4.4	NMR of cPAAm.....	43
Figure 4.5	Schematic of synthesis of NVIBAm.....	44
Figure 4.6	NMR spectrum for N-vinylisobutyramide.....	45
Figure 5.1	QCM-D data for change in frequency Δf and dissipation ΔD for poly(NIPAAm-co-MaBP) coated crystal for three cycles as a function of temperature for $n=9^{\text{th}}$ overtone.....	53
Figure 5.2	The Δf and ΔD for poly(NIPAAm-co-MaBP) coating layer exposed to water as a function of thickness at 40 °C for the $n=3^{\text{rd}}$ that the layers overtone showed behave like rigid films.....	54
Figure 5.3	The deviation of Δf and ΔD from the rigid limit for poly(NIPAAm-co-MaBP) coating layer exposed to water as a function of thickness at 40 °C for the $n=9^{\text{th}}$ overtone.	55
Figure 5.4	The Δf and ΔD for the poly(NIPAAm-co-MaBP) coating exposed to water as a function of thickness at 15 °C for $n=3^{\text{rd}}$ overtone	56
Figure 5.5	The deviation of Δf and ΔD from the rigid limit for the poly(NIPAAm-co-MaBP) coating exposed to water as a function of at 15 °C thickness for $n=9^{\text{th}}$ overtone.	56
Figure 5.6	Experimental(\circ) data and simulated(\square) fits, as well as the residuals, of $\Delta f/n$ for the $n=3,5,7,9$ overtones at 15 °C.....	58
Figure 5.7	Experimental(\circ) data and simulated(\square) fits, as well as the residuals, of ΔD for the $n=3,5,7,9$ overtones at 15 °C.....	59
Figure 5.8	Variation of the shear modulus (\circ) and thickness (\blacksquare) of the 1 st integer multiple thickness poly(NIPAAm-co-MaBP) coating as a function of temperature	60
Figure 5.9	Comparison of the viscosity and thickness of the 1 st integer multiple thickness poly(NIPAAm-co-MaBP) coating as a function of temperature.	61
Figure 5.10	Dependence of the scaled retardation time and shear modulus on the volume fraction of the poly(NIPAAm-co-MaBP) coating in the three regimes of temperature: swollen, transition, and collapsed	64
Figure 5.11	Effect of salt concentration on the thickness of the poly(NIPAAm-co-MaBP) coating as a function of temperature.....	66

Figure 5.12	Scaled shear modulus of the poly(NIPAAm-co-MaBP) coating as a function of volume fraction for three different NaCl concentrations.....	66
Figure 5.13	Shear modulus and segment volume fraction of the poly(NIPAAm-co-MaBP) coating as a function of NaCl concentration in the collapsed state at 40 °C	67
Figure 5.14	Scaled retardation time of the poly(NIPAAm-co-MaBP) coating as a function of segment volume fraction and NaCl concentration.....	67
Figure 6.1	Deswelling isobars of poly(NIPAAm) and poly(DEAAm) showing a demixing temperature near 30 °C	72
Figure 6.2	Variation in thickness of poly(NIPAAm) (■) and poly(DEAAm) (Δ) at 5 °C in between 0-2.0 M salt concentration for (6.2a) Na ₂ SO ₄ (6.2b) NaCl (6.3c) NaBr and (6.2d) NaI.....	73
Figure 6.3	Variation in thickness of poly(NIPAAm) (■) and poly(DEAAm) (Δ) at 15 °C in between 0-2.0 M salt concentration for (6.3a) Na ₂ SO ₄ (6.3b) NaCl (6.3c) NaBr and (6.3d) NaI	77
Figure 6.4	Variation in thickness of poly(NIPAAm) (■) and poly(DEAAm) (Δ) at 24 °C in between 0-2.0 M salt concentration for (6.4a) Na ₂ SO ₄ (6.4b) NaCl (6.4c) NaBr and (6.4d) NaI.....	79
Figure 6.5	Frequency shift of Amide I band as a function of degree of swelling of poly(NIPAAm) at 24 °C from 0-2.0 M salt concentrations.....	82
Figure 6.6	Frequency shift of Amide II band as a function of degree of swelling of poly(NIPAAm) at 24 °C from 0-2.0 M salt concentrations.....	83
Figure 6.7	Frequency shift of Amide I band as a function of degree of swelling of poly(DEAAm) at 24 °C from 0-2.0 M salt concentrations.....	84
Figure 6.8	CH ₃ stretch vibrations as a function of degree of swelling at 24 °C from 0-2.0 M salt concentrations for (a) poly(DEAAm) and (b) poly(NIPAAm).....	85
Figure 7.1	Deswelling isobars of N-alkylacrylamides.....	89
Figure 7.2	(a, b) Variation in thickness of poly(NnPAAm) at 1°C and 7°C in between 0-2.0M salt concentration.....	91

Figure 7.3	(a, b and c) Frequency shift of Amide I, Amide II and CH stretch as a function of degree of swelling.....	92
Figure 7.4	(a,b and c) Change in the non-dimensionless thickness of poly(NcPAAm) at 15, 24 and 40°C.....	94
Figure 7.5	(a, b) Vibration in Amide I and Amide II of poly(NcPAAm) at 24°C from 0-2.0M salt concentrations	96
Figure 7.6	(a,b and c) Variation in thickness for poly(NVIBAm) at 25, 36 and 43°C	98
Figure 7.7	(a,b) Frequency shift in Amide I and Amide II.....	100
Figure 8.1	Comparison of swelling ratio of each polymer network.....	105
Figure 8.2	Change of swelling ratio of a single layer of network as opposed to mixture.....	106
Figure 8.3	Swelling ratio of bilayers and mixture of poly(NIPAAm).....	107
Figure 8.4	Position of Amide I and Amide II of the polymer networks in dry state....	108
Figure 8.5	Polymer spectrums at 15°C and 60°C.....	109
Figure 8.6	Ellipsometry measurements of different layers	110

ABSTRACT

The overall thrust of this project is to gain an insight into a class of surface-tethered cross-linked thin films of poly(N-alkylacrylamides) that display a lower critical solution temperature (LCST). The structure of the alkyl group and the modification of the amide groups determine the LCST and resultant volume-phase transition behavior. The aim of this study involves synthesis and characterization of thin films and to correlate the volume-transition behavior to the structure of the alkyl group. For better understanding the volume-transition behavior, the polymer films are perturbed by the Hofmeister salt series to examine trends between different alkyl groups. While most of the studies have been done with bulk gels, the majority of the applications require the use of gels at surfaces and interfaces. Surface attached polymer networks provide an alternative to bulk gels showing superior response times, thus efficiency. Hence it is significant to understand the impact of confinement on the phase transition behavior of a polymer network. Anchoring a polymer network to a surface produces volume phase transition perpendicular to the substrate. The parallel swelling and collapse of the network is highly restricted due to lateral confinement, thus impacting properties such as structure, mechanical properties, dynamics and permeability of the network. Several studies have been done with poly(N-isopropylacrylamide) anchored to a substrate, which have shown significantly different behavior than unconstrained networks. Notable examples include a gradual as opposed to a sharp volume-phase transition, and significantly less swelling above and below the LCST. These studies only looked at poly(NIPAAm); therefore it

remains unknown if these results are universal and will apply to other LCST polymers. Hence, we expanded upon these studies to also investigate a library of different LCST polymers belonging to the category of N-alkylacrylamides.

I have synthesized the copolymers comprising of N-alkylacrylamides and methacryloxybenzophenone (MaBP). The benzophenone moiety in MaBP is photoreactive, allowing us to cross-link the copolymers by UV irradiation. Surface attached thin films were fabricated by spin coating the solution of copolymers and cross-linking by UV irradiation. The volume phase transitions of the coatings were studied under the influence of temperature and the salts of the Hofmeister series. Information concerning the state of responsive layers, the precise temperature at which the collapse occurs, and the changes in the molecular environment during the transition were investigated by ellipsometry and ATR-FTIR. In a longer perspective, understanding the transition behavior and the influence of salts governing this transition provides a better understanding of the interactions of biopolymers in natural systems.

CHAPTER 1: INTRODUCTION

This thesis contains an empirical investigation of volume phase transition in thermally responsive coatings. Thermally responsive coatings undergo a reversible volume change in response to a temperature variation near the lower critical solution temperature (LCST). Below the LCST the polymers expand, becoming hydrophilic and water soluble while above the LCST the polymer shrinks, becoming hydrophobic and water insoluble. The most common responsive polymers are isomers of the N-alkylacrylamides, which contain both a hydrophobic moiety and a hydrophilic amide group. The size and position of these groups control the temperature at which a volume-phase transition occurs. In this thesis, I have conducted experiments on several types of N-alkylacrylamides to determine the relationship between volume-phase behavior and monomer architecture.

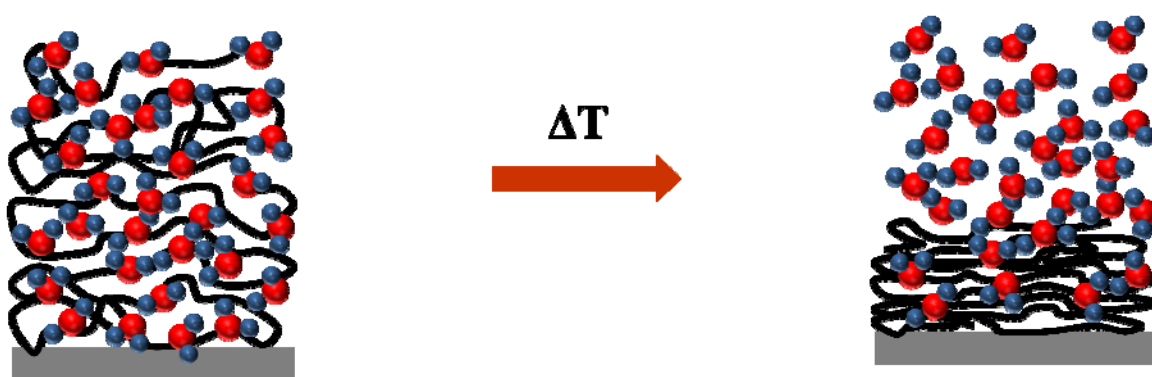


Figure 1.1 Swelling and deswelling of surface attached polymer network.

While most of the studies have been done with bulk gels, of more practical importance is the drive from industry to use less material that leads to use of gels in confined geometries. In bulk gels a small change in temperature across the critical temperature results in as much as a tenfold change in volume but at a very slow rate. Since the extent and rate of response depends on the volume of water to be absorbed or expelled from the network, scaling down the size of the gel would result in a faster response to a stimulus due to their high surface-to-volume ratio and would need minimum change in feature size to accommodate swelling and shrinking. Thin network films are materials which are confined to a surface, thus offering possibilities for a number of applications. Examples include thermally responsive coatings to control cell attachment and detachment, to control release of drugs, as scaffolds for tissue engineering and in microfluidics.

Stimuli responsive thin films fall into several categories: (1) self-assembled monolayers (SAMs); (2) grafted polymer films referred to as polymer brushes and (3) surface attached polymer networks (gels). SAMs are organic assemblies formed by the adsorption of molecular constituents from solution or gas phase onto the material surface. Polymer brushes are assemblies of polymer molecules that are tethered with one end to a substrate. The end of polymer chain is held onto the substrate by physisorption or covalent bonding, whereas the bulk of the chain extends into the solution or air interface. Surface attached polymer network are much more stable than polymer brushes, where polymer chains are attached to surface by one anchoring group while the polymer network is linked to the surface by multiple anchoring points. Unlike polymer brushes,

this thin gel film can be transferred from the surface of one material to the surface of another material. Hence it is significant to understand the impact of confinement on the phase transition behavior of a polymer network. Anchoring a polymer network to a surface exhibit a volume phase transition perpendicular to the substrate. The parallel swelling and collapse of the network is highly restricted due to lateral confinement, thus impacting the properties of polymer network such as structure, mechanical properties, dynamics and its permeability.

In order to have an in-depth understanding of this transition behavior various polymers differing in their alkyl structures, have been synthesized and characterized. By cataloging the volume-phase transition in thin cross-linked films, we can understand how transition behavior is related to chemical composition and system confinement and how those transitions can be harnessed to program specific response into materials. Ellipsometry, Attenuated Total Reflectance-Fourier Transform Infrared Spectroscopy (ATR-FTIR), QCM-D have been used to study this transition behavior. Ellipsometry is an optical technique that is used to characterize the change in the polarization ellipse upon reflection. The polarization change arises due to variations of refractive index in the interfacial zone, yielding swelling information. As a result, it provides information concerning the state of responsive layers, the precise temperature at which the collapse occurs, and the time-scales of the collapse and reswelling. QCM-D a complementary technique to ellipsometry, is a surface-sensitive instrument which allows the simultaneous measurement of frequency and dissipation changes thus giving information about the conformational changes in the polymer network. ATR-FTIR is

vibrational spectroscopy method, used to study interactions at molecular level below and above the LCST. It sheds light on the amide I and amide II bands which are sensitive to the strength of hydrogen bonds. For better understanding the volume-transition behavior, the polymer films are perturbed by the Hofmeister salt series to examine trends between different alkyl groups.

CHAPTER 2: BACKGROUND AND MOTIVATION

2.1 Background

Coatings of thin films to a surface enable the ability to control the interaction with the surrounding thus enhancing the properties of the material. Centuries these coatings were mostly used for decoration and protection purposes, but today they find their application in different high-tech areas, such as computer chips, hard disk manufacturing to their use in biomedical and aviation areas.¹⁻⁴ These coatings can be made by two different strategies, one in which the molecules bind to the substrate by physical forces, while the other by chemical bonds. In the former case the techniques applied include spin coating, dip coating, spray coating etc. However, these physical adsorption has certain limitations: they usually suffer from desorption from solvent exposure, delamination, dewetting, and displacement by molecules. In the latter case involving chemical bonds, the coatings have long term stability. The strategy employed for preparing such layers is the use of small molecules with a reactive head that can form a covalent bond with the substrate. Such layers are called as self-assembled monolayers (SAMs) and the process is self-limiting – that is, the surface reaction stops when all the reactive ends are unavailable.⁵

It was in the year 1946 that Bigelow et al ⁶ first prepared the self-assembled like monolayer, but the work by Nuzzo and Allara attracted much interest in SAMs when they prepared the layers from dilute solutions of dialkyl disulphides.⁷ SAMs can be prepared

from various methods, such as organosilicon on hydroxylated surfaces⁸⁻¹¹, alkanethiols on gold^{7, 12, 13}, silver¹⁴ and copper^{15, 16}, dialkyl sulphides on gold¹⁷, dialkyl disulphides on gold¹⁸, alcohols and amines on platinum¹⁷ and carboxylic acids on aluminium oxide^{19, 20} and silver.²¹ Recently, SAMs have been used to modify the organic polymer surfaces. Whitesides et al first made the systematic attempt to prepare SAMs on polymer surfaces.²²⁻²⁴ A “self-assembled” type molecule is created from three distinct parts. The first part is the head group that shows strong preferential adsorption to the substrate through a chemical bond. The second part is the alkyl chain that is responsible for the dense packing and crystalline structure of SAMs. The third part is the terminal functional group. The ability to tailor both the head and tail groups makes SAMs a unique method to understand the intermolecular, molecule-substrate and molecule-solvent interactions. This is a popular method to alter the interfacial properties of a surface, with molecular level control over thickness and chemical composition. SAMs offer opportunities to gain a fundamental understanding of self-organization, structure-property relationship, and interfacial phenomena. For example, by varying the alkyl chain length SAMs can be used to shield the interaction between a polymer and a substrate. Polar surfaces can be used to study the dipole-dipole interaction in surface adhesion and the surface OH can vary the wettability, thus providing an insight into the importance of H-bonding in surface phenomena.²⁵

Polymer brushes are another class of strategy for preparing stable layers. In 1950s polymer brushes (tethered polymers) gained attention when it was discovered that grafting polymer molecules to colloidal particles was a effective way to prevent flocculation.²⁶ The end-grafted polymers can be prepared with controlled length and

density and used to determine the physical properties such as thickness and density. Polymer brushes can be considered as thin films when the brush height (h) is greater than end-to-end distance ($\langle r^2 \rangle^{1/2}$) of the same non-grafted chains, and distance between grafting points (d) is smaller than end-to-end distance.²⁷

Polymer brushes have been extensively studied by various groups.²⁸⁻³⁰ Confinement of these brushes to a substrate introduces a different response from that of an isolated chain in solution. In case of polymer brushes, the chains stretch out from the substrate until the excluded volume effect is compensated by elastic energy of polymer coils. Different approaches have been adapted for the preparation of brushes; those that depend on in-situ polymerization from the substrate (grafting-from) and other use prefabricated polymer chains (grafting-to). In-situ polymerization requires a surface with attached monomers from which desired polymerization can be initiated. The growth of polymer chains from the surface leads to the formation of dense brushes. Moreover, long chains can be formed as the termination reaction is less effective than propagation. But the major disadvantage is the control on the grafting density. The exposure of the initiator carrying surface can also terminate the polymerizing reaction. Initiator efficiency, rate of diffusion of monomer to polymerization site and the limitation of initiator surface coverage makes this technique complicated. The second method of prefabricated polymers helps to determine the length and length distribution, thus enabling the selection of chains to make grafted layer and to mix chains of different length and chemical structure. Although experimentally straightforward, this strategy suffers from a few drawbacks. Firstly, due to steric repulsions it is difficult to form thick and dense brushes. Secondly, one needs chain with proper functionality at one end. Thirdly, as the

molecular weight of the polymer increases, the reaction with the polymer end-group and the complementary group on the substrate becomes less efficient.

Beside being of interest in surface modification, adhesives, separations, and lubrication³¹⁻³⁴, the polymer brushes can be used in the area of coatings, where a ultrathin and patterned organic films could be prepared to be useful in cell growth control, biomimetic material fabrication, microfluidics and drug delivery. Based on the chemical composition and architecture of the polymer chains, the conformation and structure of a polymer brush can be varied by external stimuli such as temperature, pH, solvent and salt concentration. The polymers exhibiting a conformational change in response to temperature are known as thermoresponsive polymers. Poly (N-isopropylacrylamide) poly(NIPAAm) is the most extensively studied thermoresponsive polymer. poly(NIPAAm) in solution shows a transition temperature of 32°C, but in the case of poly(NIPAAm) brushes the transition are broader, occurring over a wider temperature range, from 29°C– 40°C.³⁵⁻³⁷

As new technology advances towards smaller, thinner and lighter devices, thin polymeric gel films have attracted much attention as they can be employed for fabricating miniaturized devices with fast response time. They can also be used as responsive surfaces and interfaces, where they compete with grafted polymer layers. The 3D polymer network is much more stable than polymer brushes as it is attached to the surface by multiple anchoring points, whereas polymer brushes are attached to the substrate by one functional group.

While most of the studies have been done with bulk gels, the majority of the applications require the use of gels at surfaces and interfaces. Hence it is significant to

understand the impact of confinement on the phase transition behavior of a polymer network.³⁸

2.2 Unconstrained and Constrained Polymer Networks

If the swelling of the unconstrained polymer network (bulk gels) is isotropic, the swelling of the constrained (surface-attached) polymer networks is highly anisotropic. Figure 2.1 shows a schematic of one and three dimensional swelling. Anchoring a polymer network to a surface exhibit a volume phase transition perpendicular to the substrate. The parallel swelling and collapse of the network is highly restricted due to lateral confinement, thus impacting properties such as structure, mechanical properties, dynamics and permeability of the network.³⁹ Because swelling and shrinking of polymer networks is a diffusion controlled process, the response time of the bulk gels is very slow; therefore reducing the size of the gel can result in faster response. Polymer networks which are chemically bound to a surface allow over a wide range of film thickness, combined with mechanical and chemical stability. These networks act as 3D scaffolds hosting functional groups with a wide variety of functionalities. Due to the diversity of such systems, they can be used in a broad spectrum of applications ranging from biotechnology to microsystem engineering.⁴⁰⁻⁴⁴

Harmon and co workers predicted that surface-attached polymer networks show a different behavior than unconstrained networks. They showed that poly(NIPAAM)

networks attached to a surface undergo a volume change of around 15 fold in contrast to a 100 fold change, seen in unconstrained networks. Although the bulk gels shows a much greater volume change than the surface attached gel, the latter exhibits a much greater linear expansion.³⁸ Figure 2.1 shows a schematic of swelling of unconstrained and constrained polymer networks. Surface attachment of the poly (NIPAAm) network results in a lower LCST than the unconstrained networks, and it does not completely collapse above the LCST.^{45, 46}

For isotropic, neutral networks, the Flory-Rehner theory describes the relationship between cross-link density and the equilibrium swelling in good solvent. For low cross-link density, this theory predicts that the equilibrium swelling scales with the density of crosslinks to the $-3/5$ power.^{47, 48} It has been shown that the swelling behavior of surface-attached poly (dimethylacrylamide) (PDMAAm) is in good qualitative agreement with the Flory-Rehner theory. This theory was modified for one dimensional swelling to predict that the linear extent of swelling scales to $-1/3$ power of the crosslink density.³⁸

It was observed that the presence of a fixed substrate alter the transition temperature, especially for those containing a high concentration of ionizable groups and at high crosslink density.³⁹ Harmon and co workers showed that volume phase transition temperature started decreasing above a critical film thickness and also prevented the collapse of thin gel films above the transition temperature.⁴⁶

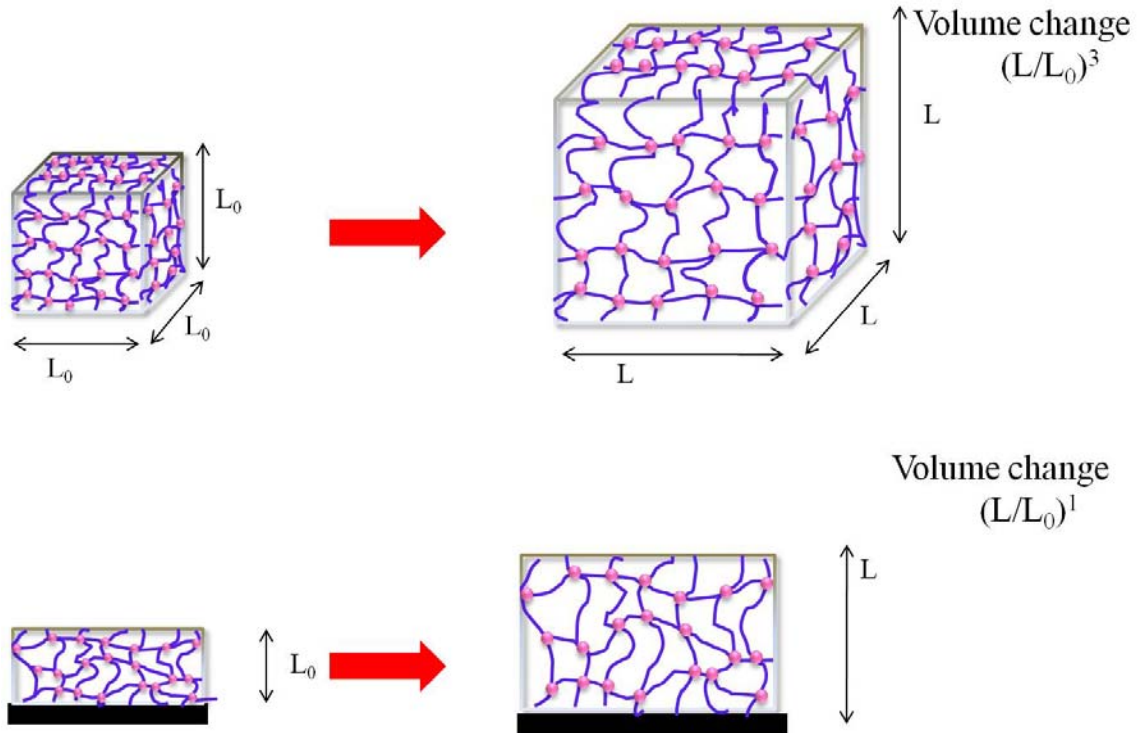


Figure 2.1: 3D Swelling of hydrogel and 1D Swelling of surface attached gel.

2.3 Cross-linked Networks of Thermally Responsive Polymers

A gel or polymer network is a system of polymer chains chemically bridged to one another. The key difference between a polymer solution and a polymer gel is that a polymer gel is elastic. When a gel is deformed, it shows a restoring force in much the same way a rubber resists external pressure. By cross-linking thermally responsive polymers, a responsive gel can be formed that can change volume in response to temperature. In much the same vein that polymer solutions phase-separate above the LCST, a thermally responsive gel collapses in volume above the LCST, expelling internal water. Thermally responsive gels, therefore, open opportunities for actuatable structures where there is no need for external power operation or feed-back circuitry.

2.4 Forces Inducing Phase Transition in Gels

The phase transition in gels results from a competitive balance between the repulsive and attractive force of the polymer network which arise from a combination of four fundamental interactions: vander waals, ionic, hydrophobic and hydrogen bonding. These four fundamental forces are shown schematically in Figure 2.2 These forces may either be independently or jointly responsible in bringing about the transition behavior in gels and play an essential role in the unique configuration and chemical reactivity of the molecules.

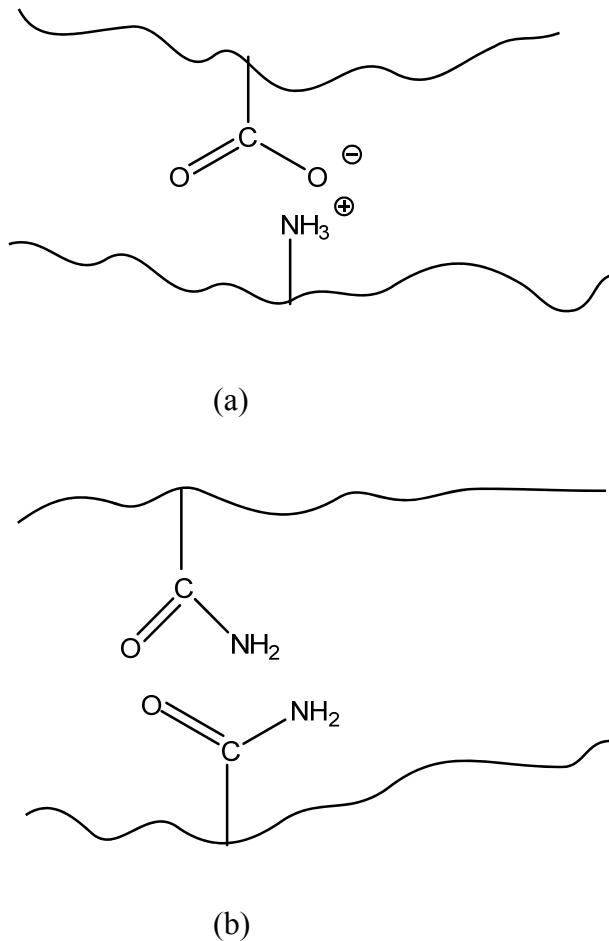
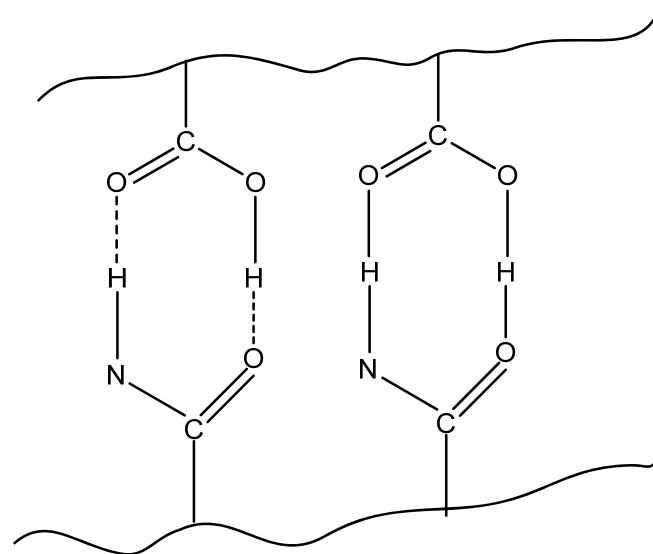
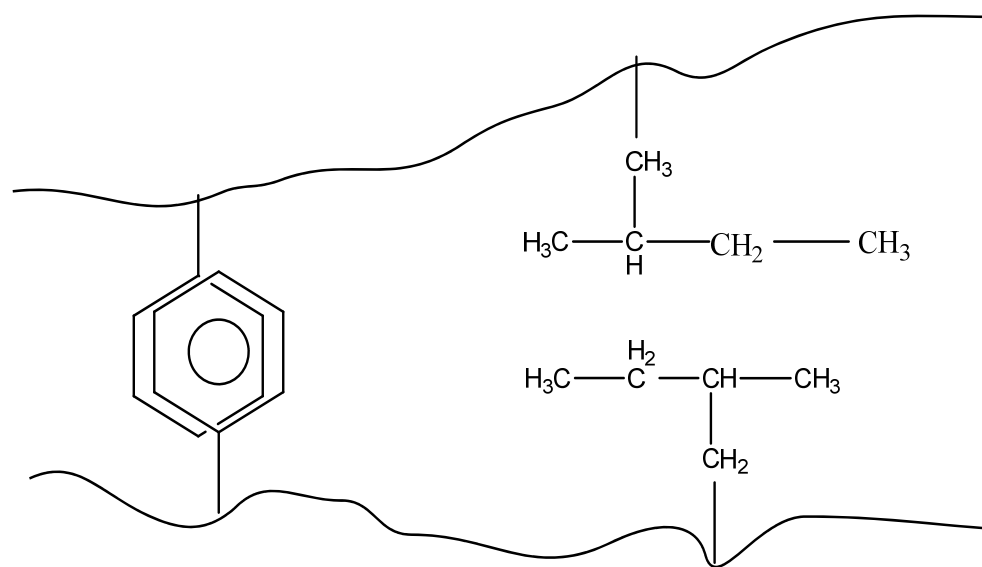


Figure 2.2 (a-d) Fundamental interactions for volume phase transition in hydrogels.



(c)



(d)

Figure 2.2 Contd.

2.5 Fundamentals of Volume- Phase Transitions in Cross-linked Thermoresponsive Polymers

Volume-phase transitions in polymer gels was first predicted by Dusek and Patterson in 1969. Ten years later, Tanaka⁴⁹ experimentally observed a volume-phase transition in polyacrylamide brought about by acetone-water mixture. Several explanations have been put forth to describe the fundamental events that drive volume-phase transitions, although none have been conclusively confirmed.

Some reports suggest that hydrogen bonding in water is responsible for the transition. Spectroscopic studies showed that the coil-globule transition takes place due to dehydration of both hydrophilic and hydrophobic moieties, enabling the formation of intra and interchain hydrogen bonds between hydrophobic moieties.⁵⁰⁻⁵² However, others have attributed the chain collapse solely due to hydrophobic interactions.⁵³⁻⁵⁷ Therefore, it is expected that the change in hydrophobicity of the polymer network would bring about a change in the transition behavior. Inomata and co-workers showed that the volume phase transition of N-substituted acrylamide gels is dependent on N-alkyl group in the side chain.⁵⁸ They observed that poly(N-n-propylacrylamide), poly(NnPAAm) showed a discontinuous volume transition similar to poly(N-isopropylacrylamide), poly(NIPAAm), whereas poly(N-cyclopropylacrylamide), poly(NcPAAm) exhibited a continuous transition. This behavior was due to the strength of the hydrophobic interaction which was believed to be proportional to the number of water molecules around the hydrophobic solutes.⁵⁵

The difference in the transition behavior and the LCST was also attributed to the dynamic volume, solvent contact area and rigidity of the side groups of N-

alkylacrylamides.⁵⁹ Dynamic volume refers to the number of water molecules which an N-alkyl substituent disrupts while surpassing the lower critical solution temperature. The rigidity of poly(NnPAAm) was found to be more than poly(NIPAAm), implying that a elongated structure of n-propyl group is more suitable for a compact confirmation than the iso-propyl group.⁵⁷ The increase in stiffness value of the poly(N-alkylacrylamides) was attributed to the hydrophobic interactions.^{57, 60, 61}

The thermoshrinking of poly(NIPAAm) is an entropically driven transition. Heskins and Guillet⁶² first proposed the thermodynamic origin of the LCST. The Gibbs free energy of the system is given by,

$$F = F_{mix} + F_{elastic} \quad (2.1)$$

Where F_{mix} and $F_{elastic}$ are the free energy of mixing and free energy of elasticity. The osmotic pressure is defined as,

$$\Pi = \frac{\partial F}{\partial V} \quad (2.2)$$

$$\frac{\partial F}{\partial V} = \frac{\partial F_{mix}}{\partial V} + \frac{\partial F_{elastic}}{\partial V} \quad (2.3)$$

At equilibrium

$$\frac{\partial F_{mix}}{\partial V} + \frac{\partial F_{elastic}}{\partial V} = 0 \quad (2.4)$$

or we can say,

$$\Pi_{mix} + \Pi_{elastic} = 0 \quad (2.5)$$

Therefore,

Osmotic stress of mixing = - (Osmotic stress of elastic)

$$\Pi_{mix} = \frac{k_B T}{\vartheta_1} [\varphi + \ln(1 - \varphi) + \chi \varphi^2] \quad (2.6)$$

$$\Pi_{elastic} = -k_B T \vartheta_0 \left[\left(\frac{\varphi}{\varphi_0} \right)^{-1} - B \left(\frac{\varphi}{\varphi_0} \right) \right] \quad (2.7)$$

$$\frac{k_B T}{\vartheta_1} [\varphi + \ln(1 - \varphi) + \chi \varphi^2] = -k_B T \vartheta_0 \left[\left(\frac{\varphi}{\varphi_0} \right)^{-1} - B \left(\frac{\varphi}{\varphi_0} \right) \right] \quad (2.8)$$

$$[\varphi + \ln(1 - \varphi) + \chi \varphi^2] = -\vartheta_1 \vartheta_0 \left[\left(\frac{\varphi}{\varphi_0} \right)^{-1} - B \left(\frac{\varphi}{\varphi_0} \right) \right] \quad (2.9)$$

Considering $\alpha = \frac{1}{\varphi}$ and $\varphi_0 = 1$ in the case of one dimensional swelling

So, we can write the above equation as,

$$\left[\alpha + \ln \left(1 - \frac{1}{\alpha} \right) + \chi \left(\frac{1}{\alpha} \right)^2 \right] = -\vartheta_1 \vartheta_0 \left[(\alpha) - \left(\frac{B}{\alpha} \right) \right] \quad (2.10)$$

$$\chi = \left[\vartheta_1 \vartheta_0 \left(\alpha - \frac{B}{\alpha} \right) - \frac{1}{\alpha} - \ln \left(1 - \frac{1}{\alpha} \right) \right] \alpha^2 \quad (2.11)$$

$$\text{Where as } \vartheta_0 = \frac{\varphi}{\vartheta_1 N} \quad (2.12)$$

$$\varphi_0 = 1 \quad (2.13)$$

$$\chi = \alpha^2 \left[-\frac{1}{N} \left(\alpha - \frac{B}{\alpha} \right) - \frac{1}{\alpha} - \ln \left(1 - \frac{1}{\alpha} \right) \right] \quad (2.14)$$

Where, k_B is the Boltzman constant, α is the elongation ratio, φ is polymer volume fraction in unswollen state, φ_0 is the polymer volume fraction in dry state, N is effective polymerization index, χ is the polymer-solvent interaction parameter, ϑ_1 is the volume of one solvent molecule, ϑ_0 is the effective crosslink number density, B is equal to $2 / f$ where f is functionality of crosslinks.

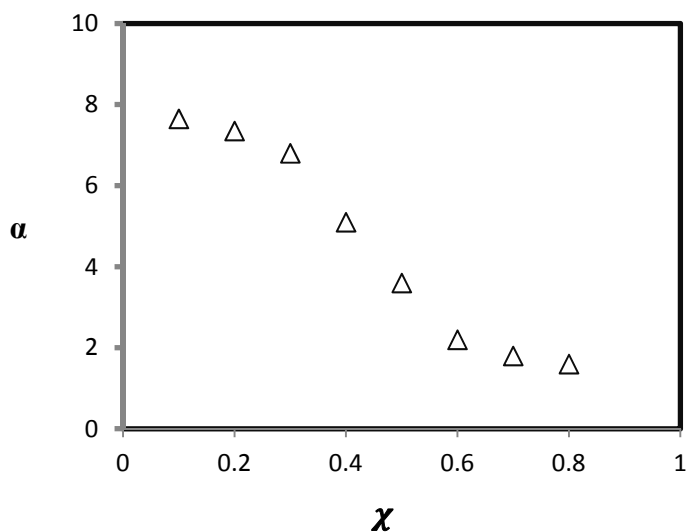


Figure 2.3 Dependence of interaction parameter in bringing up phase transition.

2.6 Benzophenone Chemistry for Fabricating Thin Films

Thin films can be fabricated by cross-linking of copolymers containing photo reactive pendant groups or monomers like benzophenone or 4-cinnamoylphenyl methacrylate with UV irradiation. This technique enables us to fabricate thin films with controllable thickness and cross-link density.^{41, 63-65} We have used this strategy to prepare thin films by photo cross-linking N-alkylacrylamides using benzophenone modified pendant groups.

Benzophenone (BP) groups are essentially used due to the following three advantages.^{66, 67}

1. BPs is chemically more stable
2. BPs can be manipulated in ambient light and activated at 350-360 nm avoiding polymer and protein damaging wavelengths.
3. BPs can preferentially react with any unreacted C-H bonds.

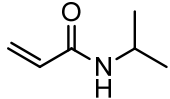
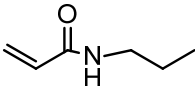
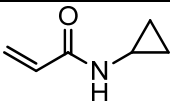
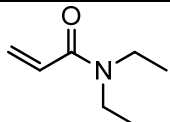
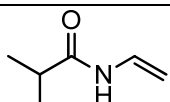
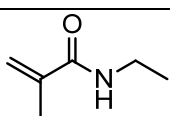
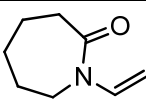
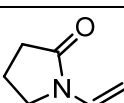
UV irradiation ($\lambda=350$ nm) triggers the $n\pi^*$ transitions in the benzophenone moieties leading to a biradicaloid triplet state that abstracts a hydrogen from the neighboring aliphatic C-H group, forming C-C bond.

2.7 Influence of Molecular Structure on the Volume Phase Transition

The phase transition behavior of thermoresponsive gels is influenced by the chemical structure of the side chains.⁶⁸ The ratio of hydrophobic to hydrophilic parts of the polymer is known to have a pronounced effect on the transition temperature of these polymer gels.⁶⁹⁻⁷²

The swelling behavior of poly (N-n-propylacrylamide) poly (NnPAAm), poly (N-isopropylacrylamide), poly (NIPAAm) and poly (N-cyclopropylacrylamide), poly (NcPAAm) have been investigated to study the influence of the alkyl groups on the transition temperature. It was found that the poly (NnPAAm) and poly (NIPAAm) had a discontinuous transition at 22°C and 32°C respectively and poly (NcPAAm) showed a continuous transition between 40 - 50°C.⁵⁵ The authors attributed this behavior to the strength of hydrophobic interaction. They predicted that the interaction is proportional to the number of water molecules surrounding the alkyl groups. Similarly Serker and others observed that the swelling behavior changed from a continuous to a discontinuous type when the alkyl group was changed from ethyl to propyl. The LCST is quite sensitive to the structure of both the amide and hydrophobic groups. For instance, subtle changes in the hydrophobic group can lead to drastic changes in the LCST, as summarized in Table 2.1

Table 2.1 LCST of aqueous solution of poly (N-alkylacryl)amides)

Poly(N-alkylacrylamides)	LCST (°C)	Ref	Figure
N-isopropylacrylamide	32-34	62, 73, 74	
N-n-propylacrylamide	22-25	52, 75, 76	
N-cyclopropylacrylamide	40-50	52, 77	
N –diethylacrylamide	30-32	73, 78, 79	
N-vinylisobutyramide	45	80-82	
N-ethylmethacrylamide	80	83-85	
N-vinylcaprolactam	32	86, 87	
N-vinylpyrrolidone	30	88	

2.8 Applications

Thermoresponsive polymers permit the development of so-called smart materials that can respond to temperature. Smart materials have the ability to detect their environment and change their properties dynamically. For instance, poly(N-

isopropylacrylamide) has facilitated advances in drug delivery, microfluidic-based separations, cell attachment detachment and tissue engineering. Each of these examples will be expanded upon below.

2.8.1 Microfluidic-Based Separations

Microvalves are one of the most important microfluidic components. Besides pumps and flow sensors, a fully functional valve is a key component in microfluidic systems that regulate the flow in it. In recent years, developing microfluidic systems for biological and chemical applications has been a major challenge.⁸⁹⁻⁹¹ Conventional microactuators (using, for example, electromagnetic, electrostatic effects) require external power for operation and are relatively complex assemblies, which limits their use in practical systems. Thermo-responsive polymers have a significant advantage over conventional microfluidic actuators due to their ability to undergo volume phase transition with respect to surrounding temperature without the requirement of an external power source. Usually, in the microfluidic system, the valves in the form of responsive polymer are fabricated within the microfluidics channels and can shrink or swell in response to temperature that in turn cause opening or closing of channels, respectively.⁹²⁻

94

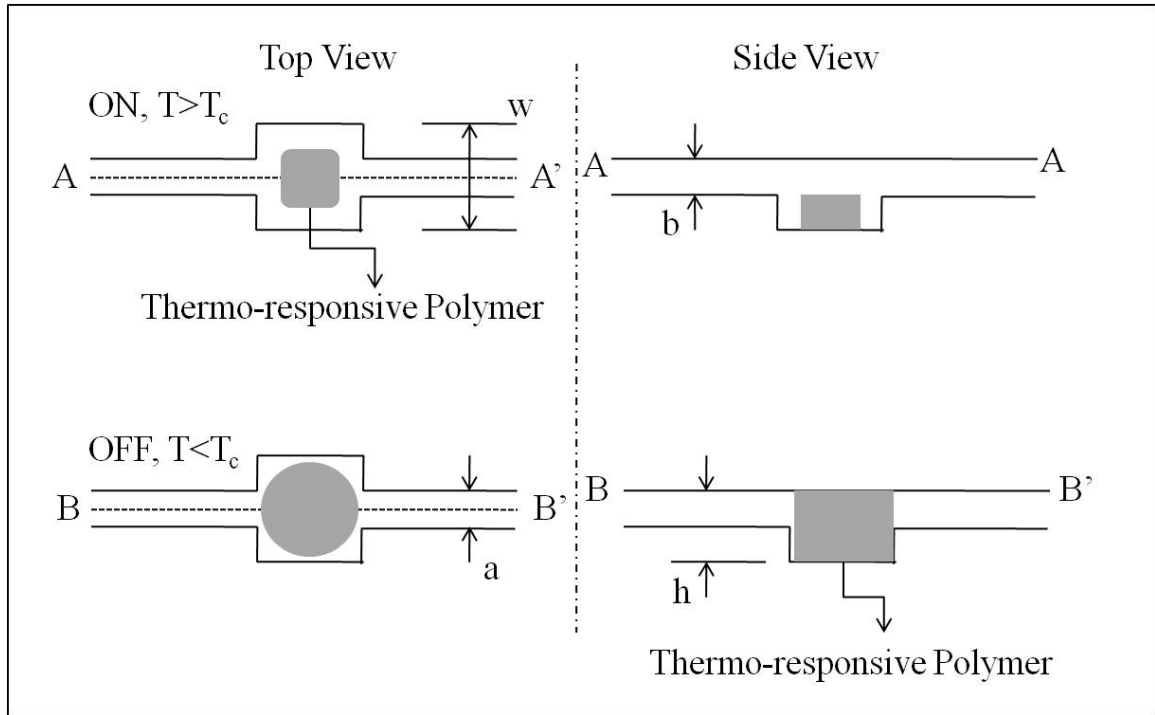


Figure 2.4 Opening and closing of a valve in the microfluidic device.

2.8.2 Tissue Engineering

The volume phase transition of poly(NIPAAm) with respect to change in temperature has been explored for designing tissue engineering scaffolds. Rat cardiac cells suspended in poly(NIPAAm)-grafted gelatin solution was developed into a synchronously contracting 3-dimensional tissue *in vitro*.⁹⁵ Using similar approach, chondrocytes suspended in poly(NIPAAm)-grafted gelatin were characterized *in vitro*⁹⁶ and *in vivo*.⁹⁷ While both systems use gelatin as the backbone, the grafted poly(NIPAAm) provides the thermoresponsive properties to allow precipitation close to the body temperature. Such polymer systems can be used in minimally invasive interventions, producing an engineered-tissue with embedded cells that are capable of living and functional.

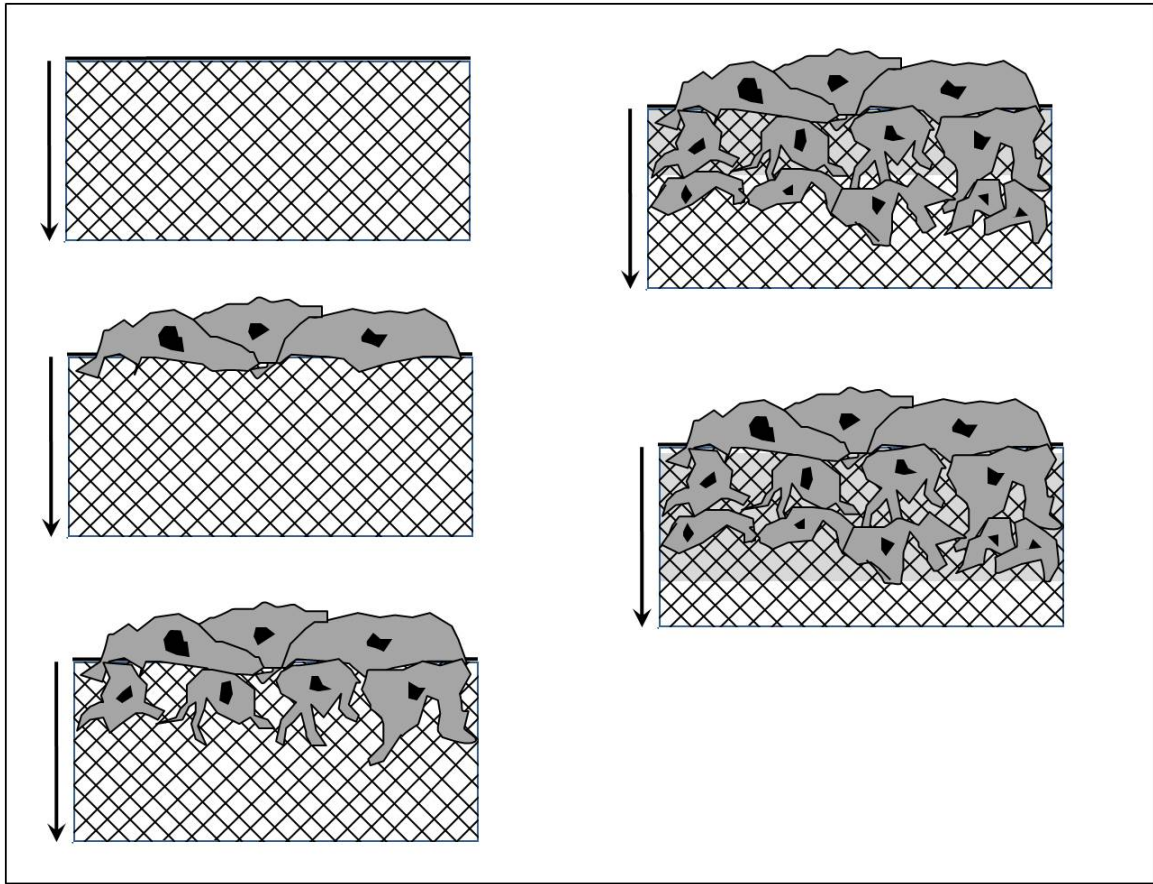


Figure 2.5 Proliferation and migration of cells into the pores of tissue engineering scaffold.

2.8.3 Drug Delivery

In drug delivery systems, it is always important to control how much of the drug is being released to the body. If the drug released too much then it can be harmful, but too little of it may limit its effectiveness. Hence, delivery of drugs at the optimal dosage for optimal lengths of time will make them more effective and more powerful. This can be achieved effectively using thermoresponsive polymer owing to its change in volume phase transition with respect to temperature. When polymer is sensibly combined with a

drug and released in the body it absorbs water and other fluids and swells. The swelling increases the aqueous solvent content within the formulation as well as the polymer mesh size, enabling the drug to diffuse through the swollen network into the external environment.⁹⁸⁻¹⁰⁰



Figure 2.6 Drug delivery.

2.8.4 Cell Attachment and Detachment

The volume phase transition behavior of thermoresponsive polymers can be used to culture dishes for cells.¹⁰¹⁻¹⁰³ Experiments have shown that e-beam grafted poly (NIPAAm) on tissue culture polystyrene dishes resulted in the detachment of cells below the LCST. But above the LCST the cells attach, spread and proliferate.¹⁰⁴ Cell removal from these surfaces provides an alternative to the traditional methods such as mechanical dissociation and enzymatic digestion. The traditional methods have been shown to be damaging to both cells and underlying extra cellular matrix.^{105, 106}

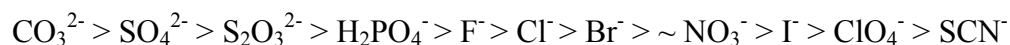


Figure 2.7 Cell detachment and attachment.

2.9 Influence of Different Compounds on Transition Behavior of Thermoresponsive Polymers

2.9.1 Hofmeister Series Effect on Volume Phase Transition

The addition of salts can alter the transition behavior of the polymer network and the magnitude of this change depends on the nature of the individual ions.^{107, 108} It is believed that the relative efficiency of the ions follows the Hofmeister series.^{109, 110} The Hofmeister series is a rank of ions based on their propensity to precipitate a mixture of hen egg white protein.¹¹¹ This behavior is more pronounced for anions than cations and is a general phenomenon. The ordering of the anion series is:



The species to the left of Cl^- are called as kosmotropes or “water makers” and to the right are called as chaotropes or “water breakers”.¹¹²

Influence of salts on phase separation of synthetic polymers was also observed. The effects of anions and cations on the cloud point of poly(NiPAAm) oligomers were investigated by Freitag et.al.¹¹³ They observed that the cloud point was lowered as a function of the salt concentration by the presence of different anions (salting-out effect) with the exception of iodine which showed a slight rise in the cloud point at low concentration. Cations showed no significant effect. The phase separation is described as an effect of the hydrophobic interactions and the disruption of hydrogen bonds.¹¹³ The ordering and disordering of ions on the solvent structure was interpreted in terms of viscosity B coefficients, which are used to represent the ion-solvent interactions. Ions with negative viscosity B coefficient break the structure of water and those with positive coefficients strengthen the water structure.¹¹⁴

In case of poly(NIPAAm) hydrogel, the LCST decreased with an increase in salt concentration. It was also shown that the volume of the gel decreased as the salt concentration increased.^{115, 116} When probed with a (QCM-D) it was seen that poly(NIPAAm) brushes grafted from a QCM-D crystals also showed a decrease in transition temperature with an increase in salt concentration.¹¹⁷

Originally, it was thought that the influence of ions on the macromolecular properties was caused by “making” or “breaking” bulk water structures. However recent experiments suggest that they cause negligible change in bulk water structure.^{118, 119} Due to the complexity of processes, which carry out in the polymer chain, water solution and solvate shell of immersed molecules, the mechanism of this process is still not clear. Studies have showed that the effect of ions can be explained by three types of interactions of ions with polymer and its hydration waters. First, ions can polarize adjacent water molecule and weaken hydrogen bonding between polymer and water. Second, ions can interfere with the hydrophobic hydration of the macromolecule by increasing surface tension of the hydrophobic moieties. Third, ions may bind directly to the polymer.¹²⁰

CHAPTER 3: MATERIALS AND METHODS

3.1 Reagents

N-isopropylacrylamide (NIPAAm), N-vinylcaprolactam (NVCL), N-vinylpyrrolidone (NVP), N, N-diethylacrylamide (N,N-DEAAm), azobisisobutyronitrile (AIBN), the various solvents as mentioned in chapter 3 were purchased from sigma-aldrich. N-n-propylacrylamide and N-ethylacrylamide were purchased from Monomer-Polymer and Dajac Labs and purified by distillation. 4-hydroxybenzophenone, methacryloyl chloride and triethylamine used in the synthesis of methacryloxybenzophenone (MaBP) were purchased from sigma-aldrich. Cyclopropylamine and acryloyl chloride were also purchased from Aldrich. Table 3.1 shows the structure and functions of the reactants used for the polymer synthesis in this work.

Table 3.1 Role of the different reactants in polymerization

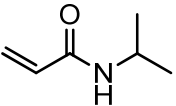
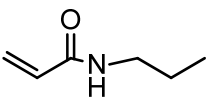
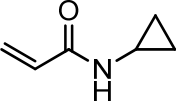
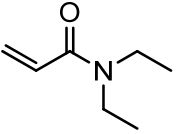
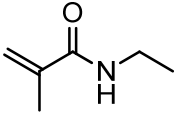
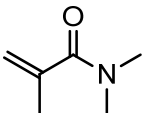
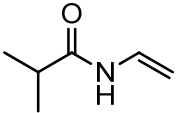
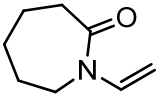
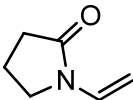
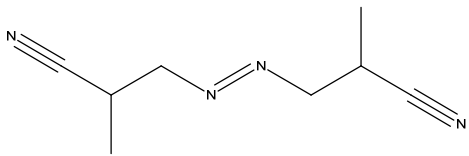
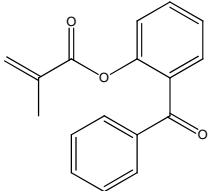
Structure	Name	Function
	N-isopropylacrylamide	Monomer, thermoresponsive component
	N-n-propylacrylamide	Monomer, thermoresponsive component
	N-cyclopropylacrylamide	Monomer, thermoresponsive component

Table 3.1 (Contd.)

	N,N-diethylacrylamide	Monomer, thermoresponsive component
	N-ethylacrylamide	Monomer, thermoresponsive component
	N,N- dimethylmethacrylamide	Monomer, thermoresponsive component
	N-vinylisobutyramide	Monomer, thermoresponsive component
	N-vinylcaprolactam	Monomer, thermoresponsive component
	N-vinylpyrrolidone	Monomer, thermoresponsive component
	Azobisisobutyronitrile	Initiator
	Methacryloxybenzophenone	Monomer, crosslinking component

3.2 Synthesis

The polymers in this work were prepared by free radical polymerization. In this method the primary monomer, the crosslinker and initiator were dissolved in an appropriate solvent and added to a schlenk tube. The reaction mixture was purged with nitrogen to remove any dissolved oxygen that otherwise retards the polymerization. Figure 3.1 illustrates the polymerization mechanisms. Details of polymerization for each monomer are explained in chapter 3.

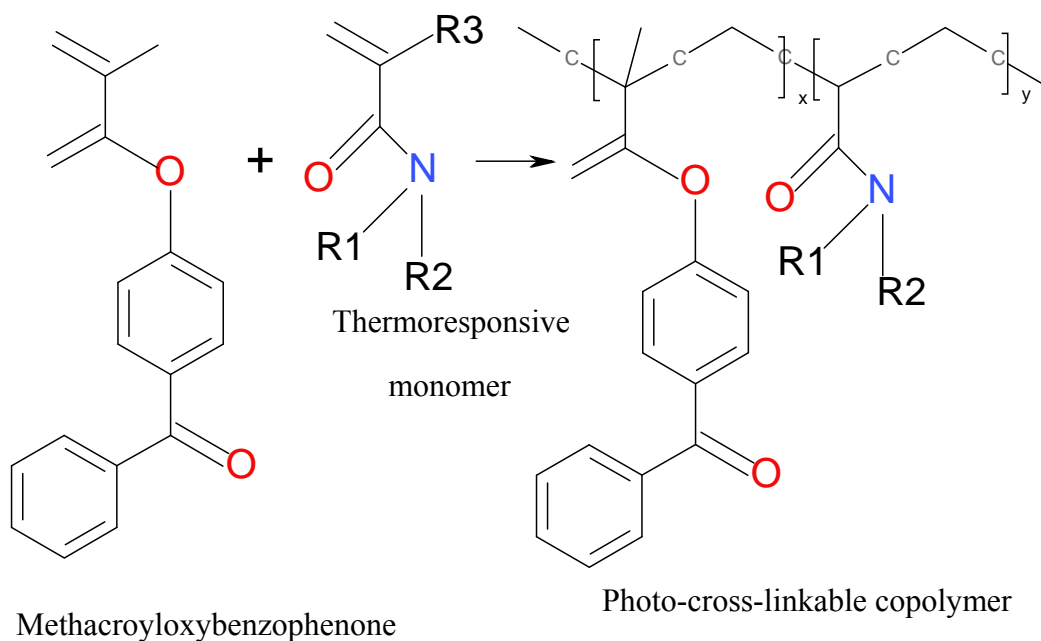


Figure 3.1 Copolymerization of MaBP and N-alkylacrylamides.

3.3 Formation of Surface-Attached Thin Films

Thin polymer films were prepared by spin-casting solutions of the polymer at the appropriate spin speed for 1 min. Typical solvents were cyclohexanone and methanol. For QCM-D the gold substrate was cleaned with ozone, piranha solution and ozone to remove any organic impurities followed by spin casting a solution of polymer at a speed of 3500 for 1 min. In the case of ellipsometry, the quartz substrate was cleaned with plasma followed by a deposition of 1wt % solution of 3-aminopropyltriethoxysilane in acetone and spin casting a solution of polymer at a speed of 2000 rpm for 1 min. Once the film was formed, cross-linking and surface attachment were accomplished by exposing the film to UV light (360nm) for 30 minutes. Figure 3.2 shows the photochemical cross-linking reaction for the N-alkylacrylamides copolymers.

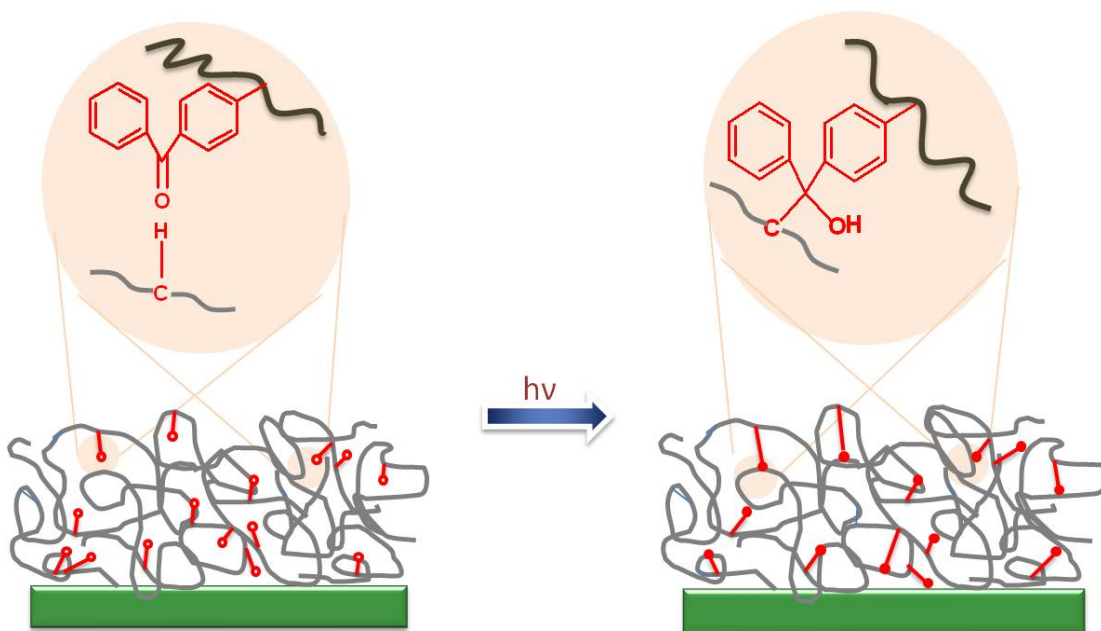


Figure 3.2 Photochemical techniques for the surface fabrication of thermoresponsive polymers.

3.4 Characterization Technique

3.4.1 Ellipsometry

3.4.1.1 Theory of Ellipsometry

Ellipsometry is a technique used to measure the optical properties and physical structure of thin films. It is a non destructive technique that is based on the principle that upon reflection of a monochromatic linear polarized light on a substrate under the angle of incidence, θ the relative phases of its electrical components are changed and an ellipse is formed. Figure 3.3 The power of ellipsometry derived from its ability to provide two parameters (Ψ , Δ), called ellipsometric angles, in a single measurement. They are expressed in the following equation, also called the fundamental equation of ellipsometry as:

$$\bar{\rho} = \frac{r_p}{r_s} = \tan\Psi e^{i\Delta} \quad (3.1)$$

Here, Ψ can vary between 0° and 90° and Δ between 0° and 360° and measures the differential change in amplitude and phase, respectively. These values are related to the Fresnel reflection coefficients, r_p and r_s , which are complex quantities that describe the ratio of the reflected electric field to that of the incident field in the p and s that is in the parallel and perpendicular direction respectively.

$$r_p = \frac{E_p^{reflected}}{E_p^{incident}} \quad r_s = \frac{E_s^{reflected}}{E_s^{incident}} \quad (3.2)$$

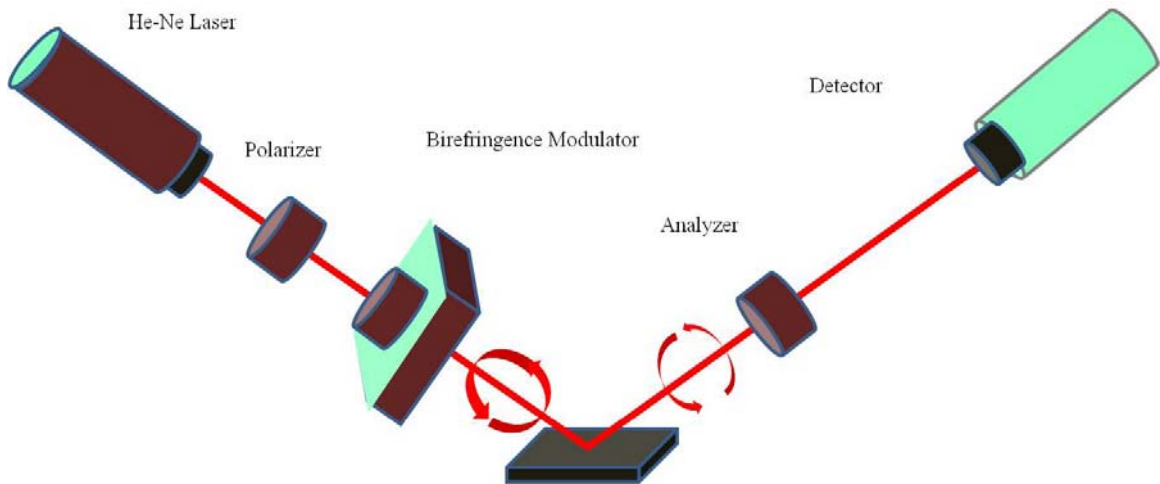
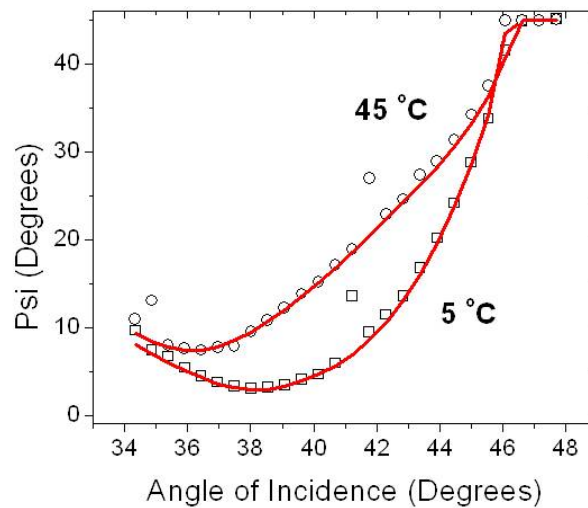


Figure 3.3 Schematic diagram of ellipsometry.

3.4.1.2 Experimental Protocol

1. The substrate, LaSFN9 prism is cleaned with plasma followed by a deposition of 1 wt% 3-aminopropyltriethoxysilane in acetone.
2. Polymer solution was spin cast on the freshly prepared substrate.
3. The film was then cross-linked by irradiating with UV light ($\lambda=365\text{nm}$) for 30 minutes.
4. Straight line alignment was done by rotating the sample holder and detector to 90° position.
5. One end of the solution cell was sealed against the sample holder.
6. The substrate was vacuum sealed against the open end of the solution cell.
7. Then the alignment was done at 45° by rotating the sample holder and detector to 45° .
8. Bring the sample holder to 0° so that the laser beam hits the centre of the edge of the prism.
9. Rotate back the sample holder to 45° and check for alignment.

10. Find the Brewster angle, Ψ and Δ for the dry film by scanning from 20° to 45° .
 11. Add solvent (DI water and salt solution in our case) to the solution cell. Wait for sometime so that Ψ and Δ remain constant. Measure the new Brewster angle, Ψ and Δ by scanning from 36° to 55° .
 12. Finally an iterative procedure (least-squares minimization) is applied by varying the refractive indices and thickness and Ψ and Δ values are calculated using the Fresnel equation. The calculated Ψ and Δ values, which match the experimental data best, provide the optical constants and thickness parameters of the sample.
- Figure 3.4 elucidates the ellipsometry data and fits.



(a)

Figure 3.4 (a, b) Ellipsometry data and fits.

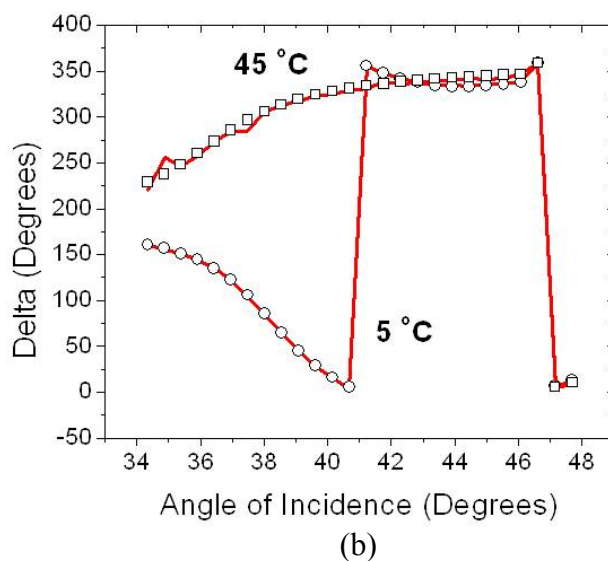


Figure 3.4 Contd.

3.4.2 Attenuated Total Reflectance-Fourier Transform Infrared Spectroscopy (ATR-FTIR)

3.4.2.1 Principles of ATR-FTIR

FTIR spectroscopy analyses the interaction of IR radiation with a sample. It measures the frequency and the intensity of the absorption (Figure 3.4). Determining the frequency helps to study the chemical bond transformation, since chemical functional groups absorb radiation at specific frequencies. The key components of the instrument source, interferometer, beamsplitter and detector. The purpose of the beamsplitter is to split the light beam in two so that some of the light reflects off the moving mirror and some reflects off the fixed mirror. Interferometer is an optical device that causes two beams of light to travel different distances. Thus, it measures all the frequencies simultaneously by modulating the intensity of individual frequencies before the detector records the signal. The product of an interferometer scan, termed interferogram (a plot of

infrared detector response versus optical path difference) cannot be interpreted in its original form. These are Fourier transformed to give infrared spectra. ATR (attenuated total reflectance) utilizes the phenomenon of total internal reflection. In ATR, a beam of infrared radiation impinges on the crystal of high refractive index. The infrared radiation sets up an evanescent wave which being slightly bigger than the crystal penetrates a small distance beyond the crystal surface. Samples brought in contact with the surface absorb the evanescent wave giving rise to an infrared spectrum. The distance to which the wave penetrates the sample is known as the depth of penetration (DP). DP is given by the following equation

$$DP = \frac{1}{2\pi W N_c (\sin^2 \Theta - N_{sc}^2)^{1/2}} \quad (3.3)$$

where:

DP = depth of penetration

W = wavenumber

N_c = refractive index of crystal

Θ = angle of incidence

$N_{sc} = N_{\text{sample}} / N_{\text{crystal}}$

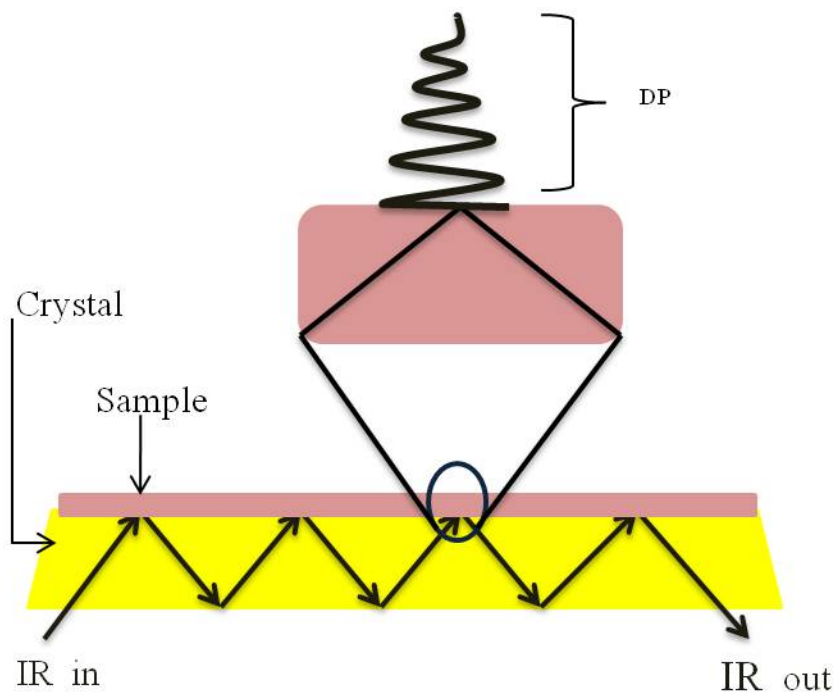


Figure 3.5 Schematic representation of ATR-FTIR.

3.4.2.2 Experimental Protocol

1. The background spectrum of the bare crystal was taken.
2. Then 0.5 wt % of the polymer solution was cast on to the ZnSe crystal.
3. The crystal was heated to the boiling point of the solvent to evaporate the solvent and form a thin film.
4. The film was then cross-linked by irradiating with UV light ($\lambda=365\text{nm}$) for 30 minutes.
5. Spectrum of the sample was taken in neat and aqueous phase for a temperature range from below the transition temperature to above the transition temperature of the various thermoresponsive polymers. The spectrum was collected in absorbance mode.

6. The number of scans was 100, resolution 4cm^{-1} and spectral ranges were in the region between $4000\text{-}400\text{cm}^{-1}$.
7. The crystal background was subtracted from the samples for each run.

3.4.3 Quartz Crystal Microbalance with Dissipation Monitoring (QCM-D)

3.4.3.1 Principles of QCM-D

Quartz crystal microbalance is an ultrasensitive weighing device that uses the principle that a piezoelectric crystal changes its oscillation frequency when a mass is deposited or removed from the crystal surface. With the advent of QCM-D technique, the dissipation factor (D), essentially a measure of the damping characteristics of the film, was concurrently measured with the resonant frequency and then used to extract information on the viscoelastic and structural properties of thin films. Sauerbrey¹²¹ showed that if the film is thin and rigid the decrease in frequency is proportional to the mass of the film according to the following equation:

$$\Delta f = -C_m \Delta m = -C_m \rho_F \Delta t_F \quad (3.4)$$

$$C_m = \frac{2f_n^2}{n\rho_q v_q} \quad (3.5)$$

where:

Δf = change in frequency	Δm = mass of film added
ρ_F = density of film	Δt_F = film thickness
C_m = proportionality constant	f_n^2 = resonant frequency of bare crystal
n = overtone	ρ_q = density of crystal
v_q = shear wave velocity of the crystal	

But in the case of a viscoelastic film the above equation is inappropriate to analyze the data and we interpret the data in context of Kelvin-Voigt model adopted from Voinova et al.¹²² This model is based on the spring dashpot mechanism as shown in Figure 3.6. Here the spring & dashpot are in parallel. When a shear stress is applied to the Voigt element, the spring captures the elastic response (energy stored) and the dashpot captures the viscous resistance (energy lost). The following equations describes the shifts in resonant frequency Δf and dissipation ΔD :

$$\Delta f = -\frac{h\rho\omega}{2\pi\rho_q h_0} \left[1 - \frac{\eta_s}{\eta} \left(\frac{(\tau_r\omega)^2}{1+(\tau_r\omega)^2} \right) \right] + \Delta f_s \quad (3.6)$$

$$\Delta D = \frac{h\rho}{\rho_q h_0} \left[\frac{\eta_s}{\eta} \left(\frac{\tau_r\omega}{1+(\tau_r\omega)^2} \right) \right] + \Delta D_s \quad (3.7)$$

where ρ_q and h_0 are the density and thickness of the quartz resonator, respectively and η_s is the viscosity of the solvent. The product $\tau_r\omega$ is the ratio of the loss modulus to the storage modulus, also known as $\tan \delta$. The terms Δf_s and ΔD_s correspond to the changes in the resonant frequency and dissipation of the uncoated crystal.

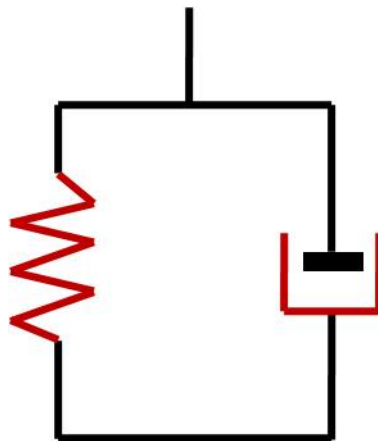


Figure 3.6 Schematic diagram of spring-dashpot model.

3.4.3.2 Experimental Protocol

1. The gold coated crystal were first treated with UV ozone followed by base piranha solution (5:1:1 mixture of DI water, ammonium hydroxide and hydrogen peroxide) at 70°C for 10 min. The crystals were then rinsed thoroughly in DI water, dried by nitrogen purge and finally treated again with UV ozone.
2. The flow modules were first cleaned with SDS solution followed by DI water for 15 min and finally dried by purging nitrogen.
3. Then a bare crystal was mounted and its frequency and dissipation measured, followed by flowing DI water and recording the resultant changes in frequency and dissipation.
4. To the above crystal 1wt % polymer solution in cyclohexanone was deposited and spun at 3500rpm for 30seconds to get a uniform thin coating.
5. The above coating was then cross-linked by UV irradiating for 30 min and mounted on the module.
6. The frequency and dissipation changes of the coated crystal in air and water were recorded.
7. The flow rate was kept constant at 0.1 mL/min and the temperature was ramped at 1.0 °C/min in between 15 and 40 °C.
8. QCM-D data was interpreted by implementing the model presented by Voinova.¹²²
9. We used the Risk Solver Platform to fit the simulated and experimental Δf and ΔD to determine the shear modulus, retardation time, and thickness of polymer.

The viscosity of water was calculated at the given temperature and entered as a fixed value. The density of water and polymer was considered to be 1000 kg/m^3 at all temperatures. Initial guesses of shear modulus (μ), viscosity (η), and thickness (h) were provided and the fitting routine was carried out until the sum of the squares of the residuals was minimized. Figure 3.7 shows the workflow for data fitting.

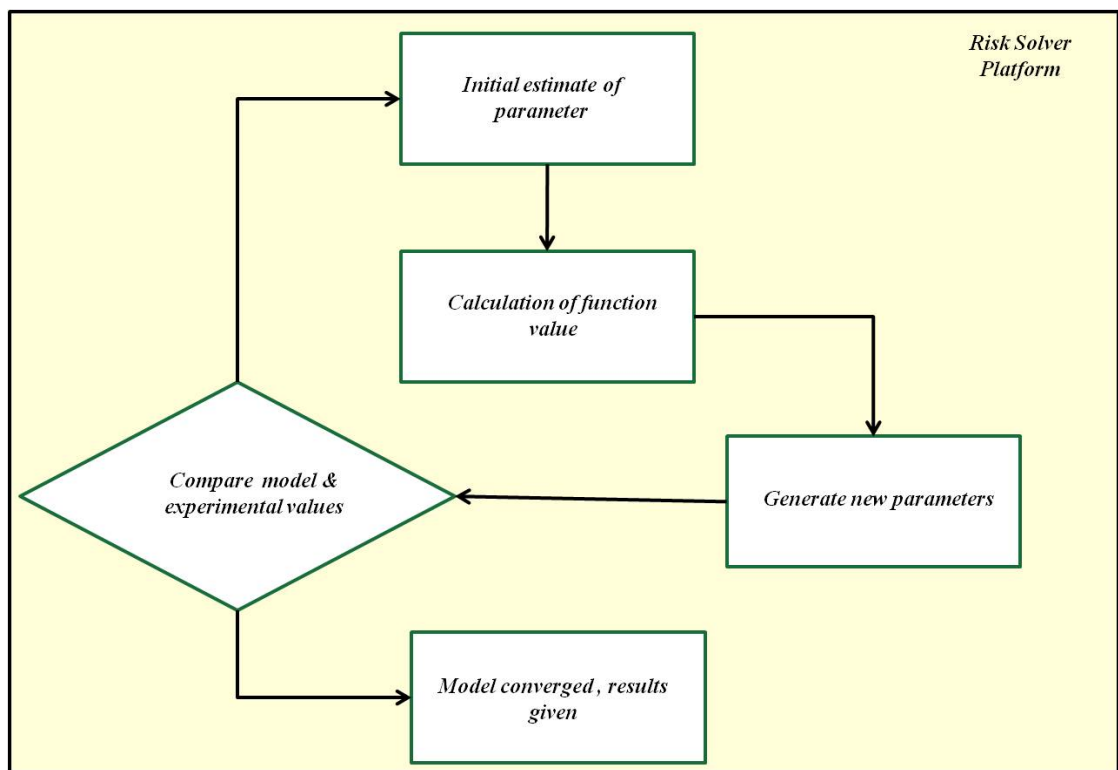


Figure 3.7 Workflow for data fitting

CHAPTER 4: SYNTHESIS AND CHARACTERIZATION OF N- ALKYLACRYLAMIDE POLYMERS

4.1 Synthesis of Methacryloxybenzophenone (MaBP)

Synthesis of methacryloxybenzophenone was carried out at 0°C in acetone by using 4-hydroxybenzophenone and methacryloyl chloride. Triethylamine (TEA) was used as an acid scavenger. Prior to synthesis acetone and triethylamine was distilled. 4-hydroxybenzophenone, methacryloyl chloride and triethylamine were used in a ratio of 1:2:2 respectively. Fig 3.1 shows the schematic of the reaction. Being, an exothermic reaction, methacryloyl chloride was added dropwise to a round bottom flask containing 4-hydroxybenzophenone, TEA and acetone. The flask was kept in an ice bath. The reaction was run for 5-6 hours, after which the product was collected. The purification of the product was done by column chromatography using silica gel as the stationary phase and benzene as the mobile phase. Finally, the product collected was dried under vacuum and characterized using nuclear magnetic resonance (NMR).

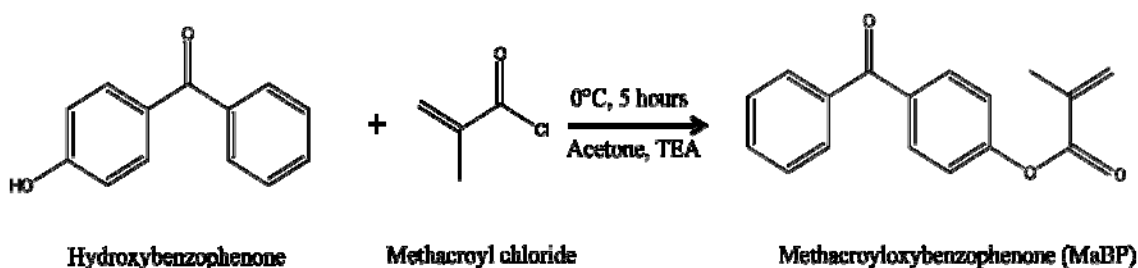


Fig 4.1 Schematic of synthesis of MaBP.

4.2 Characterization of MaBP

MaBP was characterized using an INOVA 400 NMR spectrometer. An aromatic peak between 7.2-8.0 and methyl peak at 1.0 (Figure 4.2).

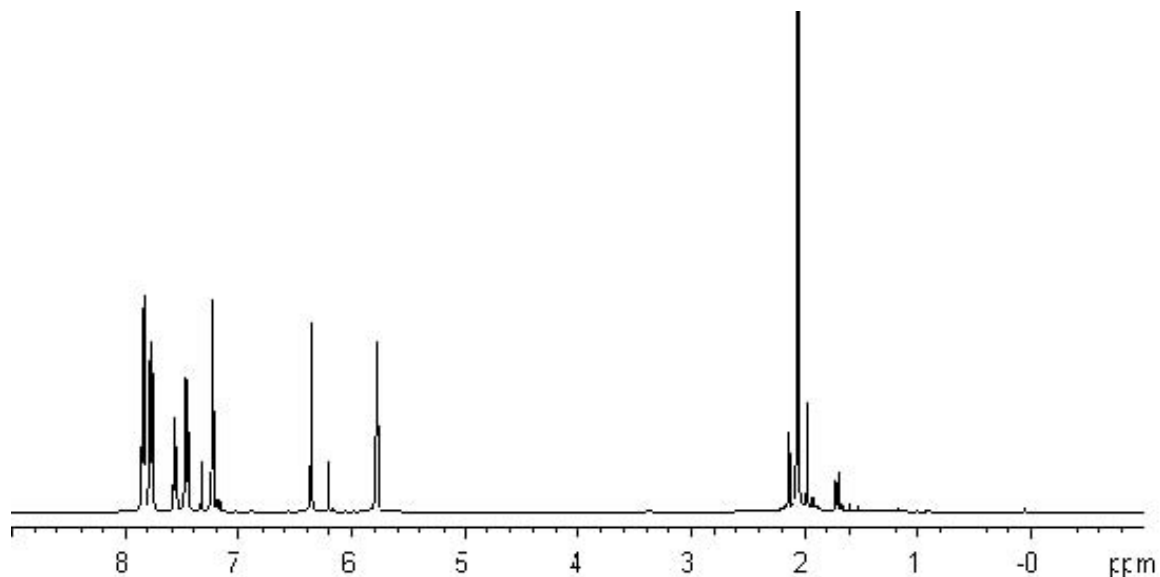


Figure 4.2 NMR spectrum of MaBP.

4.3 Synthesis of Cyclopropylacrylamide (cPAAm)

Synthesis of cyclopropylacrylamide (cPAAm) was carried out at 0°C by using cyclopropylamine, acryloyl chloride and triethylamine in a ratio of 1:1:2 (Figure 4.3). Benzene was used as the solvent. A three mouth round bottom flask (reaction flask), reflux condenser, additional funnel, stir bar and single mouth round bottom flask was used. All the glassware's were rinsed with benzene and purged with argon. In the single mouth round bottom flask appropriate amount of benzene was taken and purged with argon. One end of a long needle was put to the round bottom flask containing benzene and the other end was to the additional funnel and the required amount of benzene was taken in the additional funnel and then the additional funnel was turned on to collect the

benzene in the reaction flask. Now take acryloyl chloride and add it with the help of a syringe to the reaction flask. After this a small amount of benzene was added in the additional funnel followed by triethylamine. Now under argon atmosphere the required amount of cyclopropylamine was transferred into the additional funnel and the funnel was shaken for a while, followed by dropwise addition of the solution mixture into the reaction flask. The reaction was run overnight in an ice bath under the argon atmosphere. After that the reaction mixture was filtered and the product subjected to freeze-thaw cycle and dried under vacuum. Finally NMR was done on the product.

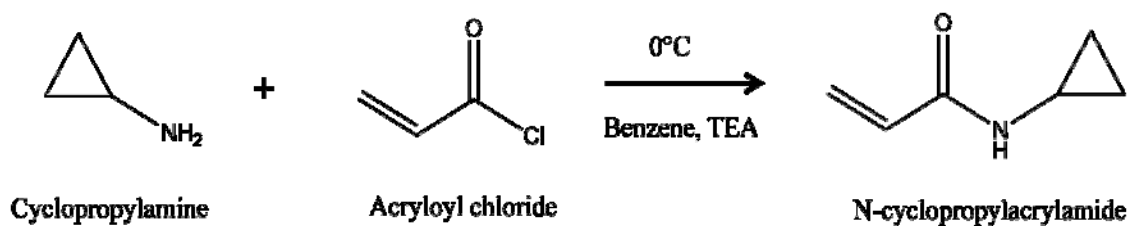


Figure 4.3 Schematic of synthesis of cPAAm.

4.4 Characterization of cPAAm

cPAAm was characterized using NMR.

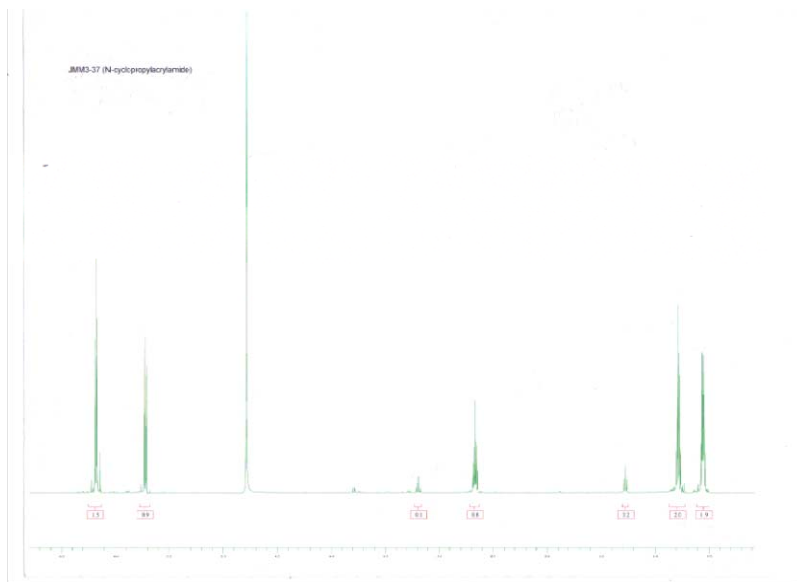


Figure 4.4 NMR of cPAAm.

4.5 Synthesis of NVIBAm

NVIBAm was synthesized in a two step process. In the first step 3-isobutyryloxalidin-2-one was prepared using oxazolidin-2-one, butyl lithium and THF. A two mouth round bottom flask with an additional funnel was purged with argon prior to the addition of the reactants. Oxazolidin-2-one was added to the round bottom flask, followed by drop wise addition of THF from the additional funnel. The reaction flask was kept in a dry ice bath on the top of a stir plate for the reactants to mix properly. After that butyl lithium was added drop wise to the round bottom flask and the reaction went on for few hours. Finally, with the help of a syringe isobutyrylchloride was added directly to the round bottom flask and stirred for 1 hour, followed by quenching the above solution in an

aqueous sodium bicarbonate solution. The above solution was transferred to a separatory funnel and extracted four times with methylene chloride to get the desired fraction. Sodium sulfate was added to the organic fraction to remove moisture, followed by filtrating the solution and removing the solvent under reduced pressure. All the reactants were transferred with a precision syringe and in the presence of argon (Figure 4.5).

The second step involves the reaction between 3-isobutyryloxalidin-2-one from step one and lithium diisopropylamide (LDA) to produce N-vinylisobutyramide. In a two mouth round bottom flask LDA and THF were added. The addition was done inside a glove box. After that the flask was taken out from the glove box and brought below a previously argon purged additional funnel. The product from step one was diluted in THF purged with argon and then transferred with a syringe into the additional funnel. This diluted solution was then added drop wise to the reactants in the round bottom flask and the reaction went on for few hours. After that the above solution was quenched in ammonium chloride followed by extraction in dichloromethane and removal of the moisture in sodium sulfate. Then the solution was filtered and subjected under a rotovap for removal of solvents (Figure 4.6).

Step 1:

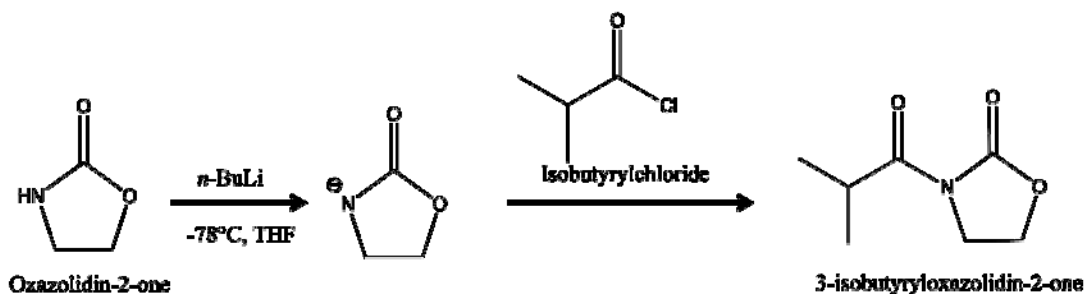


Figure 4.5 Schematic of synthesis of NVIBAm.

Step 2:

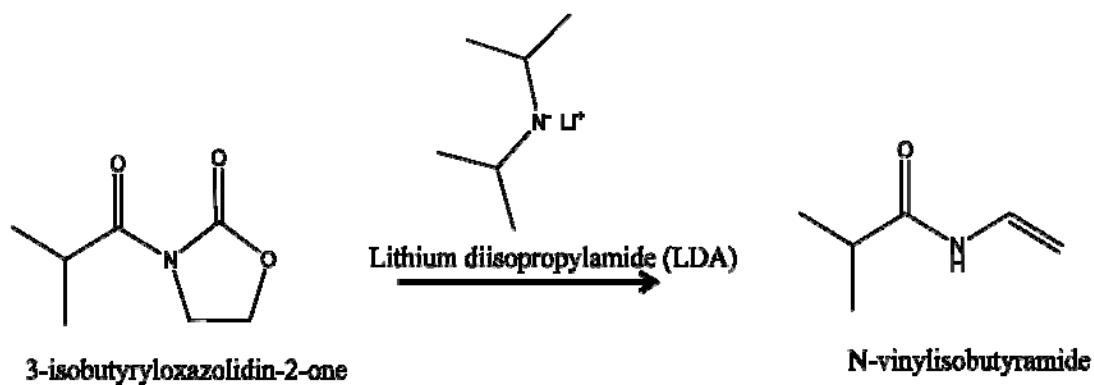


Figure 4.5 Contd.

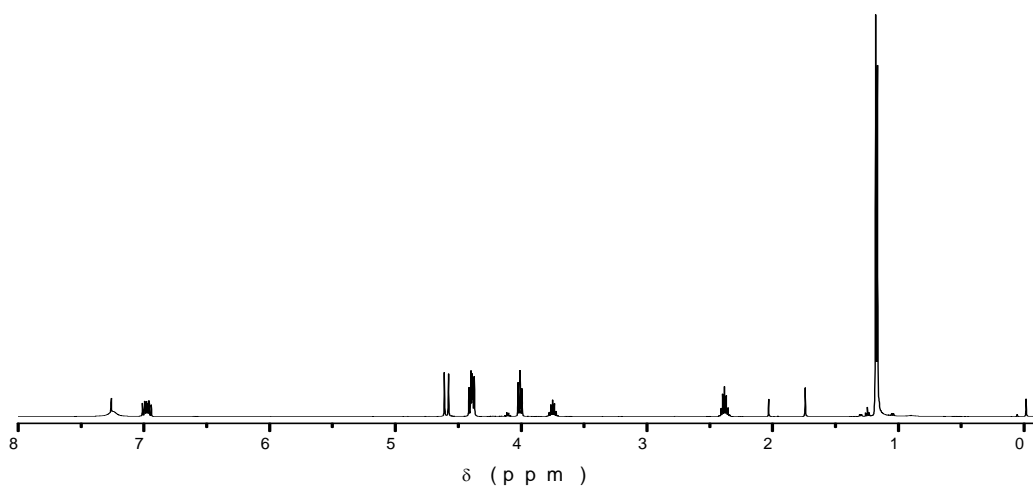


Figure 4.6 NMR spectrum for N-vinylisobutyramide.

4.6 Co-polymer Synthesis of N-alkylacrylamides

4.6.1 Synthesis of Poly (NIPAAm-co-MaBP)

Poly (NIPAAm-co-MaBP) was copolymerized with 3 mol% MaBP and 1mol % azobisisobutyronitrile (AIBN) as the initiator. Dioxane used as the solvent was distilled

prior to the reaction. In a schlenk tube appropriate amount of the reactants was taken and the mixture degassed with nitrogen by freeze-thaw cycle. After that the reaction mixture was kept in a water bath at 70°C for 18 hours, followed by precipitating in diethyl ether. The product obtained was white in color, which was transferred into another schlenk tube and dried under vacuum. NMR was finally done to confirm the product.

4.6.2 Synthesis of Poly (nPAAm-co-MaBP)

Synthesis of Poly (nPAAm-co-MaBP) was carried out using 3 mol% MaBP and 1 mol% AIBN in 20 ml dioxane. After adding the reactants it was subjected to freeze-thaw cycle for four times to remove the oxygen bubbles. The mixture was then kept for polymerization in the water bath at 60°C for 18 hours. Aluminum foil was wrapped around the schlenk tube to avoid the exposure to light. The solution turned viscous after the polymerization and this mixture was kept under vacuum to remove the solvent. After the solvent removal we are left with white polymer chunks, which was dissolved in little acetone and precipitated in diethyl ether, followed by vacuum to get a purified product.

4.6.3 Synthesis of Poly (cPAAm-co-MaBP)

Poly (cPAAm-co-MaBP) was copolymerized with 3 mol% MaBP and 1 mol % AIBN as the initiator. The reactants were added to round bottom flask having a stir bar. Methanol was used as the solvent. The reaction mixture was stirred for few minutes to dissolve the reactants. The flask was then kept in an ice bath under the argon atmosphere for 20 minutes. Polymerization was then carried out overnight by placing the reaction flask in the oil bath at 70°C. After polymerization the mixture was precipitated first in hexane followed by reprecipitation in acetone. Then the product was dried under vacuum to get a white powder.

4.6.4 Synthesis of Poly (N, N-DEAAm-co-MaBP)

Co-polymerization of N, N-DEAAm-co-MaBP was carried out using 3 mol % MaBP and 1 mol % AIBN in a schlenk tube. Toulene was used as the solvent. The reaction mixture was freeze thawed for 3-4 times, followed by nitrogen purging for few minutes. Then the mixture was kept for polymerization in water bath at 60°C for 22 hours. After the polymerization the schlenk tube was kept under vacuum for solvent removal. Purification was done by precipitating in n-hexane.

4.6.5 Synthesis of Poly (N-EMAAm-co-MaBP)

Poly (N-EMAAm-co-MaBP) was synthesized using 3 mol% MaBP and 1 mol% AIBN in dioxane. The reaction mixture was freeze thawed for 3-4 times, followed by nitrogen purging for few minutes. Then the mixture was kept for polymerization in water bath at 60°C for 18 hours. After the completion of the reaction it precipitated in diethyl ether, flowed by drying under vacuum to get a purified product.

4.6.6 Synthesis of Poly (NVCL-co-MaBP)

Polymerization of NVCL-co-MaBP was carried out using N-vinylcaprolactam, 3 mol% MaBP and 1 mol % AIBN in dioxane. Prior to polymerization N-vinylcaprolactam was distilled under vacuum and stored at 4°C. In a schlenk tube NVCL, MaBP and AIBN was added with a stir bar and flushed with nitrogen for 15 min. Then deoxygenated dioxane was added and degassed 3 times by freeze-thaw cycle. After that the tube was kept in a water bath at 70°C for 24 hrs for polymerization. Once the polymerization is done, the product was dissolved in DMF, followed by precipitation in diethyl ether to get a purified product.

4.6.7 Synthesis of Poly (NVP-co-MaBP)

Prior to synthesis, NVP was first dried successively over KOH and CaH_2 , followed by distillation under reduced pressure and storing at 4°C . Distilled dioxane was used as the solvent. In a schlenk tube NVP, 3 mol % MaBP and 1 mol% AIBN was taken along with a stir bar and purged with nitrogen. Then dioxane was added to it and the reaction mixture was deoxygenated 3 times by freeze-thaw cycle. Synthesis of (NVP-co-MaBP) was carried out in a water bath at 70°C for 18 hrs. Then the co-polymer was dissolved in little acetone and precipitated in diethyl ether to get a purified product.

4.6.8 Synthesis of Poly (NVIBAm-co-MaBP)

NVIBAm-co-MaBP was synthesized using N-vinylisobutyramide, 3 mol% MaBP and 1 mol % AIBN in ethanol. All the reactants were added in a round bottom flask and deoxygenated by freeze-thaw cycle, followed by nitrogen purging. Polymerization was carried out by keeping the reaction mixture overnight for 18 hours in an oil bath at a temperature of 70°C . Once the polymerization was done, the product was purified by precipitating 3 times into hexanes from THF.

CHAPTER 5: VISCOELASTIC RESPONSE OF PHOTO-CROSS-LINKED POLY(N-ISOPROPYLACRYLAMIDE) COATINGS BY QCM-D

5.1 Introduction

Surface-confined responsive polymers are important in a number of diverse applications that benefit from active surfaces, including sensors¹²³, biocompatible coatings¹²⁴, drug delivery vehicles^{125, 126}, and separation schemes.^{45, 127} Responsive polymers are attractive in the sense that they swell or deswell in response to subtle changes in the environment and provide reversible actuation. Among the many polymeric systems studied, poly(N-isopropylacrylamide), or poly(NIPAAm), has been widely exploited as it responds to changes in temperature near normal body conditions.¹²⁸ The transition in swelling has been attributed to small shifts in the balance of hydrophobic/hydrophilic interactions between segments of the polymer.¹²⁹ Below the demixing temperature, the enthalpy of mixing dominates and the polymer swells. Above the demixing temperature, hydrophobic interactions dominate and drive the collapse of the polymer.

While macroscopic gels are hindered by slow response kinetics, the response times of surface-confined coatings are several orders of magnitude faster due to their microscopic dimensions. Nonetheless, the impact of confinement on the swelling behavior remains an unresolved issue.¹³⁰ A surface coating swells in a single direction normal to confining interface. It is expected that such films have different properties from

those of bulk materials due to interfacial interactions and confinement, necessitating the need for surface sensitive experiments.¹³¹

Techniques such as plasmon resonance¹³², ellipsometry^{38, 133} and neutron reflectivity^{134, 135} are sensitive to the spatial profile of a surface-confined coating and can provide extent of swelling. The quartz-crystal microbalance with dissipation (QCM-D) provides both solvent uptake and viscoelastic response.^{136, 137} While there have been several QCM investigations of responsive surface coatings in contact with liquid media¹³⁸⁻¹⁴³, rigorous analysis and interpretation of the data can be challenging.

Johannsmann et al. have pointed out that acoustic measurements can yield different values in thickness than those obtained by optical methods as a result of relaxation processes excited at resonance.^{144, 145} The exact nature of these relaxation processes are strongly correlated to the structure, density, and coupled water within the coating. A study by Ma et al. showed that poly(oligo(ethylene glycol) brushes submerged in water displayed a viscosity very close to that of pure water, implying that the relaxation of the system was mediated to a large extent by dissipation of water.¹⁴⁶ Belfort et al. in turn found a considerable change in the viscous response of a poly(L-lysine) layer before and after cross-linking, signifying greater frictional loss in the gel-like layer.¹⁴⁷ Hook et al. explained that the increase in friction can be related to the role of coupled water.^{148, 149}

Most studies are limited to a single thickness of the sample, and confidence in the fitted parameters is limited. In this study, responsive coatings were analyzed in which the thickness was systematically varied to overcome such ambiguities. The coatings were prepared from photo-cross-linkable poly(NIPAAm) copolymers with benzophenone-

pendant monomers. The 3rd through 9th overtones of the QCM-D data were analyzed in the context of the Kelvin-Voigt viscoelastic model.¹²² Based on the thickness variation data, the responsive coatings showed rigid-like behavior at the 3rd overtone. At the 9th overtone, the films show significant deviation from the rigid-film limit. The timescale of this relaxation is on the order of nanoseconds, which is 2 orders of magnitude slower than expected if hydrodynamic interactions are completely screened within a correlation blob. The slow relaxation perhaps is a consequence of significant polymer-polymer coil overlap between cross-links. The addition of salt, which increases the modulus of the networks, has no impact on timescale of the relaxation.

5.2 Results and Discussion

A polymer gel can be thought of as a two-fluid medium comprising interconnected polymer segments in contact with a penetrating solvent.¹³⁰ If sheared with an oscillating strain at frequency $\omega/2\pi$ the gel will respond, in general, with a complex shear modulus. The polymer segments relax with a velocity that is determined by the balance between the elastic restoring force of the gel and the frictional force between solvent and gel segments. The timescale of this event, or the retardation time, can be expressed as $\tau_r = \frac{\eta}{G_o}$, where G_o is the shear modulus and η is the effective viscosity of the two-fluid medium. If a single event occurs on the timescale of the experiment the so-called Kelvin-Voigt viscoelasticity is expressed as $G = G_o + \eta \frac{d\epsilon}{dt}$. The Kelvin-Voigt constitutive relationship describes an elastic body where stress relaxation is instantaneous but the propagation of strain is determined by the retardation time. Rigid materials that have slow internal dynamics have little dissipative loss and consequently low retardation times.

Flexible materials that have considerable internal motion have significant dissipative loss and large retardation times.

We consider here an oscillating piezoelectric plate that shear strains a polymer gel of density ρ and thickness h in a bulk liquid also of density ρ_0 . The shifts in the resonant frequency Δf and dissipation ΔD are, to first order in thickness (adapted from Voinova et al.¹²²)

$$\Delta f = -\frac{h\rho\omega}{2\pi\rho_0h_0} \left[1 - \frac{\eta_s}{\eta} \left(\frac{(\tau_r\omega)^2}{1+(\tau_r\omega)^2} \right) \right] + \Delta f_s \quad (5.1)$$

$$\Delta D = \frac{h\rho}{\rho_0h_0} \left[\frac{\eta_s}{\eta} \left(\frac{\tau_r\omega}{1+(\tau_r\omega)^2} \right) \right] + \Delta D_s \quad (5.2)$$

where ρ_0 and h_0 are the density and thickness of the quartz resonator, respectively and η_s is the viscosity of the solvent. The product $\tau_r\omega$ is the ratio of the loss modulus to the storage modulus, also known as $\tan \delta$. The terms Δf_s and ΔD_s correspond to the changes in the resonant frequency and dissipation of the oscillator in contact with the bulk solvent but in the absence of the gel coating ($h=0$). In the limit of a linear elastic material where strain is transmitted instantaneously, $\tau_r\omega \rightarrow 0$ and Δf reduces to the well-known Sauerbrey relation for a lossless oscillator with a correction for solvent viscosity. In this limit, Δf is linear with respect to the gel thickness. The change in dissipation, ΔD , on the other hand, is invariant to gel thickness and depends only on the viscosity of the contacting solvent.

Figure 5.1 shows the 9th overtone values of Δf and ΔD for a poly(NIPAAm-co-MaBP) coating (dry thickness=36 nm) in contact with water as a function of temperature for three temperature cycles. The rate of temperature change was 1.0 °C/min. The cooling cycle depended strongly on the rate of temperature change, and the degree of hysteresis narrowed by slowing the temperature change. The heating curve, on the other hand, was relatively independent of the rate below 1.0 °C/min. All subsequent analysis was

conducted on the heating curve. In a similar vein, Δf and ΔD were recorded for three integer multiples of the dry thickness ($h = k \cdot 36$ nm, where $k = 2,3,4$). In order to understand whether the coatings display viscoelasticity on the timescale of the experiment, the Δf and ΔD values associated with the heating curves were plotted against the rigid film prediction of Equations 5.1 and 5.2.

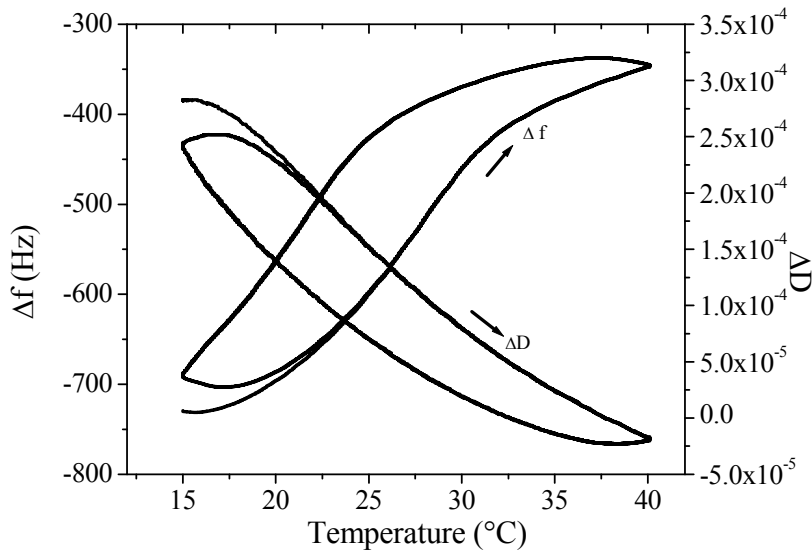


Figure 5.1. QCM-D data for change in frequency Δf and dissipation ΔD for poly(NIPAAm-co-MaBP) coated crystal for three cycles as a function of temperature for $n=9^{\text{th}}$ overtone. The dry thickness of the coating was 36 nm. The arrowhead indicates that Δf increases and ΔD decreases with increase in temperature.

Figures 5.2 and 5.3 show the 3^{rd} and 9^{th} overtones, respectively, for all four integer multiple thicknesses ($k=1,2,3,4$) at 40 °C. Figures 5.4 and 5.5 show the 3^{rd} and 9^{th} overtones, respectively, for all integer multiple thicknesses ($k=1,2,3,4$) at 15 °C. The dashed lines on the figures correspond to the Δf and ΔD values of equivalent rigid coatings in the limit $\tau_r\omega \rightarrow 0$. At the 3^{rd} overtone, it can be seen that the coatings appear as

rigid overlayers, both at 15 and 40 °C. While there is some deviation between the experimental ΔD and the rigid limit value at 15 °C, the deviation does not become significant until the higher thicknesses. Using this overtone, only the thickness of the coating can be ascertained. At the 9th overtone, however, the measured values of Δf were less than the rigid film prediction, appearing as a constant offset at 40 °C and a weakly varying offset at 15 °C. These offsets indicate that the coatings do display viscoelasticity in the 9th overtone. At 15 °C, the measured dissipation was greater than the rigid film prediction by 500% at the largest thickness, whereas at 40 °C it was greater by only 5%. For both the 15 and 40 °C experiments, the values of ΔD curve up with increasing thickness, and hence the linearized Equations 5.1 and 5.2 are inappropriate to analyze the data.

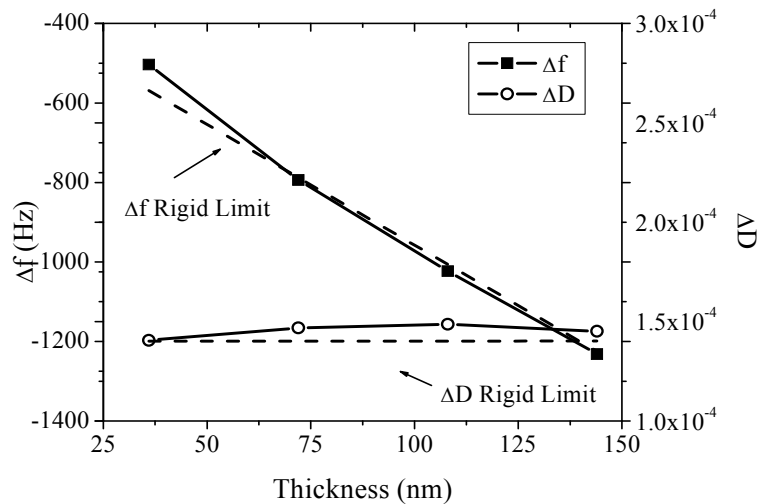


Figure 5.2. The Δf and ΔD for poly(NIPAAm-co-MaBP) coating layer exposed to water as a function of thickness at 40 °C for the $n=3^{\text{rd}}$ overtone showed that the layers behave like rigid films. Dashed lines indicate the rigid limit and solid lines are the experimental results.

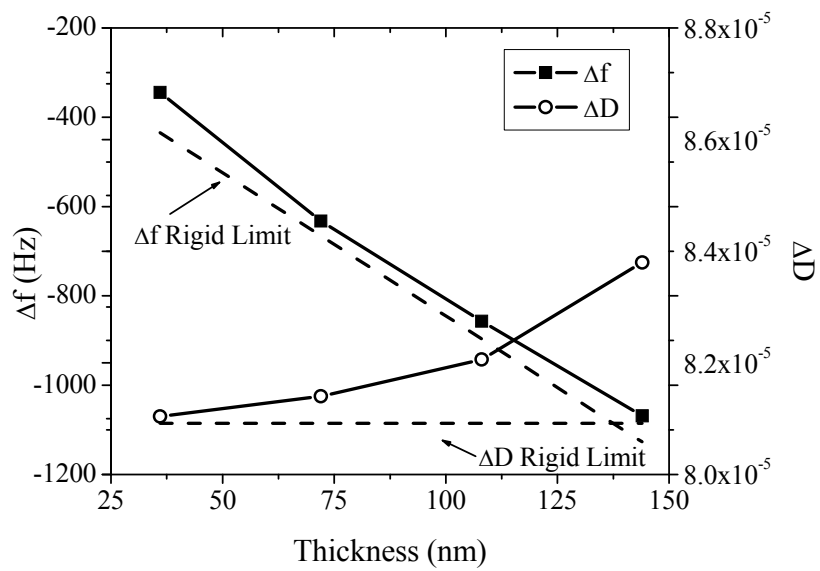


Figure 5.3. The deviation of Δf and ΔD from the rigid limit for poly(NIPAAm-co-MaBP) coating layer exposed to water as a function of thickness at 40 °C for the $n=9^{\text{th}}$ overtone. Dashed lines indicate the rigid limit and solid lines are the experimental results.

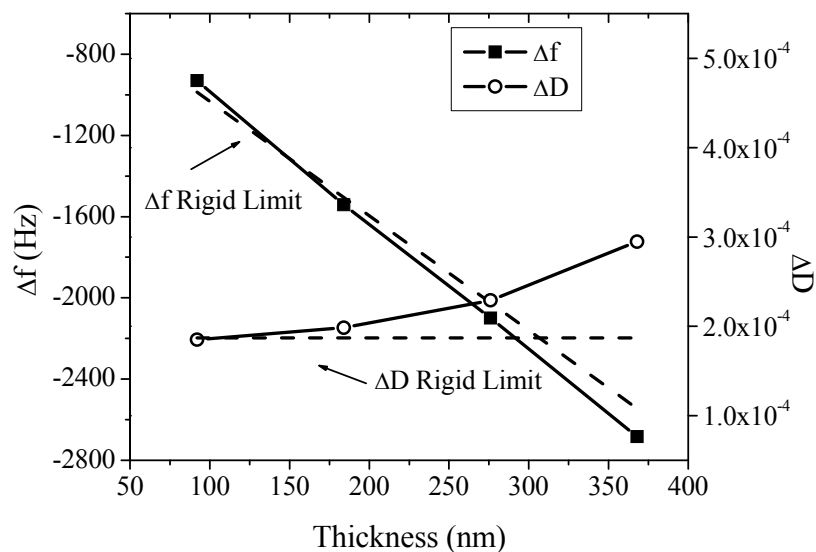


Figure 5.4. The Δf and ΔD for the poly(NIPAAm-co-MaBP) coating exposed to water as a function of thickness at 15 °C for $n=3^{\text{rd}}$ overtone.

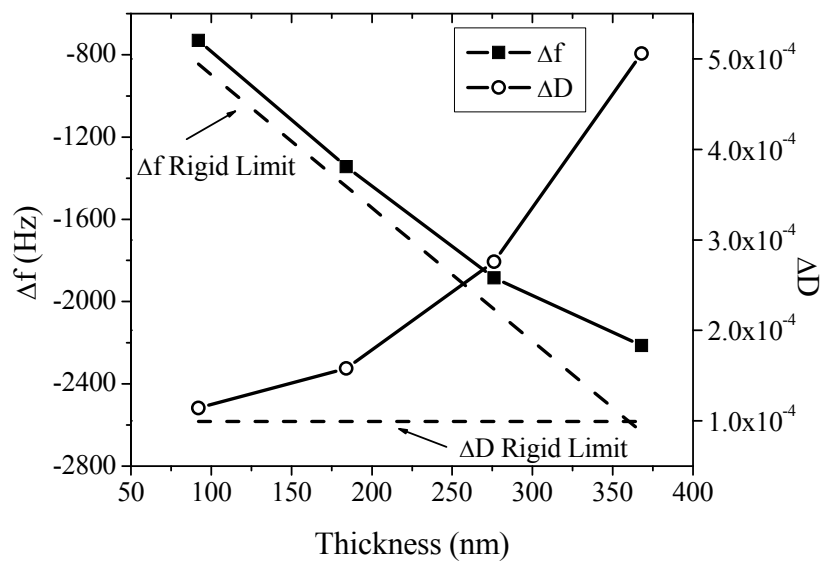


Figure 5.5. The deviation of Δf and ΔD from the rigid limit for the poly(NIPAAm-co-MaBP) coating exposed to water as a function of thickness at 15 °C for $n=9^{\text{th}}$ overtone.

The acoustic response of a Voigt viscoelastic layer in a bulk liquid of equal density is defined by the β -function (adopted from Voinova.¹²²)

$$\beta = -2\pi\rho_o h_o \left(\frac{f}{2} \Delta D - i\Delta f \right) = -i\sqrt{-i\rho G^*} \frac{1 - Ae^{2\xi h}}{1 + Ae^{2\xi h}} \quad (5.3)$$

where

$$G^* = G_o + i\omega\eta \quad (5.4)$$

$$A = \left(\sqrt{\frac{-iG^*}{\omega\eta_s}} - 1 \right) / \left(\sqrt{\frac{-iG^*}{\omega\eta_s}} + 1 \right) \quad (5/5)$$

$$\xi = \omega \sqrt{-\frac{\rho}{G^*}} \quad (5.6)$$

The β -function is highly nonlinear and can lead to unphysical solutions. In order to create confidence in the fits, the four multiple integer thicknesses were fit simultaneously using the 3rd-9th overtones (with the assumption that the shear modulus and retardation time do not change appreciably over the frequency and thickness in this range). Figures 5.6 and 5.7 show the experimental data and simulated fits as well as the residuals for the 15 °C samples. Shown on each plot are the four integer multiple thicknesses for the 3rd, 5th, 7th, and 9th overtones. Generally speaking, the best fits yielded residuals within +/- 10% of both the $\Delta f/n$ and ΔD experimental values.

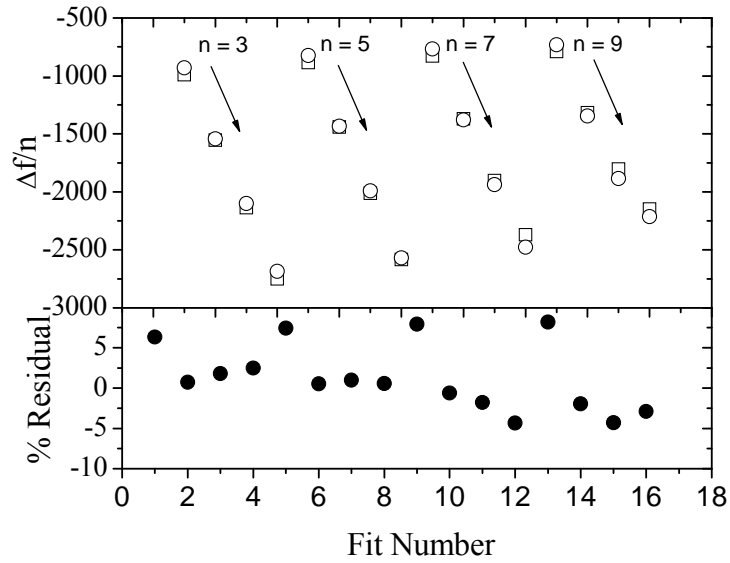


Figure 5.6. Experimental(\circ) data and simulated(\square) fits, as well as the residuals, of $\Delta f/n$ for the $n=3,5,7,9$ overtones at 15 °C. The arrow direction corresponds to the 4 integer multiple thicknesses.

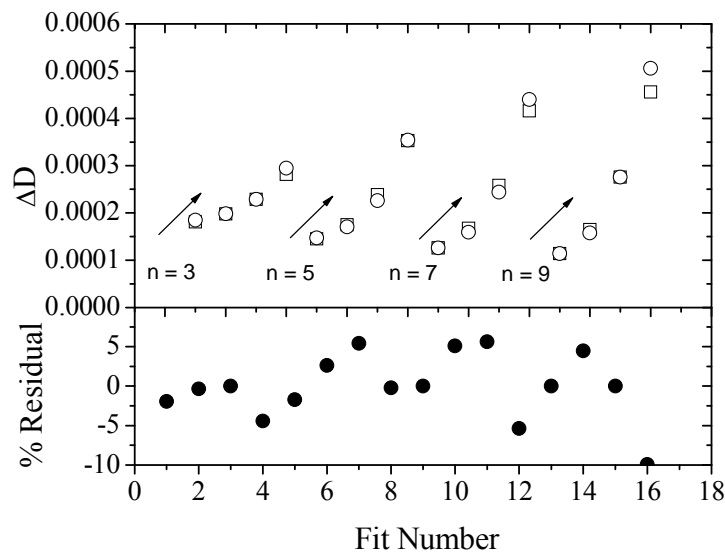


Figure 5.7. Experimental(\circ) data and simulated(\square) fits, as well as the residuals, of ΔD for the $n=3,5,7,9$ overtones at 15 °C. The arrow direction corresponds to the 4 integer multiple thicknesses.

Figures 5.8 and 5.9 shows the fitted values of shear modulus, thickness, and viscosity as a function of temperature for the 36 nm thick coating. The poly(NIPAAm-co-MaBP) coating shows a gradual reduction in thickness between 15 and 25 °C (decreasing from 93 nm to 75 nm) followed by a sharp reduction in thickness between 25 and 30 °C. At all temperatures, the QCM-D derived thickness was close to the ellipsometry derived thickness. At 15 °C, the QCM-D thickness of 93 nm was approximately 15% lower than the ellipsometry thickness. At 40 °C, the QCM-D thickness of 36 nm was within 5% of the ellipsometry thickness.

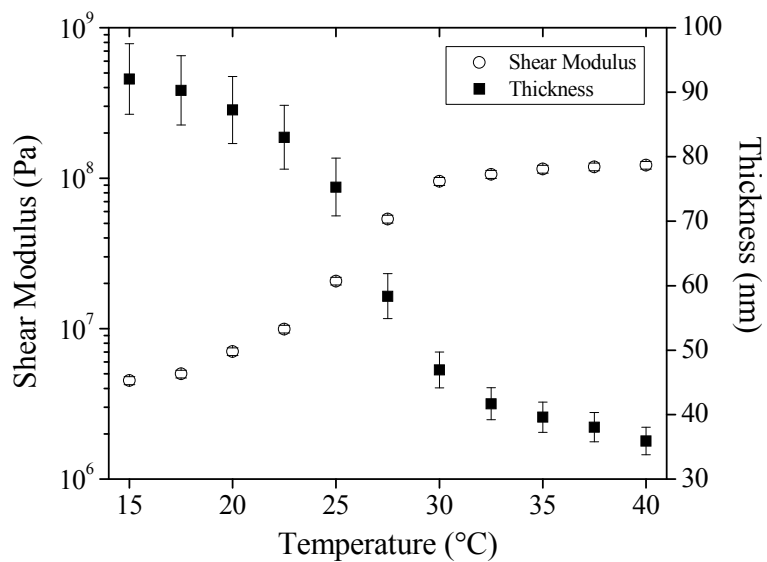


Figure 5.8. Variation of the shear modulus (○) and thickness (■) of the 1st integer multiple thickness poly(NIPAAm-co-MaBP) coating as a function of temperature. Error bars for shear modulus lie within the data points.

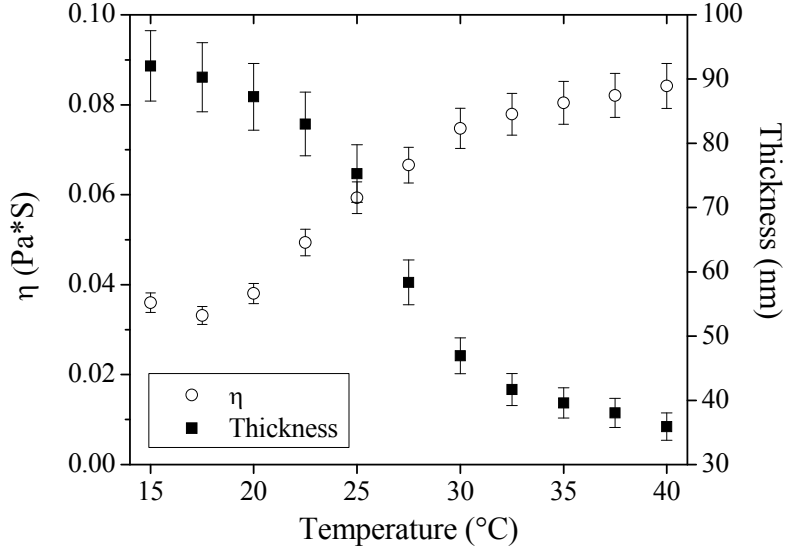


Figure 5.9. Comparison of the viscosity and thickness of the 1st integer multiple thickness poly(NIPAAm-co-MaBP) coating as a function of temperature. The frequency ω was based on the $n=9^{\text{th}}$ overtone.

Over the temperature range 15 – 40 °C, the thickness changes by a factor of 3; however, the shear modulus changes by a factor of 24 and the viscosity changes by a factor of two. In the low-frequency limit, the shear modulus G_o is a measure of the number of effective crosslinks per unit volume of the network and is expressed as¹⁵⁰

$$G_o \cong \frac{kT}{a^3} \left(\frac{\phi}{N_e} \right) \quad (5.7)$$

Where N_e is the number segments between cross-links, ϕ is the segment volume fraction and a^3 is the segmental volume. The maximum limit of N_e is set by the cross-link density, nevertheless formation of knots and entanglements may act to reduce the effective crosslink density. The value of G_o (based on complete cross-linking of the gel coating) is expected to be ~1MPa, but as seen from Figure 5.6, it plateaus two orders of magnitude

higher. It is well-known that the shear modulus in the high-frequency regime (or the glassy regime) can be 2-3 orders of magnitude higher than the rubbery regime due to incomplete relaxation of segmental dynamics.

Moreover, if it is assumed the gel is affinely deformed by the shear resonator, an individual “correlation blob” is deformed in the same manner. The blob will relax to recover its equilibrium dimensions, the motion corresponding to the relaxation of a stretched one-dimensional chain, whose characteristic time scale in a good solvent is on order of ¹⁵⁰

$$\tau \cong \eta_s \frac{a^3}{\phi kT} \quad (5.8)$$

This relationship assumes that hydrodynamic interactions are completely screened within the correlation blob, which may not properly reflect the exact range of frictional forces acting against the movement of a chain at high frequencies. Indeed, based on Equation 5.8, at 15 °C, the retardation time is expected to be on the order of 10 ps. The best fit at 15 °C, however, yields a retardation time $\tau_r = \eta/G_o$ on the order of 10 ns, which corresponds to $\tau_r\omega \approx 2$ (for the 9th overtone). The slower response time may be the result of significant coil-coil overlap between cross-links, which is not surprising considering that the polymer films were spin-casted prior to cross-linking.

While the phenomenological expressions described by Equations 5.7 and 5.8 may not be entirely appropriate, they do suggest that for data to be compared at different temperatures and solvent viscosities, the retardation ratio τ_r should be scaled by T/η_s and G_o should be scaled by $1/T$. Figure 5.10 shows the dependence of these values on the segmental volume fraction of the coatings, with three regions denoted: the swollen regime, the transition regime, and the collapsed regime. The segmental volume fraction

of a collapsed layer at 40 °C was determined to be 0.72 from neutron reflection experiments¹⁵¹ hence, the volume fraction ϕ at each temperature was estimated to be $\phi = 0.72h_T/h_{40}$, where h_T is the thickness at temperature T and h_{40} is the thickness at 40 °C. In the swollen regime, G_o/T displays a strong dependence on the volume fraction (a power law of order 6), which most likely is not universal but a reflection of varying retardation timescales in the swelling process. An enhancement in the local segmental dynamics due to dilution could very well cause the strong concentration dependence. The retardation time $\tau_r T/\eta_s$, also shows a strong dependence on the volume fraction, although a slightly weaker power law of order -3. In the collapsed regime, G_o/T scales linearly in concentration whereas $\tau_r T/\eta_s$ shows almost no concentration dependence. This observation may be a result of significant interpenetration between polymer segments in the collapsed state. It has been noted elsewhere that high-frequency relaxation in concentrated polymer solutions is rather insensitive to concentration and quality of the solvent.¹⁵²

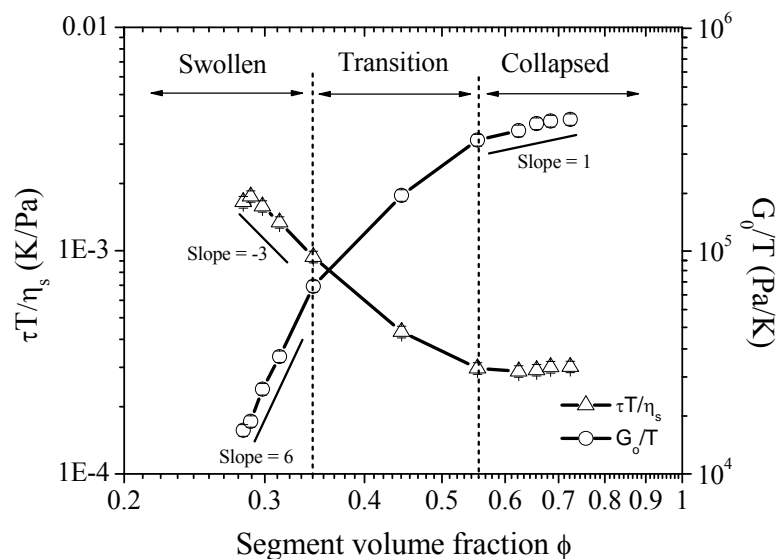


Figure 5.10. Dependence of the scaled retardation time and shear modulus on the volume fraction of the poly(NIPAAm-co-MaBP) coating in the three regimes of temperature: swollen, transition, and collapsed. Error bars are within the data points.

To further complete the picture, inorganic salts are known to have a strong effect on the volume-phase transition behavior of poly(NIPAAm).¹⁵³⁻¹⁵⁸ Figure 5.11 shows the effect of NaCl concentration on the thickness of the poly(NIPAAm) coatings. At any one particular temperature, the addition of the salt worsens the solvent quality and drives deswelling of the coating. Figure 5.12 shows the scaled G_0/T values for three samples (no added salt, 0.5 M NaCl, and 2.0 M NaCl). The scaled modulus appears to collapse for segment volume fractions below 0.6, implying that NaCl has negligible effect on chain stiffness in the swollen state. In the collapsed state, however, the modulus increases with increasing NaCl concentration. This observation is clearly shown in Figure 5.13, in which the modulus is plotted against salt concentration in the collapsed state at 40 °C. Also plotted is the segment volume fraction in the collapsed state, which increases from 0.72

under no added salt to 0.82 at 2.0M NaCl. The residual water has been attributed to weakly bound water molecules that most likely remain between amide moieties.¹⁵⁹ Salt could possibly affect the residual water through one of two effects. Salt ions that are incorporated into the collapsed layer may provide more efficient packing of the polymer chains. In the second scenario, if salt is excluded from the collapsed layer, an osmotic gradient may act to further dehydrate the collapsed layer. In either scenario, the more tightly packed configuration is registered in the elastic modulus.

On the other hand, the reduced value of $\tau_r T / \eta_s$ for all salt concentrations, as shown in Figure 5.14, appears to collapse to the same master curve when plotted against the segment volume fraction, signifying that the retardation time is strongly correlated to the volume fraction, yet short range dynamics do not appear to be significantly affected by the addition of salt.

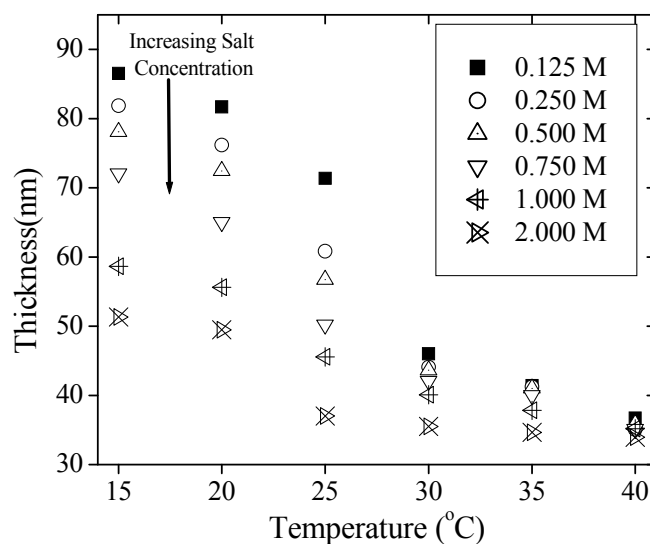


Figure 5.11. Effect of salt concentration on the thickness of the poly(NIPAAm-co-MaBP) coating as a function of temperature. The arrow indicates the increase in NaCl concentration.

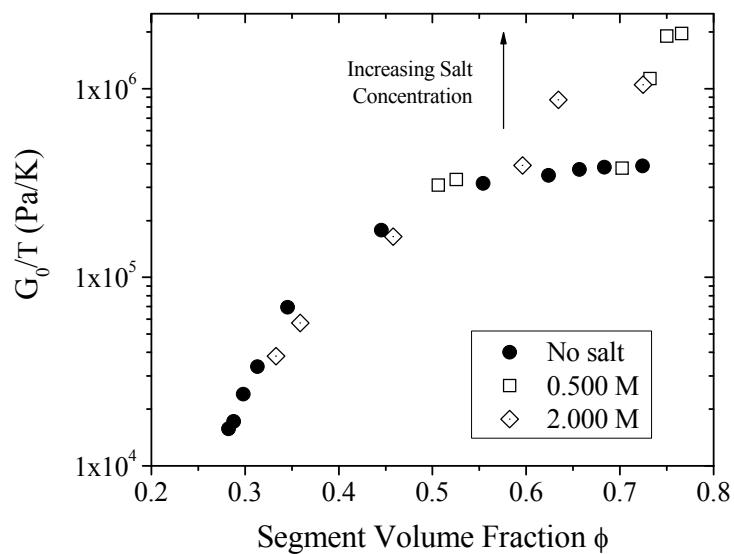


Figure 5.12. Scaled shear modulus of the poly(NIPAAm-co-MaBP) coating as a function of volume fraction for three different NaCl concentrations.

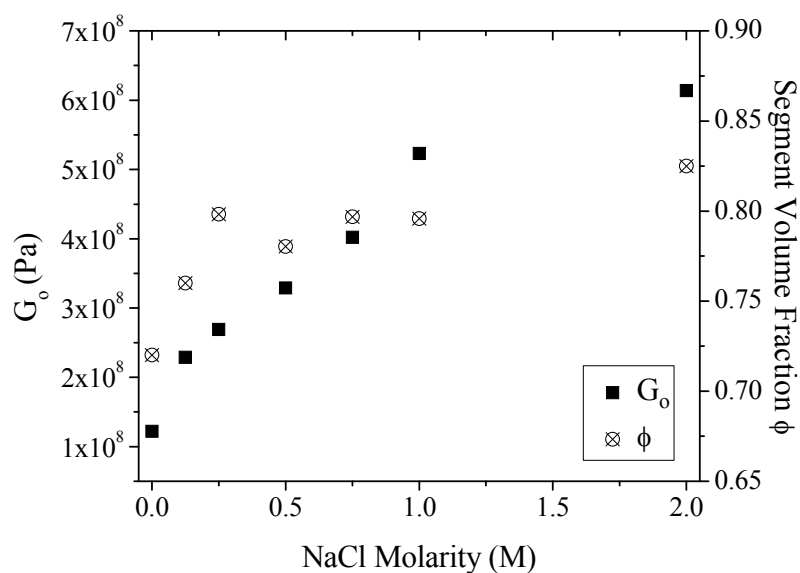


Figure 5.13. Shear modulus and segment volume fraction of the poly(NIPAAm-co-MaBP) coating as a function of NaCl concentration in the collapsed state at 40 °C.

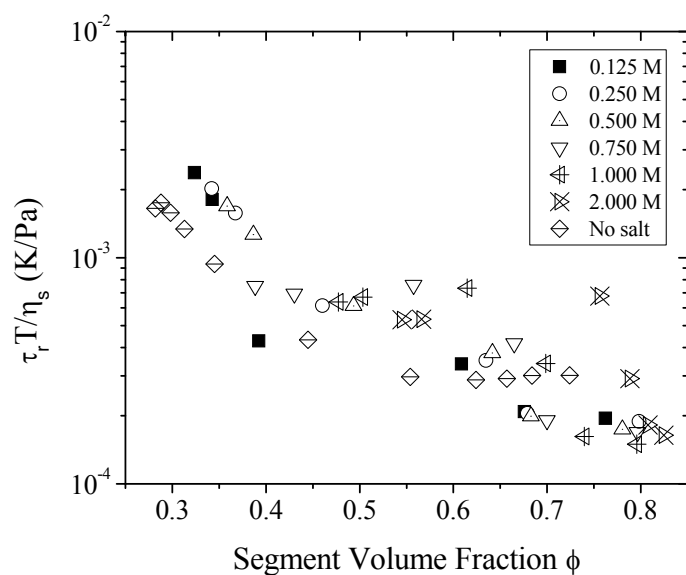


Figure 5.14. Scaled retardation time of the poly(NIPAAm-co-MaBP) coating as a function of segment volume fraction and NaCl concentration.

5.3. Conclusions

Surface-tethered poly(NIPAAm-co-MaBP) networks in contact with aqueous solutions were characterized with QCM-D. At the overtones measured, the coatings appeared to be rigid films at the 3rd overtone, where dissipation was dominated by the gel/water interface friction complicating viscoelastic analysis of the films. As the overtone increased, deviation from the rigid limit was found allowing for viscoelastic analysis. Throughout the collapse, the shear modulus increased from 5 MPa in the swollen state to 120 MPa in the collapsed state. The shear modulus in the rubbery plateau in the collapsed state is expected to be on the order of ~1MPa, hence the QCM-D probes a regime where the polymer mesh cannot adequately relax. However, due to the limited range over which frequency response is measured, it is unclear where in the rubbery-to-glassy transition zone that the experiment is taking place, making it difficult to analyze the viscoelasticity within known scaling relationships. That being said, in this frequency regime, the shear modulus is much more sensitive to the demixing temperature than the shear viscosity. This could be a consequence of significant polymer-polymer coil overlap that results in the spin-casting technique. Finally, in the collapsed state, QCM-D showed a sharp increase in the shear modulus with increasing NaCl salt concentration, yet the dynamics were not significantly perturbed. Again, this may be a consequence of polymer-polymer contacts dominating the viscous behavior.

CHAPTER 6: EFFECT OF HOFMEISTER SERIES ON THE TRANSITION BEHAVIOR OF POLY(NIPAAm) AND POLY(DEAAm)

6.1 Introduction

Lower critical solution temperature (LCST) polymers can serve as model systems for probing the effect of ions on the stability of biological macromolecules.¹⁶⁰⁻¹⁶³ It is well established that the dissolution temperature of LCST polymers, including poly(N-isopropylacrylamide), or poly(NIPAAm), is strongly affected by the addition of salt, in a manner similar to how protein stability is affected by salt.^{154, 155, 157, 164-169} The effect of ions, however, is not purely concentration dependent. The dissolution temperature depends on the “structure forming” or “structure breaking ability” of the ion and follows the Hofmeister series.¹⁷⁰⁻¹⁷³

LCST polymers contain a hydrogen-bonding group, such as an amide, and a hydrophobic group. At low temperatures, solubility of the macromolecule is engendered through favorable mixing of the hydrogen-bonding groups and water. As temperature is increased, a point is reached where mixing can no longer stabilize hydrophobic interactions and the polymer phase-separates from solution.

Despite a considerable body of research, however, questions still remain concerning the exact mechanism of the interaction of salts with macromolecules that contain both amides and hydrophobic groups. It is generally thought that the effect of the Hofmeister salts result from ion-specific interactions with both amide and nonpolar

moieties¹⁷⁰. where the amide interaction is perhaps a nonspecific ion-dipole interaction that is modulated by vicinal methyl groups.¹⁷⁴ Cremer and co-workers proposed that strong “salting out” salts act by polarizing the water molecules adjacent to the amide groups and by increasing the surface tension around the hydrophobic groups, while “salting in” salts bind directly to the amide groups.¹⁶⁵ They also suggested a two-step demixing process for strong salting out anions like SO_4^{2-} , wherein amide groups are first dehydrated followed by the dehydration of the isopropyl groups.¹⁶⁵

Near the water/air interface, all ions of the Hofmeister series increase surface tension due to exclusion of the ions near the surface.^{175, 176} Similar effects have been observed with the salting out of benzene from aqueous solution, where ions decrease the solubility of benzene in water.¹⁷⁷ It may therefore be expected that all macromolecules have decreased solubility in salt solutions. Indeed, early members of the Hofmeister series, or kosmotropes, do monotonically decrease solubility. Later members of the Hofmeister series, or chaotropes, however, can form ion-dipole pairs with hydrogen bonding moieties and increase solubility.¹⁷⁸⁻¹⁸⁰

In this paper, we explore the influence of Na_2SO_4 , NaCl , NaBr , and NaI on the swelling of thin layers of surface-attached networks of poly(NIPAAm) and poly(N,N-diethylacrylamide), or poly(DEAAm), both of which are amide-based polymers. Poly(NIPAAm) contains a secondary amide that donates and accepts a hydrogen bond; whereas, poly(DEAAm) contains a tertiary amide that only accepts a hydrogen bond. The

Hofmeister series suggests that $\text{SO}_4^{2-} > \text{Cl}^- > \text{Br}^- > \text{I}^-$ in terms of the anion's ability to salt-out neutral, LCST polymers. Within this ordering, SO_4^{2-} is kosmotropic, I^- is chaotropic, and Cl^- and Br^- are intermediate. We use both ATR-FTIR and ellipsometry to characterize the surface-attached networks. While FTIR has been extensively used to measure the frequency shifts of the vibrations associated with the amide and aliphatic groups in LCST polymers and gels upon demixing¹⁸¹⁻¹⁸⁵, interpretation of spectra is difficult without precise knowledge of the water content. To that end, we use ellipsometry to derive the average water distribution in the polymer coatings. FTIR spectra are then compared at the same water content in order to unambiguously determine the effect of ions on the vibrations of the amide and aliphatic groups.

6.2 Results and Discussion

Figure 6.1 shows the thermally-induced deswelling transition (or deswelling isobars) in both poly(NIPAAm) and poly(DEAAm) networks with 3 mole% MaBP cross-linker. Both have a demixing temperature near 30 °C. Below the deswelling temperature, poly(NIPAAm) has a higher equilibrium water content than poly(DEAAm), which is likely the result that poly(NIPAAm) can hydrogen bond to water at both the C=O and N-H positions whereas poly(DEAAm) can hydrogen bond at the C=O position. Interestingly, the two ethyl groups of poly(DEAAm) does not alter the transition temperature with respect to poly(NIPAAm); however, the deswelling isobar is more gradual than in poly(NIPAAm).

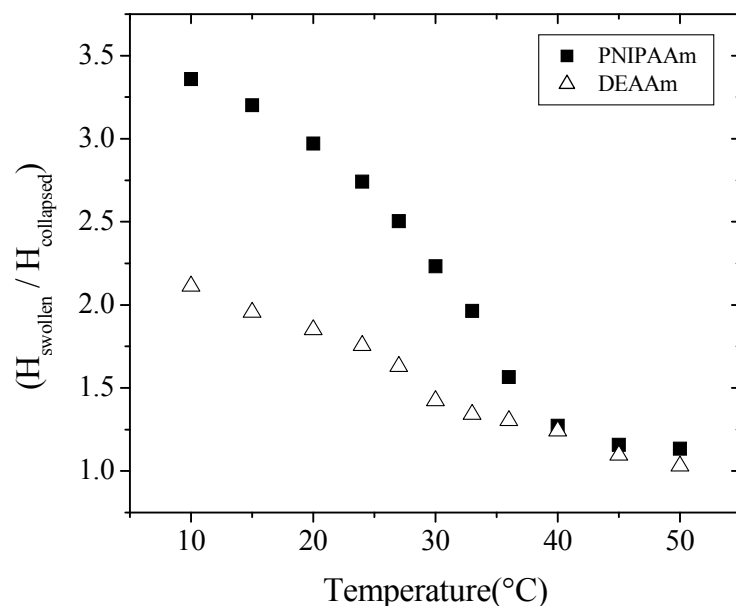
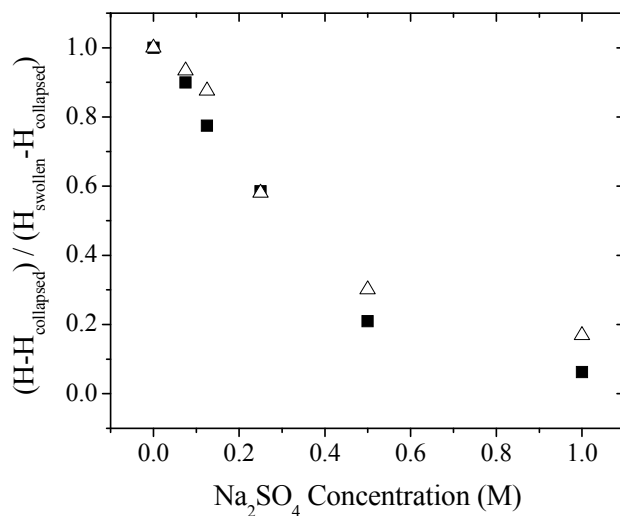


Figure 6.1 Deswelling isobars of poly(NIPAAm) and poly(DEAAm) showing a demixing temperature near 30 °C.

Figure 6.2 shows the deswelling isotherms, or the variation in the dimensionless thickness of both poly(NIPAAm) and poly(DEAAm), over a range of salt concentration (0-2.0 M) for Na₂SO₄(figure 6.2a), NaCl(figure 6.2b), NaBr(figure 6.2c), and NaI (figure 6.2d), all carried out at 5 °C. The dimensionless thickness is defined as $(H - H_{\text{collapsed}}) / (H_{\text{swollen}} - H_{\text{collapsed}})$, where H is the thickness at the respective salt concentration, H_{swollen} is the thickness in water at 5 °C and $H_{\text{collapsed}}$ is the thickness at 42 °C. Comparing poly(DEAAm) and poly(NIPAAm), despite the difference in the collapse profiles with respect to temperature, they display similar collapse profiles with each salt. If a salt concentration $C_{1/2}$ is defined for when the polymer layer reaches a dimensionless thickness value of $1/2$, the values of $C_{1/2}$ for Na₂SO₄(figure 6.2a), NaCl, (figure 6.2b), NaBr(figure 6.2c), are 0.25 M, 1.3 M, and 2.5 M, respectively, for both poly(DEAAm)

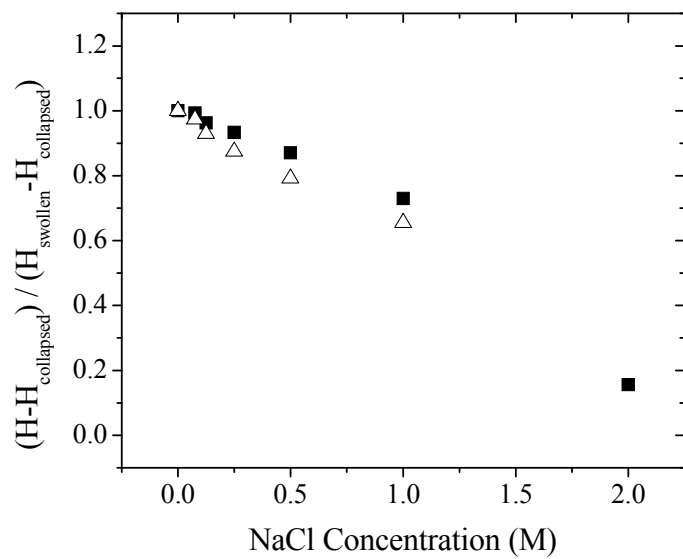
and poly(NIPAAm). At 5 °C, a $C_{1/2}$ for NaI (figure 6.2d), could not be found up to 5.0 M. NaI also leads to slight additional swelling of both layers (by ~5-10%) at low salt concentrations.

Based on the values of $C_{1/2}$ for each of the ions, it becomes readily apparent that the bulk air/water surface tension effects cannot be used to predict deswelling behavior. The surface tension increments of the individual salts in dynes/(cm*molality) are $\text{Na}_2\text{SO}_4 = 2.77$, $\text{NaCl} = 1.73$, $\text{NaBr} = 1.47$, and $\text{NaI} = 1.14$.¹⁷⁵ Hence, the increase in the bulk surface tension at $C_{1/2}$ is 0.7 dynes/cm for Na_2SO_4 , 2.5 dynes/cm for NaCl , 3.7 dynes/cm for NaBr , and greater than 5.7 dynes/cm for NaI . It is hypothesized that the differences in the bulk surface tension follow from a direct interaction of the ion with the amide group. In fact, the bulk surface tension trend is consistent with the ordering of the ions in the Hofmeister series.

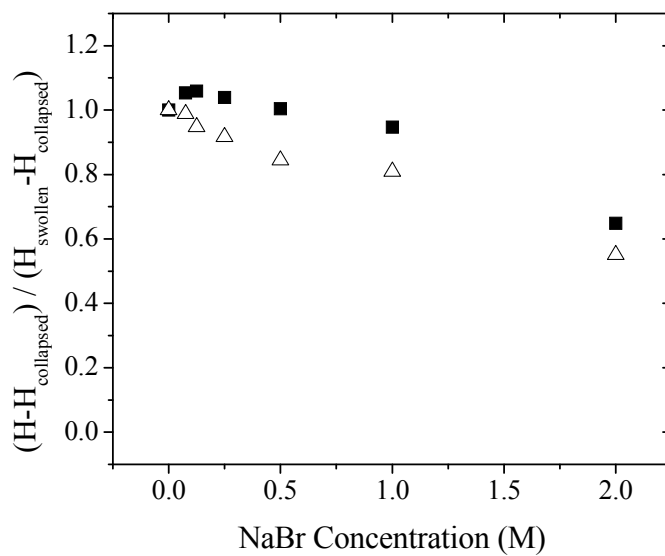


(6.2a)

Figure 6.2 Variation in thickness of poly(NIPAAm) (\blacksquare) and poly(DEAAm) (\triangle) at 5 °C in between 0-2.0 M salt concentration for (6.2a) Na_2SO_4 (6.2b) NaCl (6.2c) NaBr and (6.2d) NaI .

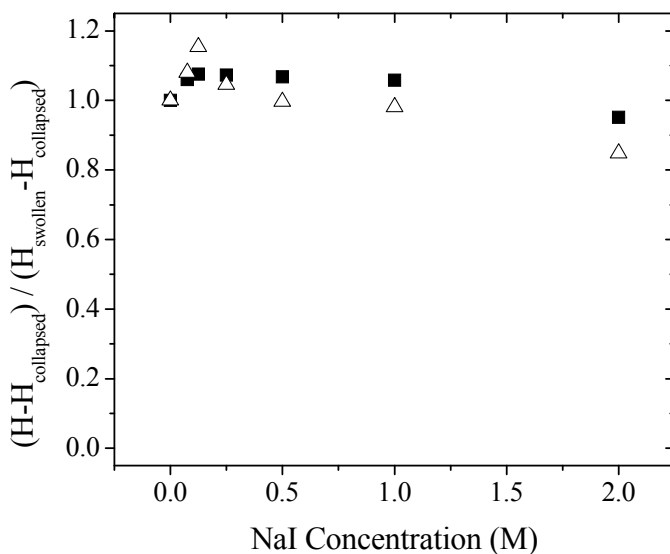


(6.2b)



(6.2c)

Figure 6.2 Contd.



(6.2d)

Figure 6.2 Contd.

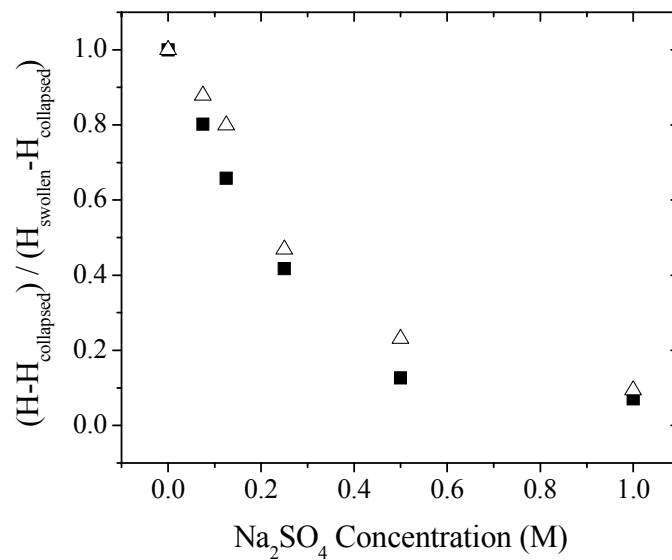
By changing the temperature of the experiment, the subtle effects of the ions can be distinctly observed. Figures 6.3 and 6.4 show similar experiments conducted at 15 and 24 °C. At both temperatures, the deswelling isotherms for poly(NIPAAm) and poly(DEAAm) overlap in Na₂SO₄ and NaCl. However, the ratio of C_{1/2} at 5 °C to C_{1/2} at 24 °C is different for the two salts. The value of C_{1/2} for Na₂SO₄ (figure 6.2a), at 5 °C is 2.2 times the value at 24 °C (figure 6.4a),; whereas, the value of C_{1/2} for NaCl (figure 6.2b), at 5 °C is 3 times the value at 24 °C (figure 6.4b),. This may be due to an increasingly stronger interaction of Cl⁻ with the amide than SO₄²⁻ as the temperature is increased.

For NaBr, there is a small difference in deswelling isotherms of poly(DEAAm) and poly(NIPAAm) at 15 °C, where NaBr is perhaps slightly more effective at salting-out poly(DEAAm). This difference becomes significant, however, at 24 °C, where C_{1/2} for poly(NIPAAm) is 1.0 M and for poly(DEAAm) it is 0.7 M. Moreover, a slight salting-in

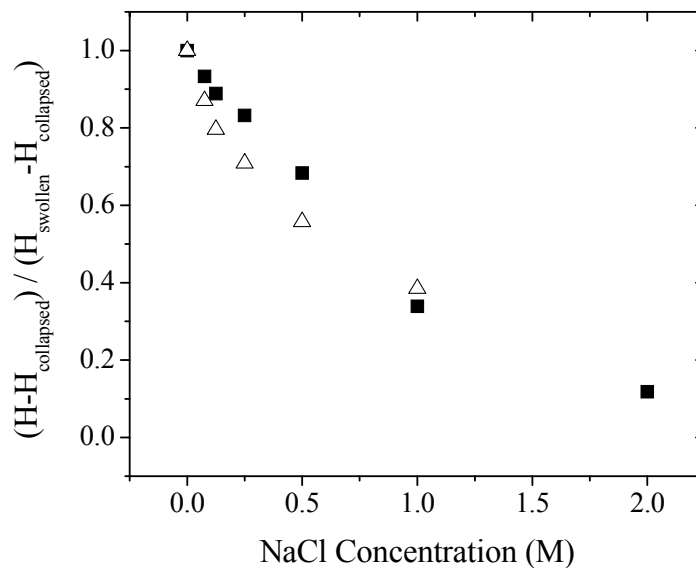
effect is measured for poly(NIPAAm), which increases with temperature. At 24 °C, the maximum degree of salting-in is 8%.

With respect to NaI, there is considerable deviation in the deswelling isotherms for poly(NIPAAm) and poly(DEAAm), with the deviation becoming more prominent as the temperature is increased. At both 15 and 24 °C, NaI is more effective at deswelling poly(DEAAm) than poly(NIPAAm). Moreover, NaI salts-in poly(NIPAAm) at low salt concentrations, with the degree of salting-in increasing with temperature. In contrast, the opposite trend is seen with poly(DEAAm), where the degree of salting-in decreases with temperature. That said, the maximum degree of salting-in is 5% for poly(DEAAm) at 5 °C and 18% for poly(NIPAAm) at 24 °C.

It was noted that that the bulk surface tension increments of the individual salts are insufficient to quantitatively interpret the deswelling isotherms. It is tempting to explain the deviation with respect to a difference in the partitioning of ions between the macromolecule surface and bulk water and the partitioning ions between an air interface and bulk water interface. At the air/water interface, ions that possess a large charge/volume ratio are generally excluded from the interface, as they are less likely to give up their hydration waters.^{175, 186} Ions with a smaller charge/volume ratio can more easily forfeit their hydration waters and therefore are able to access the interfacial zone. A question is how the presence of dipoles influences ion partitioning. Towards this end, we use ATR-FTIR to study the amide group and aliphatic CH₃ vibrations of poly(NIPAAm) and poly(DEAAm) upon exposure to salt.

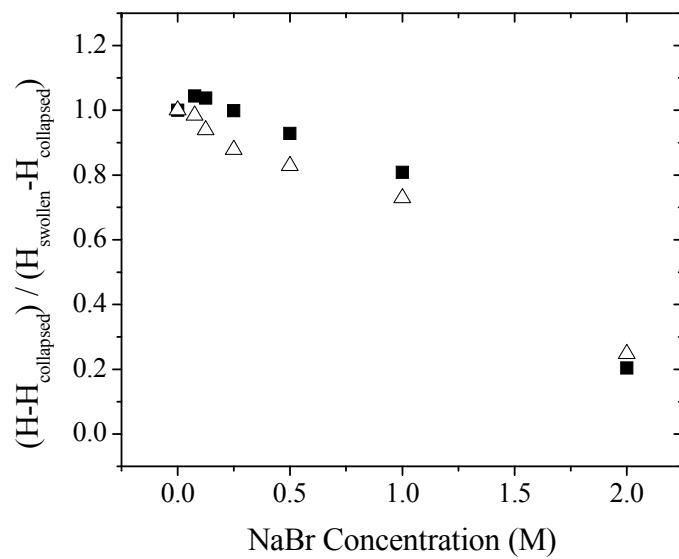


(6.3a)

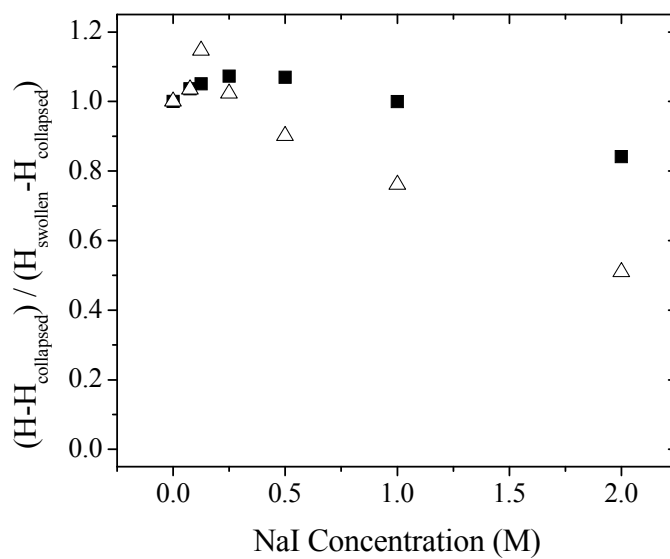


(6.3b)

Figure 6.3 Variation in thickness of poly(NIPAAm) (■) and poly(DEAAm) (△) at 15 °C in between 0-2.0 M salt concentration for (6.3a) Na_2SO_4 (6.3b) NaCl (6.3c) NaBr and (6.3d) NaI.

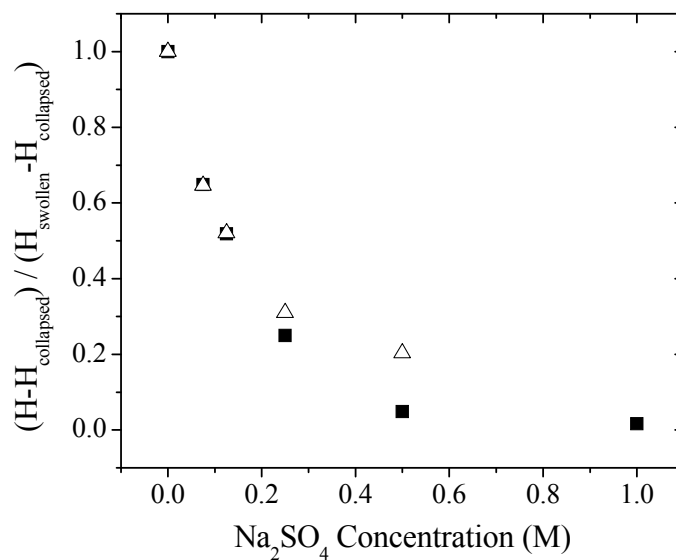


(6.3c)

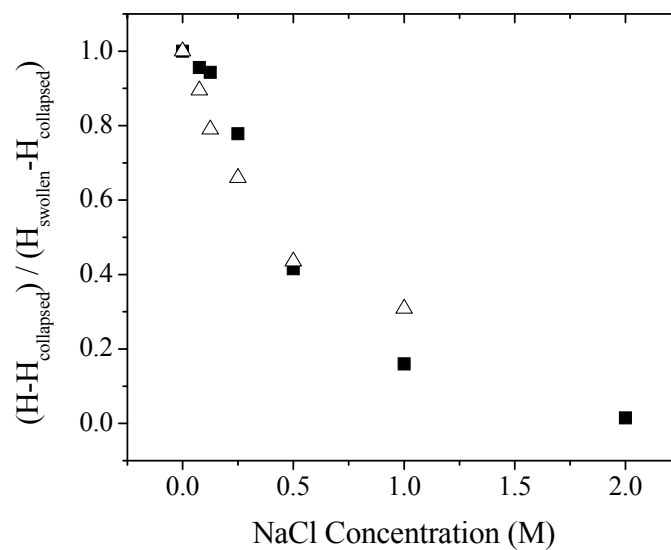


(6.3d)

Figure 6.3 Contd.

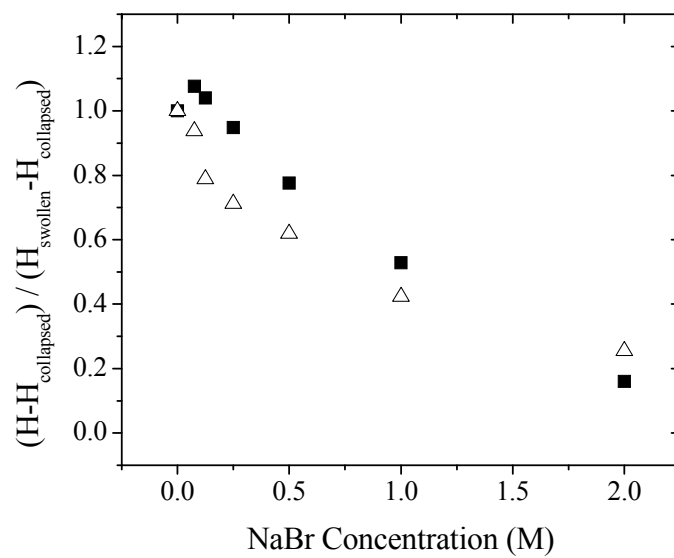


(6.4a)

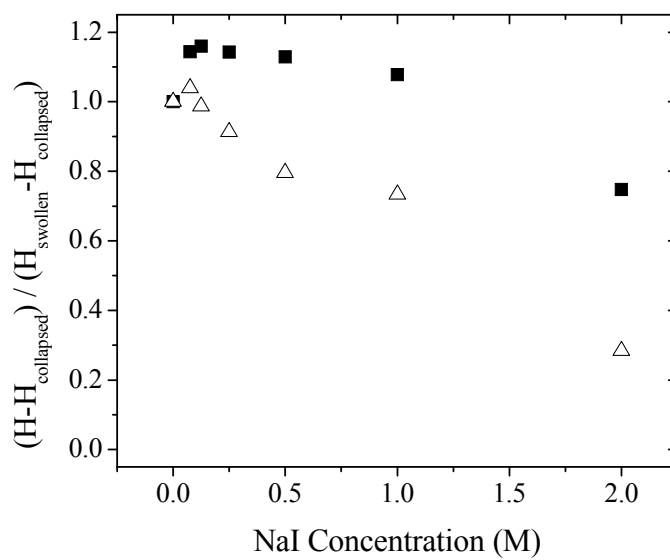


(6.4b)

Figure 6.4 Variation in thickness of poly(NIPAAm) (■) and poly(DEAAm) (Δ) at 24 °C in between 0-2.0 M salt concentration for (6.4a) Na_2SO_4 (6.4b) NaCl (6.4c) NaBr and (6.4d) NaI.



(6.4c)



(6.4d)

Figure 6.4 Contd.

As the frequency of the vibrations is clearly influenced by the amount of water in the network, rather than comparing the frequencies as a function of salt concentration, we compare the vibrational frequency at the same degree of swelling for each salt, as determined from the ellipsometry measurements.

Figure 6.5 shows the frequency of the amide I of poly(NIPAAm) versus degree of swelling in Na₂SO₄, NaCl, NaBr, and NaI at 24 °C. In all cases the amide I shows an initial decrease in the vibration frequency as salt is added followed by an increase in the frequency as the layer collapses, which is caused by the rise of the sub-band around 1651cm⁻¹. The frequency trends for all salts overlap (to within +/- 0.5 cm⁻¹); hence, the frequencies of the vibrations appear independent of ion and depend only on the degree of swelling. In contrast, Figure 6.6 shows the amide II, where now the frequencies no longer overlap. Most notably at a degree of swelling ($H/H_{\text{collapsed}}$) of 2.4, a frequency of 5 cm⁻¹ separates NaI (1551 cm⁻¹) and Na₂SO₄ (1555 cm⁻¹). The corresponding degree of swelling in pure water occurs at 30 °C, where the position of the amide II is centered at approximately 1555 cm⁻¹, the same position of Na₂SO₄. While the proximity of the two vibrations suggests negligible interaction of Na₂SO₄ with the amide, a direct comparison is probably inappropriate due to the different temperatures of the experiment (24 °C vs. 30 °C). That said, for all values of $H/H_{\text{collapsed}}$ above unity, the amide II vibration of poly(NIPAAm) is lowest in NaI, followed by NaBr, NaCl and then Na₂SO₄. Interestingly, the trend follows the order of the Hofmeister series.

We speculate that the ions are electrostatically attracted to the O=C-N dipole and destabilize or sterically inhibit hydrogen bonding at the N-H moiety, decreasing the amide II frequency. NaI, which exhibits the largest effect, thus displays the largest ion-

dipole attraction, which correlates with the salting-in effect measured with ellipsometry. Moreover, the trend in the vibration frequencies could explain the increase in the bulk air/water surface tension at $C_{1/2}$ for each of the salts; in other words, the stronger the ion-dipole attraction, the greater the required surface tension to collapse the layer. As the frequency of amide I is unaffected by the type of ion, it is presumed that binding or attraction is primarily between the anion and the partially positive end of the O=C-N and does not affect hydrogen bonding to the partially negative O=C end of the dipole.

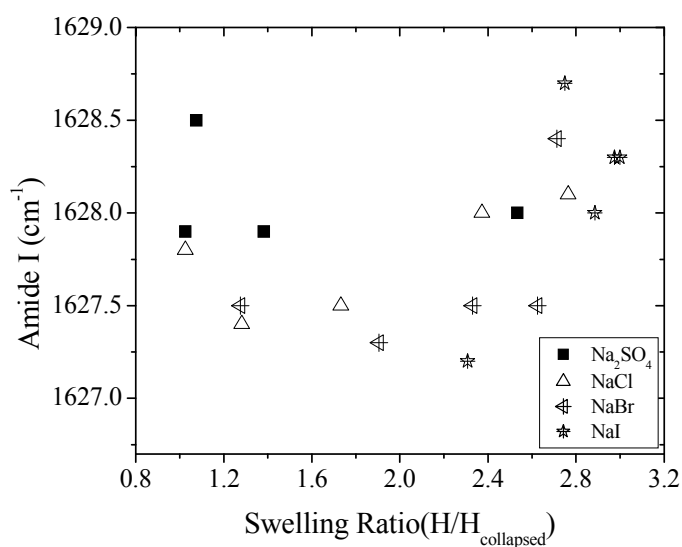


Figure 6.5 Frequency shift of Amide I band as a function of degree of swelling of poly(NIPAAm) at 24 °C from 0-2.0 M salt concentrations.

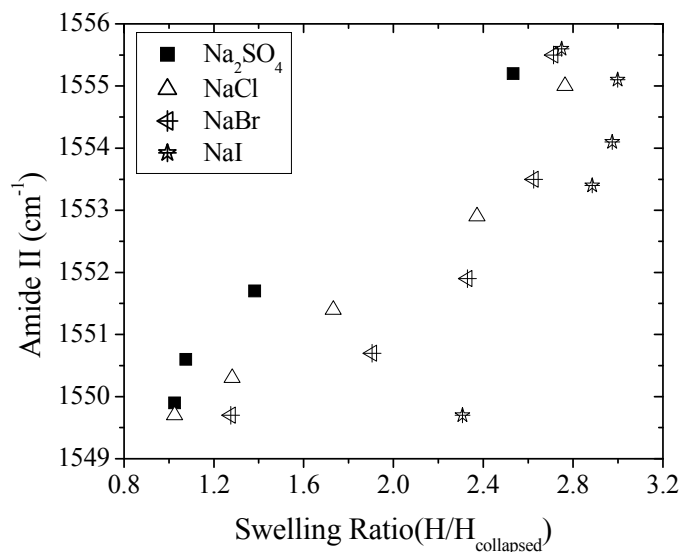


Figure 6.6 Frequency shift of Amide II band as a function of degree of swelling of poly(NIPAAm) at 24 °C from 0-2.0 M salt concentrations.

In poly(DEAAm) (which lacks a N-H moiety), the frequency of the amide I vibration now depends strongly on the ion (Figure 6.7). The vibration associated with Na₂SO₄ displays the same U-shape trend as seen in poly(NIPAAm), which is quite close to the frequency trend in pure water upon collapse. In NaCl, the depth of the minimum in the U-shape becomes shallower. In NaBr and NaI, the minimum disappears and now the frequency increases monotonically with temperature. We now speculate that in the case of poly(DEAAm), ions interact primarily with the partially positive end of C=O dipole. The interaction weakens the ability of the C=O to hydrogen bond with water and shifts the frequency of the vibration to higher frequencies. As in the case of the amide II vibration in poly(NIPAAm), the strength of the interaction follows the Hofmeister series.

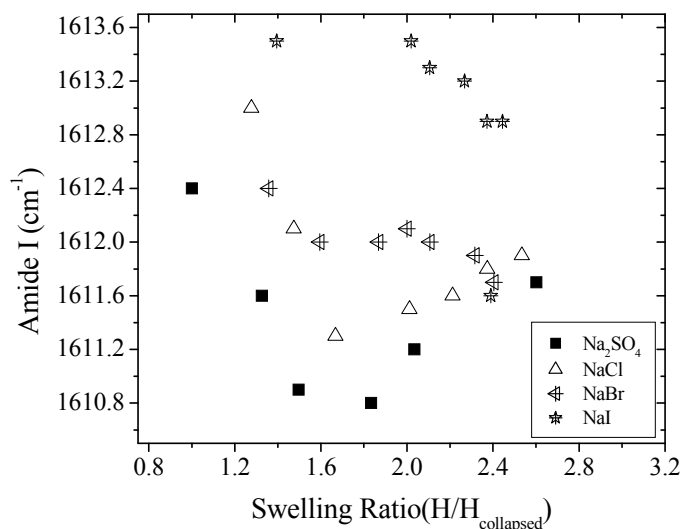


Figure 6.7 Frequency shift of Amide I band as a function of degree of swelling of poly(DEAAm) at 24 °C from 0-2.0 M salt concentrations.

Finally, it is of note to examine the CH₃ asymmetric stretching vibration in both poly(DEAAm) and poly(NIPAAm). This vibration was chosen as it is the most prominent of all the aliphatic vibrations, it shows a relatively large shift upon collapse (8 cm⁻¹), and it provides a direct comparison of the 2 terminal carbons of the isopropoyl group with the 2 terminal carbons of the ethyl groups. The CH₃ asymmetric vibrations are shown in figure 6.8 as a function of salt for both poly(NIPAAm) and poly(DEAAm). The CH₃ asymmetric stretching vibration collapses to the same curve for all the salts, with the exception of poly(DEAAm) in NaI. The relative independence of the CH₃ asymmetric stretching vibration on the salt ion suggests negligible accumulation of ions on the hydrophobic surface, as expected from bulk air/water surface tension measurements. Mysteriously, however, NaI causes an increase of 3 cm⁻¹ in the CH₃ vibration in poly(DEAAm), which is not observed in poly(NIPAAm). The increase may be a

consequence of the close proximity between an iodide and the CH₃ group resulting from attraction of the ion to the amide dipole. In contrast, the amide in poly(NIPAAm) is less sterically hindered and may better accommodate an iodide without perturbation of the CH₃ vibration.

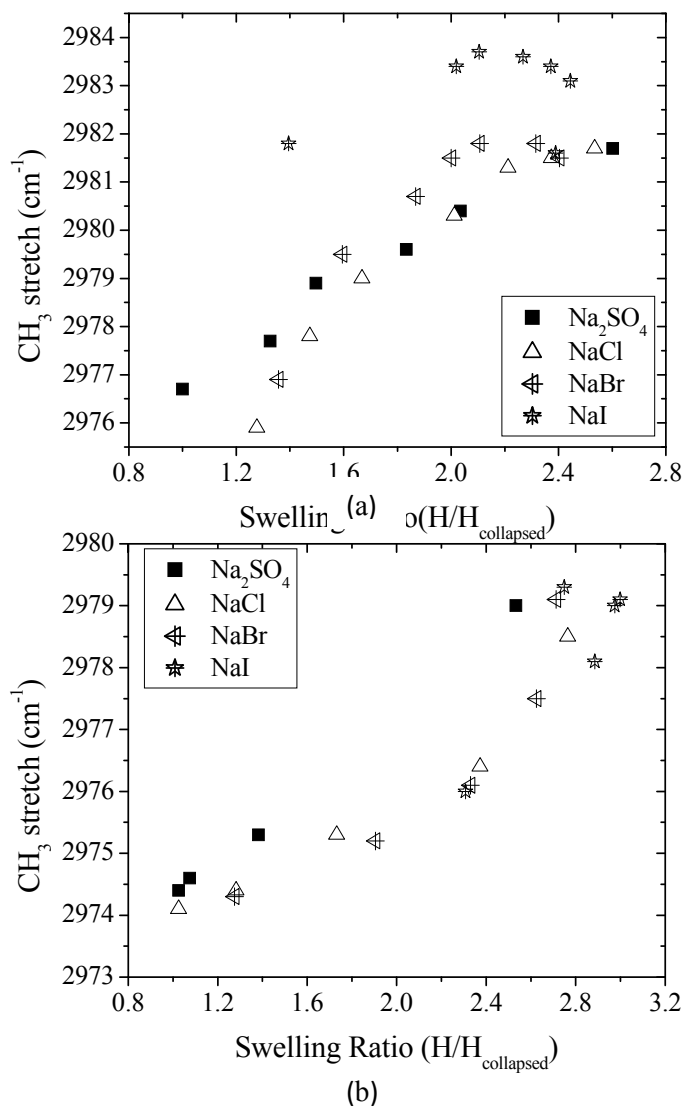


Figure 6.8 CH₃ stretch vibrations as a function of degree of swelling at 24 °C from 0-2.0 M salt concentrations for (a) poly(DEAAm) and (b) poly(NIPAAm).

6.3 Conclusion

The mechanisms by which ions affect the solubility of neutral macromolecules remain unresolved. Herein, we explored the deswelling isotherms of both poly(NIPAAm) and poly(DEAAm) induced through the addition of Na₂SO₄, NaCl, NaBr, and NaI. In the presence of early members of the Hofmeister series, the demixing isotherms of both poly(NIPAAm) and poly(DEAAm) are identical. Later members of the Hofmeister series, in contrast, impart distinct deswelling isotherms for poly(NIPAAm) and poly(DEAAm), due to differences in accumulation of ions at the amide dipole. The strength of the ion-dipole interaction appears to be dictated by surrounding hydrophobicity or steric hindrance of the amide, as later members of the Hofmeister series collapse poly(DEAAm) more quickly than poly(NIPAAm). Finally, the relative absence of a dependence on the CH₃ shift and ion suggests that ions do not adsorb to the hydrophobic moieties. The one exception is NaI and poly(DEAAm), which may not arise from adsorption but close proximity of the ion to the diethyl groups due to interaction with the amide dipole.

CHAPTER 7: STUDIES OF THE POLYMER STRUCTURE ON THE PHASE TRANSITION IN PRESENCE OF SALTS

7.1 Introduction

Studies of ion binding to model amides indicate that the ions interact with peptide groups.^{120, 187} However, the extent to which these interactions are modulated by the adjacent non-polar groups is not clear.^{188, 189} Thermoresponsive polymers can serve as a proxy to understand these interactions. These types of polymers comprise both hydrophilic and hydrophobic moieties. Since the LCST depends on the hydrophobic/hydrophilic balance of the polymer, the LCST can be tuned by variation of the side chain. Many studies have been done to show the influence of salts on the swelling and contraction of these polymers.^{190, 191} These studies have shown that the magnitude of various salt effects varies according to the Hofmeister series.

Park and Hoffman¹⁵⁷ were the first to demonstrate that aqueous solution of sodium chloride induces a volume phase transition in poly(NIPAAm). The experimental results obtained by Eeckman et al showed that the addition of salts leads to a significant decrease in the LCST of poly (NIPAAm). A 1.0M NaCl solution leads to a decrease of poly(NIPAAm) LCST by about 12 °C from approximately 32 °C in pure water to about 20 °C, while a 0.2 M Na₂SO₄ solution decreases its LCST by about 10 °C. It appears that the salt type, concentration, valence and size of the anions play important roles in influencing the LCST of poly(NIPAAm).^{192, 193} Cremer and co-workers proposed three mechanisms by which the salts interact with macromolecules. First, the anions can polarize the water

molecules adjacent to the amide groups. Second, the anions can interfere with the hydrophobic groups near the polymer backbone and isopropyl side chains, causing an increase in surface tension. Third these species can directly bind with the amide moieties.¹⁵⁸ In our previous paper we showed that the ions bind to the amide group and the ion-dipole interaction is dictated by surrounding hydrophobicity or steric hindrance of the amide.¹⁹⁴

In general, the majority of investigation concerning the Hofmeister ions focused on poly(N-isopropylacrylamide). It is still an open question how similar synthetic polymers with different alkyl groups respond to the addition of Hofmeister ions. In this contribution, we investigated the effect of Hofmeister salts on the swelling behavior of surface-attached, photocrosslinked polymer networks differing in the position of the amide and the structure of the alkyl groups. We showed that the anions ability to salt-out these polymers does not depend on the polymer structure and that $\text{SO}_4^{2-} > \text{Cl}^- > \text{Br}^- > \text{I}^-$. Ellipsometry and ATR-FTIR has been used to characterize the surface-attached poly (N-alkylacrylamides) copolymerized with 3 mol% of methacroyloxybenzophenone (MaBP). While ellipsometry was used to derive average water distribution in the polymer coatings, ATR-FTIR was used to study the intermolecular and intramolecular interaction between the polymer coating, salt and water molecules.

7.2 Results and Discussion

We investigated the deswelling transition of photo cross-linked poly (N-

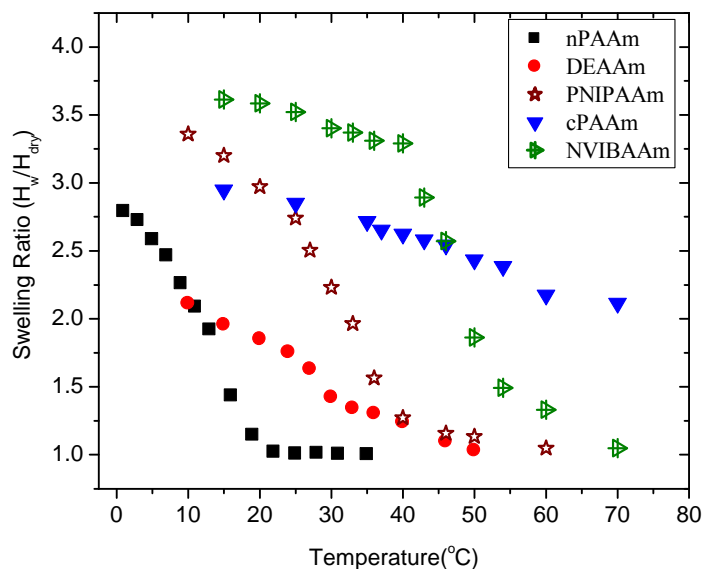
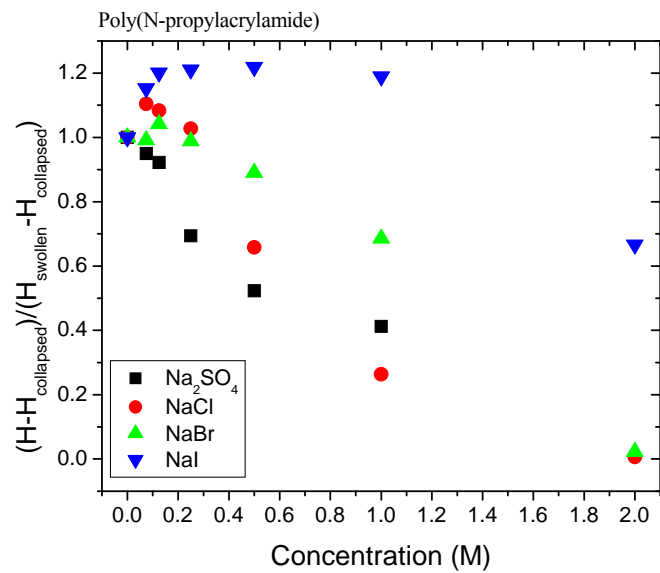


Figure 7.1 Deswelling isobars of N-alkylacrylamides.

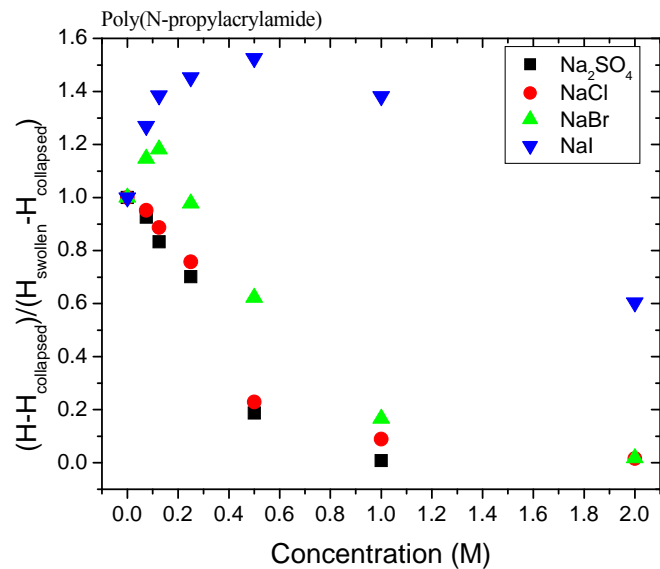
alkylacrylamides) networks with 3 mol % of MaBP as the cross-linker. Figure 7.1 shows demixing temperature of the copolymers: Poly(N-n-propylacrylamide), poly(NnPAAm) $\sim 15^{\circ}\text{C}$, poly(N-isopropylacrylamide), poly(NIPAAm) $\sim 30^{\circ}\text{C}$, poly (N,N-diethylacrylamide), poly(N,N-DEAAm) $\sim 30^{\circ}\text{C}$, poly(N-cyclopropylacrylamide), poly(NcPAAm) $\sim 45^{\circ}\text{C}$ and poly(N-vinylisobutyramide), poly(NVIBAAm) $\sim 43^{\circ}\text{C}$. By comparing all the copolymers, we observe that below the demixing temperature poly(N, N- DEAAm) swells to a lesser extent. This behavior may be attributed to the fact poly(N, N-DEAAm) which lacks the amide proton can hydrogen bond at C=O position only. Poly(NnPAAm) shows the lowest transition temperature, which is due to the fact that it is linear in structure, hence more hydrophobic. By reversing the position of the amide

groups as in the case of poly(NVIBAAm) we notice that the demixing temperature is near 43°C and the transition is more discontinuous. Despite the similarities in the poly(N-propylacrylamide), the transition behavior of poly(NcPAAm) is more continuous showing a demixing temperature of ~ 45°C. The closed structure of the propyl group has less accessibility to the solvent molecules, thus making poly(NcPAAm) more hydrophilic.

Figure 7.2 shows the variation in the dimensionless thickness of poly(NnPAAm), over a range of salt concentration (0-2.0M) for Na₂SO₄, NaCl, NaBr and NaI, all carried out at 1°C (Figure 7.2a) and 7°C (Figure 7.2b). The dimensionless thickness is defined as $(H-H_{collapsed})/(H_{swollen}-H_{collapsed})$, where H is the thickness at the respective salt concentration, $H_{swollen}$ is the thickness in water at 1°C and 7°C and $H_{collapsed}$ is the thickness at 35°C. Figure 7.2 (a and b) shows the effect of ions on the swelling behavior of poly(NnPAAm). At both the temperature, the deswelling isotherms overlap in Na₂SO₄, NaCl and NaBr, with a slight deviation in the case of NaBr at 7°C. With respect to NaI, there is a considerable deviation in the deswelling isotherms, with the deviation being more prominent at 7°C. We notice that NaBr has a slight salting-in effect, whereas the salt-in is more pronounced in the case of NaI.



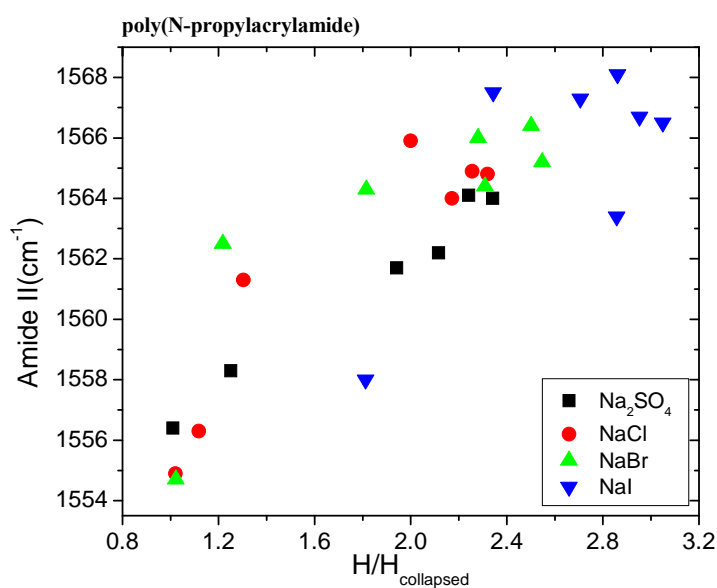
(a)



(b)

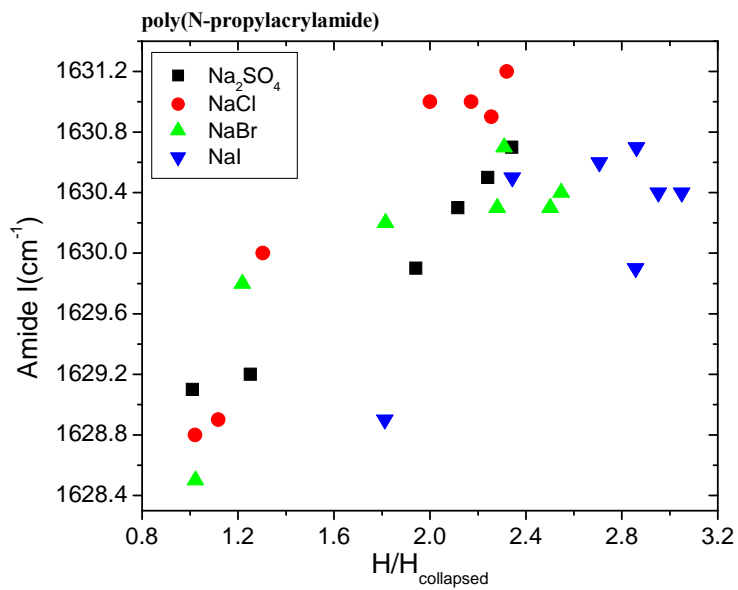
Figure 7.2 (a, b) Variation in thickness of poly(NnPAAm) at 1°C and 7°C in between 0-2.0M salt concentration.

For further understanding the influence of ions on the amide and aliphatic groups, we used ATR-FTIR to study the behavior of these species. Figure 7.3 shows the frequency of amide I (C=O bond) (Figure 7.3b), amide II (N-H bond) (Figure 7.3a) and CH stretch (Figure 7.3c) versus the degree of swelling in Na₂SO₄, NaCl, NaBr and NaI at 7°C. We observe that the frequencies of Na₂SO₄, NaCl, and NaBr overlap, with the exception of NaI, which correlates with the salting-in effect as measured with ellipsometry.

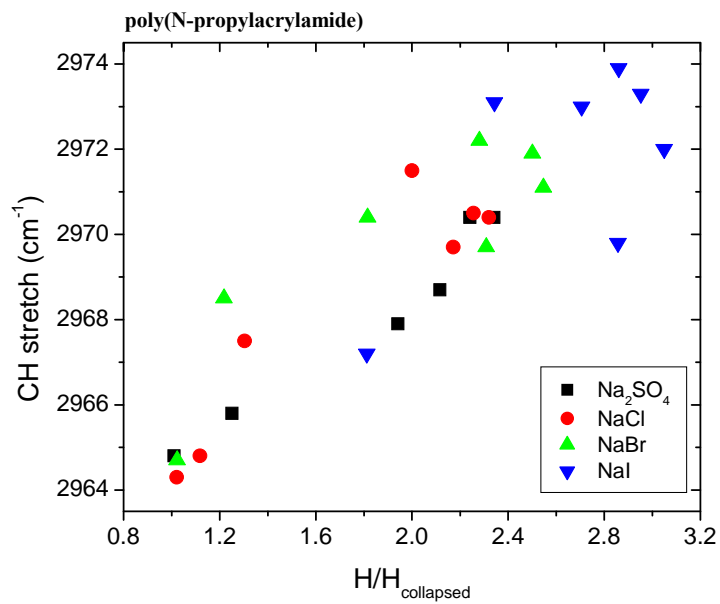


(a)

Figure 7.3 (a, b and c) Frequency shift of Amide I, Amide II and CH stretch as a function of degree of swelling.



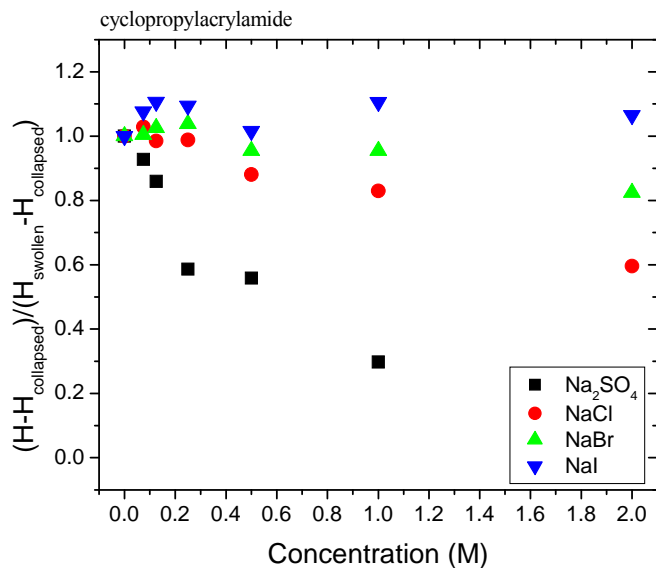
(b)



(c)

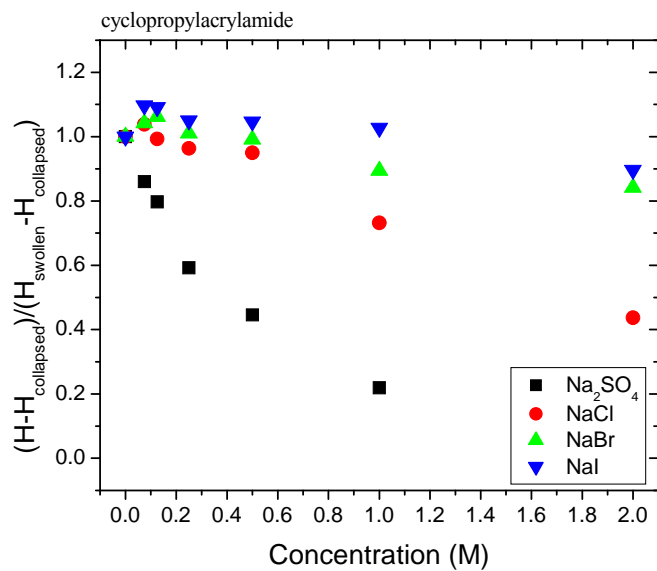
Figure 7.3 Contd.

Figure 7.4 shows the swelling behavior of poly(NcPAAm) in presence of the salts carried out at 15 (Figure 7.4a), 24 (Figure 7.4b) and 40°C (Figure 7.4c). Herein, we notice that with the exception of Na₂SO₄, the remaining salts exhibit a salt-in effect. As the temperature increases there is an increase in the salting-in effect of NaBr and NaI. We observe that even at a temperature of 40°C, a concentration of 2.0M NaBr and NaI is not enough to collapse the polymer network. This indicates that NaI shows the highest binding effect, followed by NaBr. At 15 and 24°C, we see a slight binding in the case of NaCl.

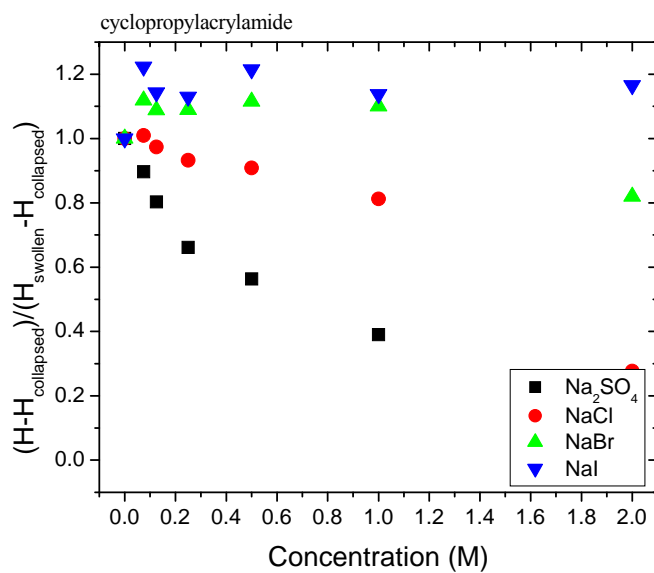


(a)

Figure 7.4 (a,b and c) Change in the non-dimensionless thickness of poly(NcPAAm) at 15, 24 and 40°C.



(b)

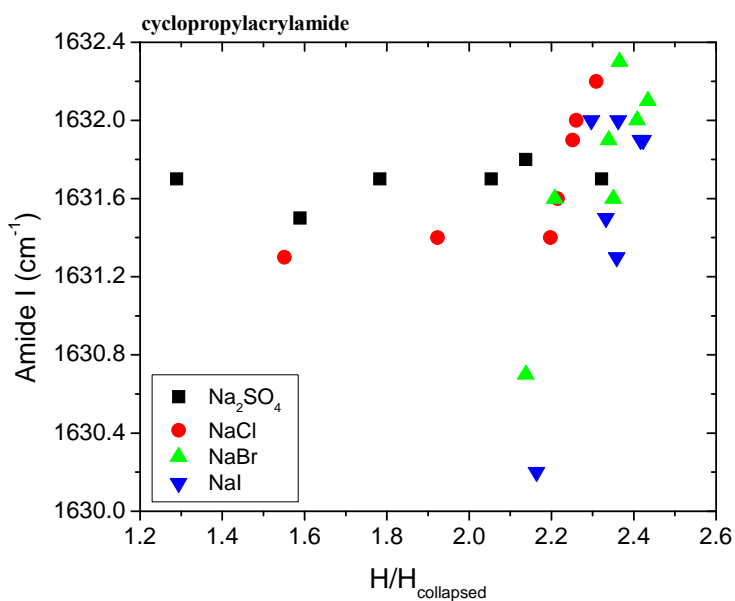


(c)

Figure 7.4 Contd.

Further investigation with ATR-FTIR showed the frequency of vibrations in the amide I and amide II band of poly(NcPAAm) at 24°C. Figure 7.5a and Figure 7.5b shows

the frequency of amide I and amide II versus degree of swelling in Na₂SO₄, NaCl, NaBr and NaI at 24°C. We notice a similar trend in the frequencies of amide band. In both the scenarios the frequencies do not overlap and trend follows the Hofmesiter series. Comparing the frequency shift of amide I and amide II, we observe that at a degree of swelling of 2.2, a frequency of 5 cm⁻¹ amide II separates NaI and Na₂SO₄. In case of amide I, at the same swelling degree of 2.2, a frequency shift of 2 cm⁻¹ separates NaI and Na₂SO₄. A greater difference in the frequencies of vibrations implies that the ions are more accessible to amide II group.



(a)

Figure 7.5 (a, b) Vibration in Amide I and Amide II of poly(NcPAAm) at 24°C from 0-2.0M salt concentrations.

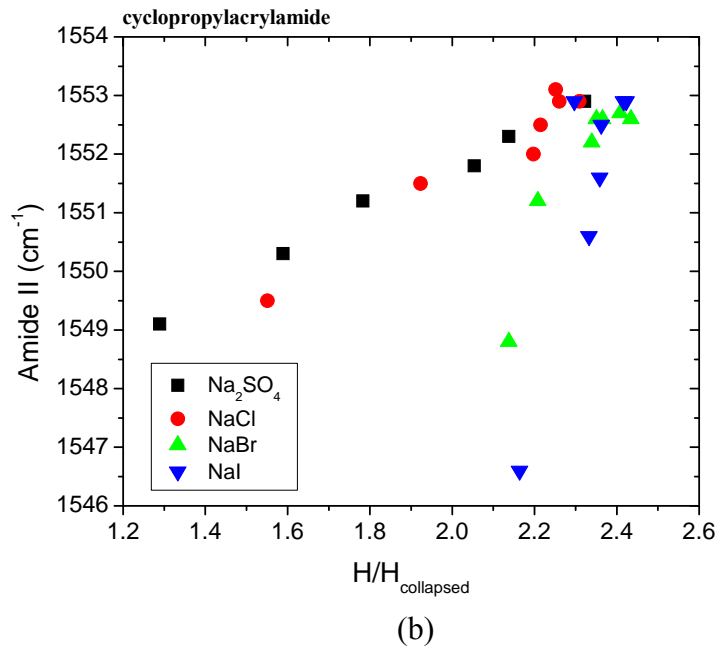
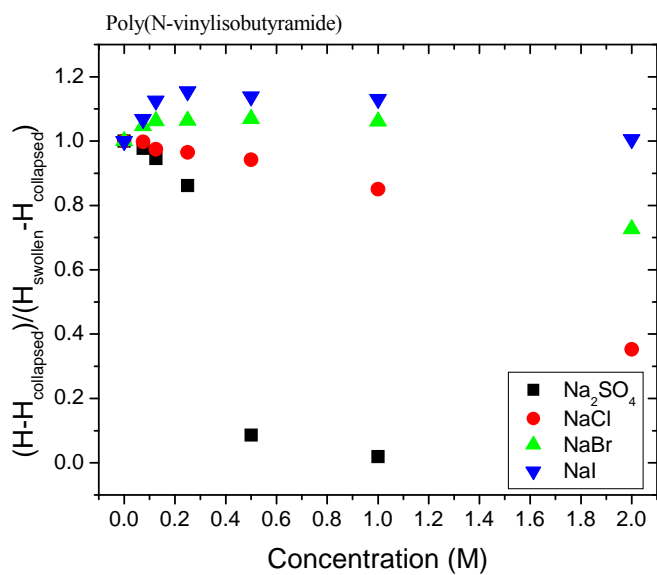
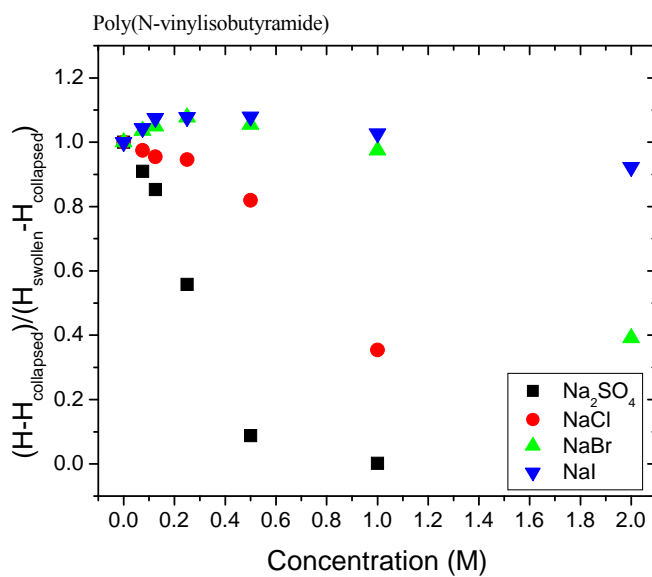


Figure 7.5 Contd.

Figure 7.6 shows the variation in thickness for poly(NVIBAm) at 25, 36 and 43°C. In poly(NVIBAm) the position of amide groups are reversely placed to that of poly(NIPAAm); that is the NH group is now attached to the backbone and C=O is attached to the side chain. Comparing the deswelling behavior at the three temperatures we notice that NaBr and NaI shows a salt-in behavior, with NaI showing a more salting-in effect at 43°C. This may be to the fact that at high temperature there is less hydrogen bonding which might be causing the NaI to bind with the polymer network. A 2.0M concentration of NaI does not drive the collapse of the network.

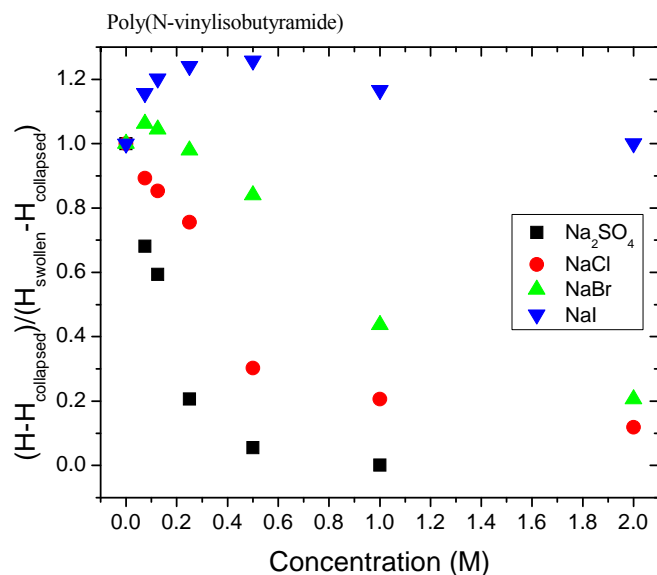


(a)



(b)

Figure 7.6 (a,b and c) Variation in thickness for poly(NVIBAm) at 25, 36 and 43°C.



(c)

Figure 7.6 Contd

Figure 7.7 shows the frequency shift in amide I (Figure 7.7a) and amide II (Figure 7.7b) versus the degree of swelling at 25°C. Here, the frequency of amide I increase in the case of Na₂SO₄, NaCl and NaBr and show a decrease for NaI. The frequency trend for amide II shows a decrease in the vibration frequency for all the salts and overlap with each other; hence the vibrations depend only on the degree of swelling.

Considering the individual shift in the amide bands for each polymer in the presence of salts, we notice that poly(NcPAAm) and poly(NVIBAm) shows a strong dependency on the ions. The average shift in the frequencies of vibration for amide II in poly(NnPAAm) is about $\sim 9 \text{ cm}^{-1}$, followed by $\sim 5 \text{ cm}^{-1}$ for poly(NIPAAm), 4 cm^{-1} for poly(NcPAAm) and $\sim 2 \text{ cm}^{-1}$ for poly(NVIBAm). For amide I the average shifts is as follows; $\sim 2 \text{ cm}^{-1}$ for poly(NnPAAm), $\sim 2 \text{ cm}^{-1}$ for poly(NIPAAm), $\sim 1 \text{ cm}^{-1}$ for poly(NcPAAm) and $\sim 2 \text{ cm}^{-1}$ for poly(NVIBAm). By comparing the shifts in amide I and amide II, it can be inferred that the amide II is more perturbed by the presence of ions, than amide I.

From the above mentioned data, it is evident that poly(NnPAAm) has a higher degree of frequency of vibration as compared to other polymers. Comparing amide I with amide II for the same polymer, it is seen that amide II has a higher frequency of vibration. As the frequency of vibration for amide II increases, it provides a negligible interaction of anions, whereas amide I having a lesser shift provides enough time for the anions to interact with them. Thus, greater shift implies a greater frequency of vibration and tends to give a tighter packing of polymer network.

By comparing the salts, we notice that NaI shows a more binding effect whereas Na_2SO_4 has a more salting-out effect. The size of I^- is larger than SO_4^{2-} . The larger the size of anion, the lesser is the binding of water molecules with it thus producing a lesser charge density. This lesser charge density of anions while interacting with the polymer network produces a higher osmotic pressure surrounding it and this in turn help the anions to be pushed towards the polymer network. On the contrast, small anions like SO_4^{2-} bind the water molecules strongly and coordinate them radially, giving rise to high

charge density of anions. This strong radial coordination of water molecules around the anion prohibits the interaction with the polymer network.

7.3 Conclusion

In this work, we have shown the deswelling of different N-alkylacrylamides when triggered by temperature and perturbed by the salts of Hofmeister series. The different structures of the hydrophobic and amide groups determine the swelling behavior: poly(NcPAAm) > poly(NIPAAm) > poly(NnPAAm). Comparing poly(NVIBAm) and poly(NIPAAm), we notice that the reversal of the amide groups causes a difference in the degree of swelling: poly(NVIBAm) > poly(NIPAAm). By perturbing the polymers with salts we show that the binding of ion is modulated by the size of hydrophobic group connected to the amide. Though dissolution by Na₂SO₄ is independent of polymer structure, dissolution by NaCl, NaBr and NaI depends on the structure of the polymer.

CHAPTER 8: SWELLING BEHAVIOR OF BILAYER AND THIN FILMS

8.1 Introduction

Self assembled layered polymer films are novel materials that are obtained by sequential adsorption of polymers of two or more types on solid substrate. First introduced by Decher and coworkers this technique is now recognized in diverse applications, such as biosensors, drug delivery systems and light emitting diodes.¹⁹⁵ The design of thin films with precise control of their structures and properties for targeted biomedical applications has become important as studies are being done to understand the influence of surface or film properties on cellular functions such as adhesion, proliferation, differentiation and so forth.

Multilayered films of thermoresponsive poly(N-isopropylacrylamide), poly(NIPAAm) polymers have shown the uptake and release of active ingredients within the films. Caruso and coworkers have shown that a dye, Rhodamine B could be reversible loaded or released from within or from the multilayer films containing poly(NIPAAm) by simply tuning the solution temperature.¹⁹⁶ Zhao et al reported that the decrease in cloud point of two different polymers chains was significant than that between polymer chains of the same kind. They attributed this behavior to the formation of interpolymer complex via intermolecular forces.¹⁹⁷

Among many techniques to fabricate functional polymer thin films, the layer-by-layer (LbL) method is one of the most simplest and versatile method to prepare multilayer thin films. LbL method utilizes the Coulombic forces between oppositely charged species to control step-wise deposition of molecular scale layers. Whereas most reports use the LbL to construct multilayers, interest is growing in other areas to fabricate multilayers as a result of the limited stability of multilayers towards water, pH and competing ions.¹⁹⁸ An alternative approach to the assembly of thin films can include the deposition of photoreactive polymers on nearly any substrate.

Multilayered films of photoreactive polymers deposited on a substrate permit a stable, covalent attachment between the layers, control over thickness of each layer and preservation of the properties of individual polymers. In this work, we have synthesized and fabricated multiayers from photo-cross-linkable copolymers of N-alkylacrylamides.

8.2 Results and Discussion

The polymer films were fabricated from photo-cross-linkable copolymers comprising of benzophenone pendant monomers. Film formation, cross-linking and surface-attachement was achieved by spin coating followed by UV irradiation. Ultraviolet radiations ($\lambda=350\text{nm}$) trigger the $n\pi^*$ transitions in the benzophenone moieties leading to a biradicaloid triplet state that abstracts a hydrogen from the neighboring aliphatic C-H group, forming a stable C-C bond. The construction of multilayer was achieved by sequential deposition and irradiation of the respective polymer network. The swollen profiles and vibration of the amide bands of these polymer networks were measured by ellipsometry and ATR-FTIR respectively. Experiments were done on bilayer of the respective polymer and on the solution mixture of these polymers.

Figure 8.1 compares the swelling ratio of each network in a single layer configuration to that of a bilayer comprising of these polymer network. Exposure of a single layer of poly(NIPAAm)-co-MaBP (3%) at 15°C produced a swell ratio of 2.8 and the demixing temperature was observed to be ~28°C. The swell ratio is defined as the swollen thickness divided by the dry thickness. Single layer of poly(NVIBAm)-co-MaBP measured a dry thickness of 84nm and had a swell ratio of 3.6. The demixing temperature in this case was found to be ~43°C.

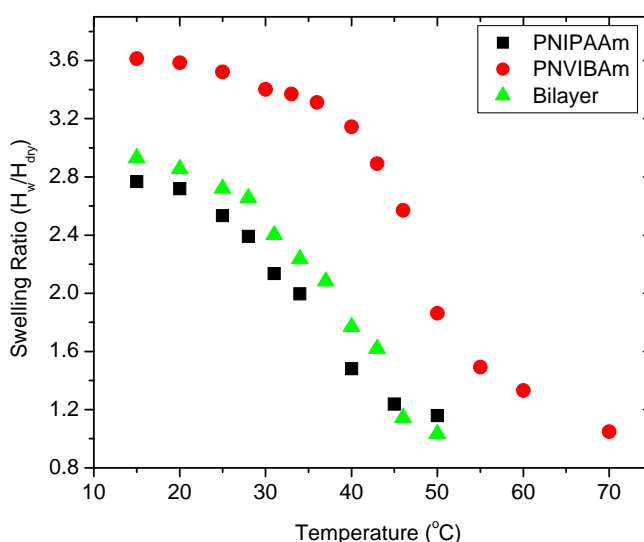


Figure 8.1 Comparison of swelling ratio of each polymer network.

In case of bilayers, poly(NIPAAm)-co-MaBP (3%) was deposited first on the substrate and then poly(NVIBAm)-co-MaBP on top of it. The dry thickness of each network was calculated to be 83nm and 76 nm respectively. These combinations of network layers when exposed to water produced an overall swelling ratio of 2.9 and a transition temperature of ~30°C. A 70% increase in swelling occurred in a two layer

model as compared to 67% and 80% increase in case of single layer model. We do not see a distinct change in the transition behavior. The thickness of the layers being too small and the similar trend in the transition behavior of poly(NIPAAm) and poly(NVIBAm) might be causing an almost continuous transition.

Figure 8.2 shows swelling change of a single layer of network as opposed to a mixture of those polymers. As described above, single layer of, poly(NIPAAm)-co-MaBP (3%) and poly(NVIBAm)-co-MaBP (3%) when exposed to water increased its thickness 2.8 and 3.6 times respectively to its dry thickness measurement. A mixture of these polymers when exposed to water produces a swelling ratio and the transition temperature of 3.8 and $\sim 43^{\circ}\text{C}$ respectively. This is calculated to be 70% increase in swelling as compared to its original thickness

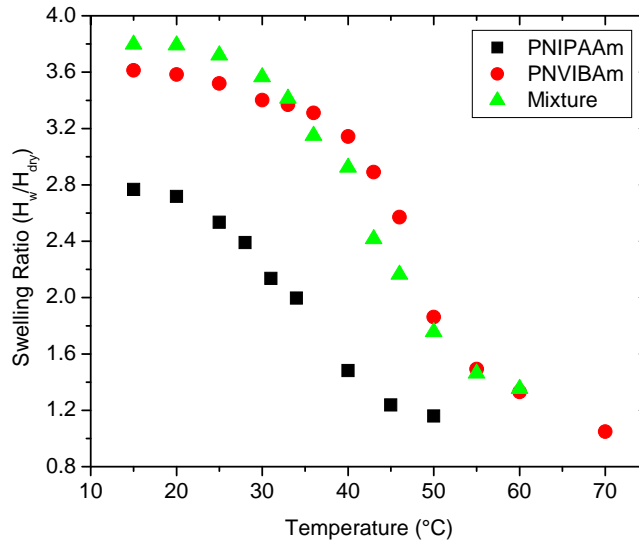


Figure 8.2 Change of swelling ratio of a single layer of network as opposed to mixture.

Figure 8.3 compares the swelling ratio of bilayers and mixture of poly(NIPAAm) and poly(NVIBAm). We observe an increment of 31% in the swelling ratio of mixture of polymers compared to its bilayers. The crosslinking within the network and in between the layers may be causing in a less degree of swelling.

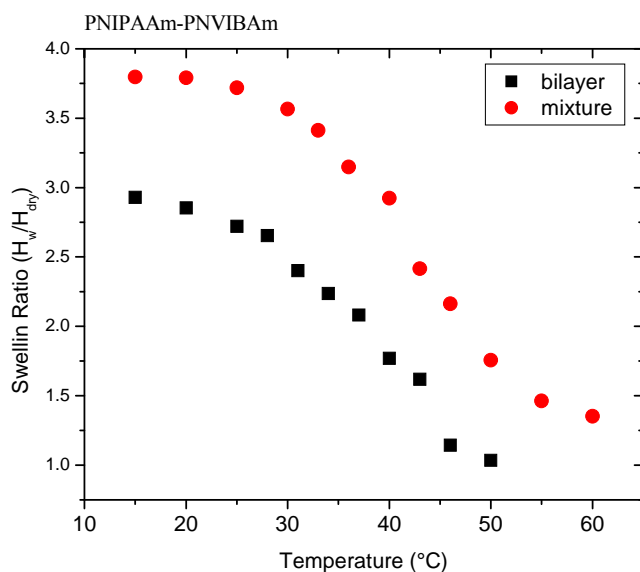


Figure 8.3: Swelling ratio of bilayers and mixture of poly(NIPAAm).

We employed ATR-FTIR to compare the vibrations of poly(NIPAAm), poly(NVIBAm) and a 50/50 mixture of both the polymers. Figure 8.4 shows the position of amide I and amide II of the polymer networks in dry state. The amide I band in poly(NIPAAm), poly(NVIBAm) and their mixture consisted of a major peak at 1625 cm^{-1} , 1646 cm^{-1} and 1644 cm^{-1} respectively. The amide II band consisted of a major peak at 1553 cm^{-1} for poly(NIPAAm), 1538 cm^{-1} for poly(NVIBAm) and 1535 cm^{-1} for the mixture. This suggests that the natural humidity is sufficient to hydrate the poly(NVIBAm) more than poly(NIPAAm).

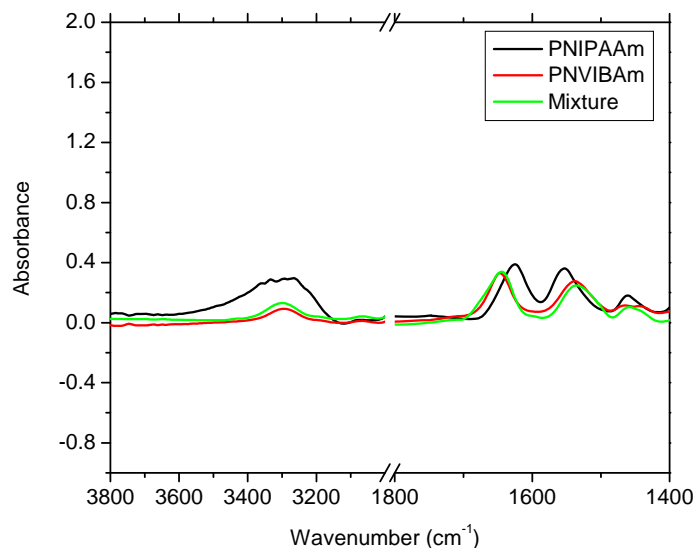


Figure 8.4 Position of Amide I and Amide II of the polymer networks in dry state.

Exposure of the polymer mixture to 15 and 60°C showed the spectral intensity of amide I and amide band. At 15°C the amide I showed a peak at 1630 cm^{-1} and amide II at 1567 cm^{-1} . Further increase of temperature to 60°C, shifted the amide I peak to 1632 cm^{-1} and amide II to 1545 cm^{-1} . The shift in amide II by 22 cm^{-1} indicates that natural humidity is sufficient to dehydrate the amide groups. The spectrum for both the temperature is shown in Figure 8.5. At high temperature CH peaks emerges, which is attributed to the loss of water molecules around the aliphatic groups resulting in hydrophobic interaction.

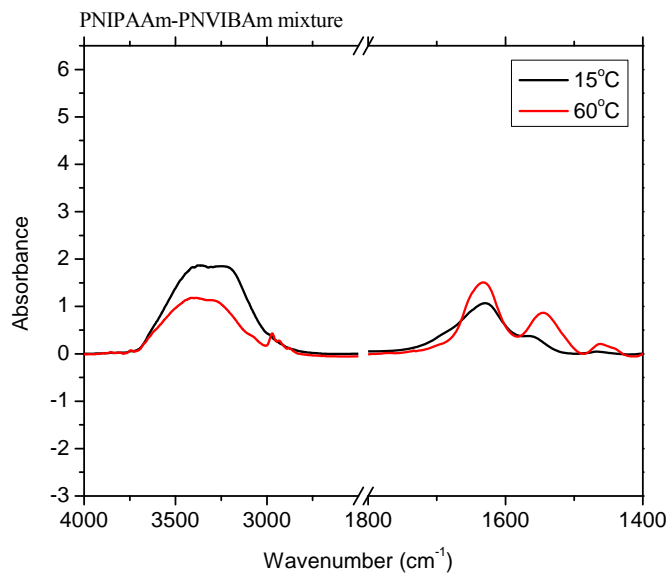


Figure 8.5 Polymer spectrums at 15°C and 60°C.

As the layers comprising of poly(NIPAAm) and poly(NVIBAm) did not show a significant change, we thought of fabricating a bilayer made up of a more hydrophobic polymer such as poly(N-n-propylacrylamide), poly(NnPAAm) and a hydrophilic polymer such as poly(NVIBAm). Figure 8.6 shows the ellipsometry measurements of these coatings.

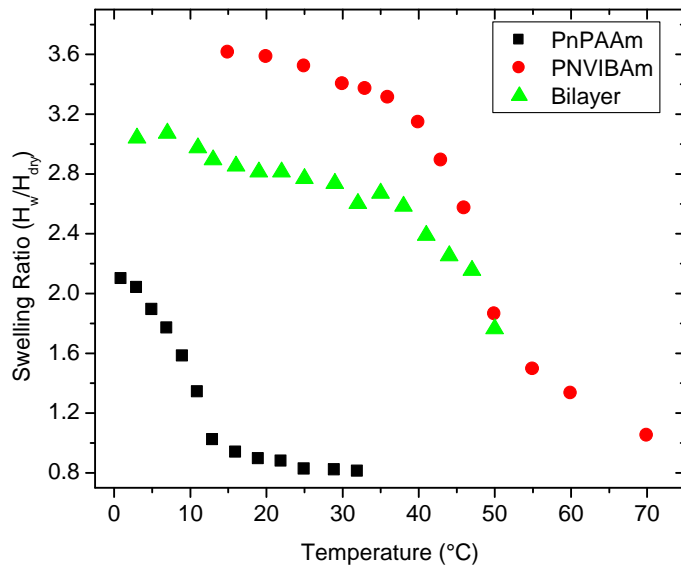


Figure 8.6 Ellipsometry measurements of different layers.

The bilayer shows a two step transition. The dry thickness of the layers is ~ 65 nm. We see the first transition near 12°C and the other near 40°C . The discontinuity in the transition is not so distinct. This ambiguity is due to fact that the layers are not so thick (Figure 8.6).

8.3 Conclusion and Future Work

A bilayer made up of poly(NIPAAm) and poly(NViBAm) shows a similar trend in the transition behavior as a single layer; whereas a bilayer made up of a more hydrophobic, poly(NnPAAm) and hydrophilic poly(NViBAm) exhibits a small discontinuity in the transition at two different temperatures. This might be due to the fact that the films are not thick enough. For future experiments, it is proposed to fabricate films with thicker coatings to have a better understanding on the swelling degree of these layers and the interactions in between them.

REFERENCES

1. Andrade, J. P., *Surface and Interfacial Aspects of Biomedical Polymers*. Plenum Press, New York, 1985.
2. J. Ruhe, V. N., T. Clarke, G. B. Street, *J. Tribol. Trans. ASME* 1996, 118.
3. L. F. Thompson, C. G. W., M. J. Bowden, *Introduction to microlithography*. 2nd Ed. ed.; American Chemical Society: Washington DC, 1994.
4. Tirrell, M.; Kokkoli, E.; Biesalski, M., The role of surface science in bioengineered materials. *Surf. Sci.* 2002, 500, (1-3), 61-83.
5. A. Ulman, *An Introduction to Ultrathin Organic Films*. Academic Press: New York, 1991.
6. Bigelow, W. C., *J. Colloid Interface Sci* 1946, 1.
7. Nuzzo, R. G.; Allara, D. L., Adsorption of bifunctional organic disulfides on gold surfaces. *J. Am. Chem. Soc.* 1983, 105, (13), 4481-3.
8. Finklea, H. O.; Robinson, L. R.; Blackburn, A.; Richter, B.; Allara, D.; Bright, T., Formation of an organized monolayer by solution adsorption of octadecyltrichlorosilane on gold: electrochemical properties and structural characterization. *Langmuir* 1986, 2, (2), 239-44.
9. Netzer, L.; Iscovici, R.; Sagiv, J., Adsorbed monolayers versus Langmuir-Blodgett monolayers - why and how? II. Characterization of built-up films constructed by stepwise adsorption of individual monolayers. *Thin Solid Films* 1983, 100, (1), 67-76.

10. Sagiv, J., Organized monolayers by adsorption. 1. Formation and structure of oleophobic mixed monolayers on solid surfaces. *J. Am. Chem. Soc.* 1980, 102, (1), 92-8.
11. Tillman, N.; Ulman, A.; Penner, T. L., Formation of multilayers by self-assembly. *Langmuir* 1989, 5, (1), 101-11.
12. Chidsey, C. E. D.; Liu, G. Y.; Rowntree, P.; Scoles, G., Molecular order at the surface of an organic monolayer studied by low energy helium diffraction. *J. Chem. Phys.* 1989, 91, (7), 4421-3.
13. Whitesides, G. M.; Laibinis, P. E., Wet chemical approaches to the characterization of organic surfaces: self-assembled monolayers, wetting, and the physical-organic chemistry of the solid-liquid interface. *Langmuir* 1990, 6, (1), 87-96.
14. Ulman, A., *J. Mat. Ed* 1989, 11.
15. Blackman, L. C. F.; Dewar, M. J. S.; Hampson, H., Compounds promoting the dropwise condensation of steam. *J. Appl. Chem.* 1957, 7, 160-71.
16. Stewart, K. R. W., G.M; Godfried, H.P; Silvera, I.F, *Surf. Sci.* 1986, 57.
17. Troughton, E. B.; Bain, C. D.; Whitesides, G. M.; Nuzzo, R. G.; Allara, D. L.; Porter, M. D., Monolayer films prepared by the spontaneous self-assembly of symmetrical and unsymmetrical dialkyl sulfides from solution onto gold substrates: structure, properties, and reactivity of constituent functional groups. *Langmuir* 1988, 4, (2), 365-85.
18. Nuzzo, R. G.; Fusco, F. A.; Allara, D. L., Spontaneously organized molecular assemblies. 3. Preparation and properties of solution adsorbed monolayers of organic disulfides on gold surfaces. *J. Am. Chem. Soc.* 1987, 109, (8), 2358-68.
19. Allara, D. L.; Nuzzo, R. G., Spontaneously organized molecular assemblies. 2. Quantitative infrared spectroscopic determination of equilibrium structures of solution-adsorbed n-alkanoic acids on an oxidized aluminum surface. *Langmuir* 1985, 1, (1), 52-66.

20. Ogawa, H.; Chihara, T.; Taya, K., Selective monomethyl esterification of dicarboxylic acids by use of monocarboxylate chemisorption on alumina. *J. Am. Chem. Soc.* 1985, 107, (5), 1365-9.
21. Schlotter, N. E.; Porter, M. D.; Bright, T. B.; Allara, D. L., Formation and structure of a spontaneously adsorbed monolayer of arachidic acid on silver. *Chem. Phys. Lett.* 1986, 132, (1), 93-8.
22. Chaudhury, M. K.; Whitesides, G. M., Direct measurement of interfacial interactions between semispherical lenses and flat sheets of poly(dimethylsiloxane) and their chemical derivatives. *Langmuir* 1991, 7, (5), 1013-25.
23. Chaudhury, M. K.; Whitesides, G. M., Correlation between surface free energy and surface constitution. *Science (Washington, D. C., 1883-)* 1992, 255, (5049), 1230-2.
24. Ferguson, G. S.; Chaudhury, M. K.; Biebuyck, H. A.; Whitesides, G. M., Monolayers on disordered substrates: self-assembly of alkyltrichlorosilanes on surface-modified polyethylene and poly(dimethylsiloxane). *Macromolecules* 1993, 26, (22), 5870-5.
25. Ulman, A., Formation and Structure of Self-Assembled Monolayers. *Chem. Rev. (Washington, D. C.)* 1996, 96, (4), 1533-1554.
26. Degennes, P. G., Conformations of polymers attached to an interface. *Macromolecules* 1980, 13, (5), 1069-1075.
27. Minko, S., Responsive polymer brushes. *Polym. Rev. (Philadelphia, PA, U. S.)* 2006, 46, (4), 397-420.
28. Halperin, A.; Tirrell, M.; Lodge, T. P., Tethered chains in polymer microstructures. *Advances in Polymer Science* 1992, 100, 31-71.
29. Milner, S. T., Polymer brushes. *Science* 1991, 251, (4996), 905-914.
30. Szleifer, I.; Carignano, M. A., Tethered polymer layers. *Advances in Chemical Physics, Vol Xciv* 1996, 94, 165-260.

31. Amiji, M.; Park, K., Surface modification of polymeric biomaterials with poly(ethylene oxide), albumin, and heparin for reduced thrombogenicity. *J. Biomater. Sci., Polym. Ed.* 1993, 4, (3), 217-34.
32. Halperin, A.; Tirrell, M.; Lodge, T. P., Tethered chains in polymer microstructures. *Adv. Polym. Sci.* 1992, 100, (Macromol.: Synth., Order Adv. Prop.), 31-71.
33. Joanny, J. F., Lubrication by molten polymer brushes. *Langmuir* 1992, 8, (3), 989-95.
34. Tadros, T., *The Effect of Polymers on Dispersion Properties*. Academic Press: London, 1982.
35. He, Q.; Kueller, A.; Grunze, M.; Li, J., Fabrication of Thermosensitive Polymer Nanopatterns through Chemical Lithography and Atom Transfer Radical Polymerization. *Langmuir* 2007, 23, (7), 3981-3987.
36. Raula, J.; Shan, J.; Nuopponen, M.; Niskanen, A.; Jiang, H.; Kauppinen, E. I.; Tenhu, H., Synthesis of Gold Nanoparticles Grafted with a Thermoresponsive Polymer by Surface-Induced Reversible-Addition-Fragmentation Chain-Transfer Polymerization. *Langmuir* 2003, 19, (8), 3499-3504.
37. Wei, Q. S., Ji, J.; Shen, J. C., *Macromolecular Rapid Communications* 2008, 29, 645-650.
38. Toomey, R.; Freidank, D.; Ruhe, J., Swelling behavior of thin, surface-attached polymer networks. *Macromolecules* 2004, 37, (3), 882-887.
39. Harmon, M. E.; Jakob, T. A. M.; Knoll, W.; Frank, C. W., A surface plasmon resonance study of volume phase transitions in N-isopropylacrylamide gel films. *Macromolecules* 2002, 35, (15), 5999-6004.
40. Beines, P. W.; Klosterkamp, I.; Menges, B.; Jonas, U.; Knoll, W., Responsive thin hydrogel layers from photo-cross-linkable poly(N-isopropylacrylamide) terpolymers. *Langmuir* 2007, 23, (4), 2231-2238.

41. Kuckling, D.; Harmon, M. E.; Frank, C. W., Photo-cross-linkable PNIPAAm copolymers. 1. Synthesis and characterization of constrained temperature-responsive hydrogel layers. *Macromolecules* 2002, 35, (16), 6377-6383.
42. Millaruelo, M.; Eichhorn, K. J.; Sieczkowska, B.; Voit, B., Photolabile carboxylic acid protected terpolymers for surface patterning. Part 1: Polymer synthesis and film characterization. *Langmuir* 2006, 22, (22), 9436-9445.
43. Revzin, A.; Russell, R. J.; Yadavalli, V. K.; Koh, W. G.; Deister, C.; Hile, D. D.; Mellott, M. B.; Pishko, M. V., Fabrication of poly(ethylene glycol) hydrogel microstructures using photolithography. *Langmuir* 2001, 17, (18), 5440-5447.
44. Zhang, Q.; Archer, L. A., Interfacial friction and adhesion of cross-linked polymer thin films swollen with linear chains. *Langmuir* 2007, 23, (14), 7562-7570.
45. Harmon, M. E.; Kuckling, D.; Frank, C. W., Photo-cross-linkable PNIPAAm copolymers. 2. Effects of constraint on temperature and pH-responsive hydrogel layers. *Macromolecules* 2003, 36, (1), 162-172.
46. Harmon, M. E.; Kuckling, D.; Pareek, P.; Frank, C. W., Photo-cross-linkable PNIPAAm copolymers. 4. Effects of copolymerization and cross-linking on the volume-phase transition in constrained hydrogel layers. *Langmuir* 2003, 19, (26), 10947-10956.
47. Flory, P. J., Statistical mechanics of swelling of network structures. *J. Chem. Phys.* 1950, 18, 108-11.
48. Flory, P. J.; Rehner, J., Jr., Statistical mechanics of cross-linked polymer networks. II. Swelling. *J. Chem. Phys.* 1943, 11, 521-6.
49. Tanaka, T., Collapse of gels and critical endpoint. *Phys. Rev Lett* 1978, 40.
50. Katsumoto, Y.; Tanaka, T.; Sato, H.; Ozaki, Y., Conformational change of poly(N-isopropylacrylamide) during the coil-globule transition investigated by attenuated total reflection/infrared spectroscopy and density functional theory calculation. *Journal of Physical Chemistry A* 2002, 106, (14), 3429-3435.

51. Meersman, F.; Wang, J.; Wu, Y. Q.; Heremans, K., Pressure effect on the hydration properties of poly(N-isopropylacrylamide) in aqueous solution studied by FTIR spectroscopy. *Macromolecules* 2005, 38, (21), 8923-8928.
52. Y.Maeda, Changes in the Hydration States of Poly(N-alkylacrylamide)s during Their Phase Transitions in Water Observed by FTIR Spectroscopy[†]. *Macromolecules* 2001, 34.
53. Favier, A.; Ladaviere, C.; Charreyre, M. T.; Pichot, C., MALDI-TOF MS investigation of the RAFT polymerization of a water-soluble acrylamide derivative. *Macromolecules* 2004, 37, (6), 2026-2034.
54. Ilmain, F.; Tanaka, T.; Kokufuta, E., Volume transition in a gel driven by hydrogen bonding. *Nature* 1991, 349, (6308), 400-401.
55. Inomata, H.; Goto, S.; Saito, S.,Phase transition of N-substituted acrylamide gels. *Macromolecules* 1990, 23, (22), 4887-4888.
56. K. Otake, Thermal Analysis of the Volume Phase Transition with N-Isopropylacrylamide Gels *Macromolecules* 1989, 23.
57. Ito, D.; Kubota, K., Solution properties and thermal behavior of Poly(N-n-propylacrylamide) in water. *Macromolecules* 1997, 30, (25), 7828-7834.
58. Inomata, H.; Saito, S.,Studies on volume phase transition of N-substituted acrylamide hydrogels. *Fluid Phase Equilibria* 1993, 82, 291-302.
59. F.Seker, Correlation of Chemical Structure and Swelling Behavior in N-alkylacrylamide Hydrogels. *J.of Polymer Science:Part A:Polymer Chemistry* 1998, 36.
60. Ulbrich, K.; Kopecek, J.,Cross-linked co-polymers of N,N-diethylacrylamide with improved mechanical properties. *Journal of Polymer Science Part C-Polymer Symposium* 1979, (66), 209-219.

61. Harmon, M. E.; Kuckling, D.; Frank, C. W., Photo-cross-linkable PNIPAAm copolymers. 5. Mechanical properties of hydrogel layers. *Langmuir* 2003, 19, (26), 10660-10665.
62. M.Heskins, Solution properties of Poly(N-isopropylacrylamide) *J.of Macromol.Sci* 1968, 2.
63. Guenther, M.; Kuckling, D.; Corten, C.; Gerlach, G.; Sorber, J.; Suchanek, G.; Arndt, K. F., Chemical sensors based on multiresponsive block copolymer hydrogels. *Sens. Actuators, B* 2007, B126, (1), 97-106.
64. Gupta, S.; Kuckling, D.; Kretschmer, K.; Choudhary, V.; Adler, H.-J., Synthesis and characterization of stimuli-sensitive micro- and nanohydrogels based on photocrosslinkable poly(dimethylaminoethyl methacrylate). *J. Polym. Sci., Part A: Polym. Chem.* 2007, 45, (4), 669-679.
65. Matsukuma, D.; Yamamoto, K.; Aoyagi, T., Stimuli-Responsive Properties of N-Isopropylacrylamide-Based Ultrathin Hydrogel Films Prepared by Photo-Cross-Linking. *Langmuir* 2006, 22, (13), 5911-5915.
66. Dorman, G.; Prestwich, G. D., Benzophenone Photophores in Biochemistry. *Biochemistry* 1994, 33, (19), 5661-73.
67. Prestwich, G. D.; Dorman, G.; Elliott, J. T.; Marecak, D. M.; Chaudhary, A., Benzophenone photoprobes for phosphoinositides, peptides and drugs. *Photochem. Photobiol.* 1997, 65, (2), 222-234.
68. Ito, S., Phase transition of aqueous solution of poly(N-alkylacrylamide) derivatives. Effects of side chain structure. *Kobunshi Ronbunshu* 1989, 46, 437-43.
69. Brazel, C. S.; Peppas, N. A., Synthesis and Characterization of Thermo- and Chemomechanically Responsive Poly(N-isopropylacrylamide-co-methacrylic acid) Hydrogels. *Macromolecules* 1995, 28, (24), 8016-20.

70. Inomata, H.; Wada, N.; Yagi, Y.; Goto, S.; Saito, S., Swelling behaviors of N-alkylacrylamide gels in water: effects of copolymerization and crosslinking density. *Polymer* 1995, 36, (4), 875-7.
71. Katakai, R.; Yoshida, M.; Hasegawa, S.; Iijima, Y.; Yonezawa, N., Phase Transition of Hydrogels by "Pinpoint-Variation" of Polymer Side Chains. *Macromolecules* 1996, 29, (3), 1065-6.
72. Shibayama, M.; Mizutani, S.-y.; Nomura, S., Thermal Properties of Copolymer Gels Containing N-Isopropylacrylamide. *Macromolecules* 1996, 29, (6), 2019-24.
73. Galaev, I. Y.; Mattiasson, B., Thermoreactive water-soluble polymers, non-ionic surfactants, and hydrogels as reagents in biotechnology. *Enzyme and Microbial Technology* 1993, 15, (5), 354-366.
74. Schild, H. G., Poly(N-isopropylacrylamide)-experiment, theory and application. *Progress in Polymer Science* 1992, 17, (2), 163-249.
75. Ito, D.; Kubota, K., Thermal response of poly(N-n-propylacrylamide). *Polymer Journal* 1999, 31, (3), 254-257.
76. Wada, N.; Kajima, Y.; Yagi, Y.; Inomata, H.; Saito, S., Effect of surfactant on the phase transition of N-alkylacrylamide gels. *Langmuir* 2002, 9, (1), 46-49.
77. Kuramoto, N.; Shishido, Y., Property of thermo-sensitive and redox-active poly(N-cyclopropylacrylamide-co-vinylferrocene) and poly(N-isopropylacrylamide-co-vinylferrocene). *Polymer* 1998, 39, (3), 669-673.
78. Liu, H. Y.; Zhu, X. X., Lower critical solution temperatures of N-substituted acrylamide copolymers in aqueous solutions. *Polymer* 1999, 40, (25), 6985-6990.
79. Panayiotou, M.; Freitag, R., Synthesis and characterisation of stimuli-responsive poly(N,N'-diethylacrylamide) hydrogels. *Polymer* 2005, 46, (3), 615-621.

80. Akashi, M.; Nakano, S.; Kishida, A., Synthesis of poly(N-vinylisobutyramide) from poly(N-vinylacetamide) and its thermosensitive property. *J. Polym. Sci., Part A: Polym. Chem.* 1996, 34, (2), 301-3.
81. Kunugi, S.; Tada, T.; Tanaka, N.; Yamamoto, K.; Akashi, M., Microcalorimetric study of aqueous solution of a thermoresponsive polymer, poly(N-vinylisobutyramide) (PNVIBA). *Polym. J. (Tokyo, Jpn.)* 2002, 34, (5), 383-388.
82. Suwa, K.; Wada, Y.; Kishida, A.; Akashi, M., Synthesis and functionalities of poly(N-vinylalkanamide). VI. A novel thermosensitive hydrogel crosslinked poly(N-vinylisobutyramide). *J. Polym. Sci., Part A: Polym. Chem.* 1997, 35, (16), 3377-3384.
83. Bohdanecky, M.; Horsky, J.; Petrus, V.; Mrkvickova, L.; Ulbrich, K., Cloud point curves of aqueous solutions of poly(N-ethylmethacrylamide). *Collect. Czech. Chem. Commun.* 1993, 58, (10), 2370-82.
84. Hazot, P.; Chapel, J. P.; Pichot, C.; Elaissari, A.; Delair, T., Preparation of poly(N-ethyl methacrylamide) particles via an emulsion/precipitation process: the role of the crosslinker. *J. Polym. Sci., Part A: Polym. Chem.* 2002, 40, (11), 1808-1817.
85. Upadhyay, N. B.; Sawan, S. P., Aqueous solution properties of poly(N-ethylmethacrylamide). *Polym. Prepr. (Am. Chem. Soc., Div. Polym. Chem.)* 1986, 27, (1), 253-4.
86. Mikheeva, L. M.; Grinberg, N. V.; Mashkevich, A. Y.; Grinberg, V. Y.; Thanh, L. T. M.; Makhaeva, E. E.; Khokhlov, A. R., Microcalorimetric study of thermal cooperative transitions in poly(N-vinylcaprolactam) hydrogels. *Macromolecules* 1997, 30, (9), 2693-2699.
87. Solomon, O. F.; Corciovei, M.; Ciuta, I.; Boghina, C., Properties of solutions of poly(N-vinylcaprolactam). *J. Appl. Polym. Sci.* 1968, 12, (8), 1835-42.
88. Takano, M.; Ogata, K.; Kawauchi, S.; Satoh, M.; Komiyama, J., Ion-specific swelling behavior of poly(N-vinyl-2-pyrrolidone) gel: correlations with water hydrogen bond and non-freezable water. *Polym. Gels Networks* 1998, 6, (3-4), 217-232.

89. Chen, Z. Y.; Qian, S. Z.; Abrams, W. R.; Malamud, D.; Bau, H. H., Thermosiphon-based PCR reactor: Experiment and modeling. *Analytical Chemistry* 2004, 76, (13), 3707-3715.
90. Lagally, E. T.; Scherer, J. R.; Blazej, R. G.; Toriello, N. M.; Diep, B. A.; Ramchandani, M.; Sensabaugh, G. F.; Riley, L. W.; Mathies, R. A., Integrated portable genetic analysis microsystem for pathogen/infectious disease detection. *Analytical Chemistry* 2004, 76, (11), 3162-3170.
91. Zangmeister, R. A.; Tarlov, M. J., DNA displacement assay integrated into microfluidic channels. *Analytical Chemistry* 2004, 76, (13), 3655-3659.
92. Pelton, R., Temperature-sensitive aqueous microgels. *Advances in Colloid and Interface Science* 2000, 85, (1), 1-33.
93. Richter, A.; Howitz, S.; Kuckling, D.; Arndt, K. F., Influence of volume phase transition phenomena on the behavior of hydrogel-based valves. *Sensors and Actuators B-Chemical* 2004, 99, (2-3), 451-458.
94. Richter, A.; Kuckling, D.; Howitz, S.; Gehring, T.; Arndt, K. F., Electronically controllable microvalves based on smart hydrogels: Magnitudes and potential applications. *Journal of Microelectromechanical Systems* 2003, 12, (5), 748-753.
95. Naito, H.; Takewa, Y.; Mizuno, T.; Ohya, S.; Nakayama, Y.; Tatsumi, E.; Kitamura, S.; Takano, H.; Taniguchi, S.; Taenaka, Y., Three-dimensional cardiac tissue engineering using a thermoresponsive artificial extracellular matrix. *Asaio Journal* 2004, 50, (4), 344-348.
96. Ibusuki, S.; Fujii, Y.; Iwamoto, Y.; Matsuda, T., Tissue-engineered cartilage using an injectable and in situ gelable thermoresponsive gelatin: Fabrication and in vitro performance. *Tissue Engineering* 2003, 9, (2), 371-384.
97. Ibusuki, S.; Iwamoto, Y.; Matsuda, T., System-engineered cartilage using poly(N-isopropylacrylamide)-grafted gelatin as in situ-formable scaffold: In vivo performance. *Tissue Engineering* 2003, 9, (6), 1133-1142.

98. Bae, Y. H.; Okano, T.; Kim, S. W., On off thermocontrol of solute transport .1. temperature-dependence of swelling of N-isopropylacrylamide networks modified with hydrophobic components in water. *Pharmaceutical Research* 1991, 8, (4), 531-537.
99. Bae, Y. H.; Okano, T.; Kim, S. W., On off thermocontrol of solute transport.2. solute release from thermosensitive hydrogels. *Pharmaceutical Research* 1991, 8, (5), 624-628.
100. Okano, T.; Bae, Y. H.; Jacobs, H.; Kim, S. W., Thermally on-off switching polymers for drug permeation and release. *Anderson, J. M., S. W. Kim and K. Knutson (Ed.). Advances in Drug Delivery Systems, Vol. 4; International Symposium on Recent Advances in Drug Delivery Systems, Salt Lake City, Utah, USA, February 21-24, 1989. X+359p. Elsevier Science Publishers B.V.: Amsterdam, Netherlands; New York, New York, USA. Illus* 1990, 255-266.
101. Ebara, M.; Yamato, M.; Aoyagi, T.; Kikuchi, A.; Sakai, K.; Okano, T., Temperature-Responsive Cell Culture Surfaces Enable "On-Off" Affinity Control between Cell Integrins and RGDS Ligands. *Biomacromolecules* 2004, 5, (2), 505-510.
102. Kushida, A.; Yamato, M.; Konno, C.; Kikuchi, A.; Sakurai, Y.; Okano, T., Decrease in culture temperature releases monolayer endothelial cell sheets together with deposited fibronectin matrix from temperature-responsive culture surfaces. *J. Biomed. Mater. Res.* 1999, 45, (4), 355-362.
103. Okano, T.; Yamada, N.; Sakai, H.; Sakurai, Y., A novel recovery system for cultured cells using plasma-treated polystyrene dishes grafted with poly(N-isopropylacrylamide). *J. Biomed. Mater. Res.* 1993, 27, (10), 1243-51.
104. Yamada, N.; Okano, T.; Sakai, H.; Karikusa, F.; Sawasaki, Y.; Sakurai, Y., Thermo-responsive polymeric surfaces; control of attachment and detachment of cultured cells. *Makromol. Chem., Rapid Commun.* 1990, 11, (11), 571-6.
105. Auernheimer, J.; Dahmen, C.; Hersel, U.; Bausch, A.; Kessler, H., Photoswitched Cell Adhesion on Surfaces with RGD Peptides. *J. Am. Chem. Soc.* 2005, 127, (46), 16107-16110.

106. Kleinman, H. K.; Philp, D.; Hoffman, M. P., Role of the extracellular matrix in morphogenesis. *Curr. Opin. Biotechnol.* 2003, 14, (5), 526-532.
107. Hoffman, A. S., Applications of thermally reversible polymers and hydrogels in therapeutics and diagnostics. *J. Controlled Release* 1987, 6, 297-305.
108. Von, H. P. H.; Schleich, T., Ion effects on the solution structure of biological macromolecules. *Accounts Chem. Res.* 1969, 2, (9), 257-65.
109. Hofmeister, F., *Arch. Exp. Pathol. Pharmacol* 1888, 24.
110. Voet, A., Quantitative lyotropy. *Chem. Rev.* 1937, 20, 169-79.
111. Kunz, W.; Lo Nostro, P.; Ninham, B. W., The present state of affairs with Hoffmeister effects. *Current Opinion in Colloid & Interface Science* 2004, 9, (1-2), 1-18.
112. Zhang, Y., Interactions between macromolecules and ions: the Hofmeister series. *Current Opinion in Chemical Biology* 2006, 10.
113. Freitag, R., Salt Effects on the Thermoprecipitation of Poly-(N-isopropylacrylamide) Oligomers from Aqueous Solution. *Langmuir* 2002, 18.
114. Jones, G.; Dole, M., The viscosity of aqueous solutions of strong electrolytes with special reference to barium chloride. *Journal of the American Chemical Society* 1929, 51, 2950-2964.
115. Inomata, H.; Goto, S.; Otake, K.; Saito, S., Effect of additives on phase-transition of N-isopropylacrylamide gels. *Langmuir* 1992, 8, (2), 687-690.
116. Park, T. G., Hoffman, A.S, Sodium Chloride-Induced Phase Transition in Nonionic Poly(N-isopropylacrylamide) Gel. *Journal of Applied Polymer Science* 1992, 46, (4).

117. Young, J. K., Salt-Induces Depression of lower Critical Solution Temperature in a Surface-Grafted Neutral Thermoresponsive Polymer. *Macromolecular Rapid Communications* 2006, 27.
118. Gurau, M. C., On the mechanism of the Hofmeister series. *J.of the American Chemical Society* 2004, 126.
119. Omta, A. W., Negligible effect of ions on the hydrogen-bonded structure in liquid water. *Science* 2003, 301, 347.
120. Zhang, Y. J., Specific ion effects on the water solubility of macromolecules: PNIPAM and the Hofmeister series. *Journal of the American Chemical Society*. 2005, 127.
121. Sauerbrey, G., The use of quartz oscillators for weighing thin layers and for microweighing. *Z. Phys.* 1959, 155, 206-22.
122. Voinova, M. V.; Rodahl, M.; Jonson, M.; Kasemo, B., Viscoelastic acoustic response of layered polymer films at fluid-solid interfaces: Continuum mechanics approach. *Physica Scripta* 1999, 59, (5), 391-396.
123. Wisniewski, N.; Reichert, M., Methods for reducing biosensor membrane biofouling. *Colloids and Surfaces B: Biointerfaces* 2000, 18, (3-4), 197-219.
124. Werner, C.; Maitz, M. F.; Sperling, C., Current strategies towards hemocompatible coatings. *Journal of Materials Chemistry* 2007, 17, (32), 3376-3384.
125. Jeong, B.; Gutowska, A., Lessons from nature: stimuli-responsive polymers and their biomedical applications. *Trends in Biotechnology* 2002, 20, (7), 305-311.
126. Qiu, Y.; Park, K., Environment-sensitive hydrogels for drug delivery. *Advanced Drug Delivery Reviews* 2001, 53, (3), 321-339.

127. Huber, D. L.; Manginell, R. P.; Samara, M. A.; Kim, B. I.; Bunker, B. C., Programmed adsorption and release of proteins in a microfluidic device. *Science* 2003, 301, (5631), 352-354.
128. Heskins, M., Solution properties of poly(N-isopropylacrylamide) *J. Macromol. Sci* 1968, 2, 1441-1445.
129. Schild, H. G., *Prog Polym Sci* 1992, 17, 163-249.
130. Onuki, A., Theory of Phase Transitions in Polymer Gels. *Advances in Polymer Science* 1993, 109, 63-121.
131. Gianneli, M.; Roskamp, R. F.; Jonas, U.; Loppinet, B.; Fytas, G.; Knoll, W., Dynamics of swollen gel layers anchored to solid surfaces. *Soft Matter* 2008, 4, (7), 1443-1447.
132. Balamurugan, S.; Mendez, S.; Balamurugan, S. S.; O'Brie, M. J.; Lopez, G. P., Thermal Response of Poly(N-isopropylacrylamide) Brushes Probed by Surface Plasmon Resonance. *Langmuir* 2003, 19, (7), 2545-2549.
133. Habicht, J.; Schmidt, M.; Ruhe, J.; Johannsmann, D., Swelling of Thick Polymer Brushes Investigated with Ellipsometry. *Langmuir* 1999, 15, (7), 2460-2465.
134. Yim, H.; Kent, M. S.; Mendez, S.; Balamurugan, S. S.; Balamurugan, S.; Lopez, G. P.; Satija, S., Temperature-Dependent Conformational Change of PNIPAM Grafted Chains at High Surface Density in Water. *Macromolecules* 2004, 37, (5), 1994-1997.
135. Yim, H.; Kent, M. S.; Satija, S.; Mendez, S.; Balamurugan, S. S.; Balamurugan, S.; Lopez, G. P., Evidence for vertical phase separation in densely grafted, high-molecular-weight poly(N -isopropylacrylamide) brushes in water. *Physical Review E* 2005, 72, (5), 051801.
136. Plunkett, M. A.; Claesson, P. M.; Rutland, M. W., Adsorption of a Cationic Polyelectrolyte followed by Surfactant-Induced Swelling, Studied with a Quartz Crystal Microbalance. *Langmuir* 2002, 18, (4), 1274-1280.

137. Rodahl, M.; Hook, F.; Fredriksson, C.; Keller, C. A.; Krozer, A.; Brzezinski, P.; Voinova, M.; Kasemo, B., Simultaneous frequency and dissipation factor QCM measurements of biomolecular adsorption and cell adhesion. *Faraday Discussions* 1997, 107, 229-246.
138. Annaka, M.; Yahiro, C.; Nagase, K.; Kikuchi, A.; Okano, T., Real-time observation of coil-to-globule transition in thermosensitive poly(N-isopropylacrylamide) brushes by quartz crystal microbalance. *Polymer* 2007, 48, (19), 5713-5720.
139. Hongwei Ma, L. F., Wei Li, Yaozhong Zhang and Mingwu Li, Real-time measurement of the mass of water expelled by poly(N-isopropylacrylamide) brushes upon thermo-induced collapse. *Chem. Commun* 2009, 3428 - 3430.
140. Liu, G.; Zhang, G., Collapse and Swelling of Thermally Sensitive Poly(N-isopropylacrylamide) Brushes Monitored with a Quartz Crystal Microbalance. *The Journal of Physical Chemistry B* 2004, 109, (2), 743-747.
141. Zhang, G., Study on Conformation Change of Thermally Sensitive Linear Grafted Poly(N-isopropylacrylamide) Chains by Quartz Crystal Microbalance. *Macromolecules* 2004, 37, (17), 6553-6557.
142. Ishida, N.; Biggs, S., Direct Observation of the Phase Transition for a Poly(N-isopropylacrylamide) Layer Grafted onto a Solid Surface by AFM and QCM-D. *Langmuir* 2007, 23, (22), 11083-11088.
143. Jhon, Y. K.; Bhat, R. R.; Jeong, C.; Rojas, O. J.; Szleifer, I.; Genzer, J., Salt-induced depression of lower critical solution temperature in a surface-grafted neutral thermoresponsive polymer. *Macromolecular Rapid Communications* 2006, 27, (9), 697-701.
144. Domack, A.; Prucker, O.; Ruhe, J.; Johannsmann, D., Swelling of a polymer brush probed with a quartz crystal resonator. *Physical Review E* 1997, 56, (1), 680-689.
145. Plunkett, M. A.; Wang, Z.; Rutland, M. W.; Johannsmann, D., Adsorption of pNIPAM Layers on Hydrophobic Gold Surfaces, Measured in Situ by QCM and SPR. *Langmuir* 2003, 19, (17), 6837-6844.

146. Fu, L.; Chen, X.; He, J.; Xiong, C.; Ma, H., Study Viscoelasticity of Ultrathin Poly(oligo(ethylene glycol) methacrylate) Brushes by a Quartz Crystal Microbalance with Dissipation. *Langmuir* 2008, 24, (12), 6100-6106.
147. Dutta, A. K.; Belfort, G., Adsorbed Gels versus Brushes: Viscoelastic Differences. *Langmuir* 2007, 23, (6), 3088-3094.
148. Hook, F.; Kasemo, B.; Nylander, T.; Fant, C.; Sott, K.; Elwing, H., Variations in Coupled Water, Viscoelastic Properties, and Film Thickness of a Mefp-1 Protein Film during Adsorption and Cross-Linking: A Quartz Crystal Microbalance with Dissipation Monitoring, Ellipsometry, and Surface Plasmon Resonance Study. *Analytical Chemistry* 2001, 73, (24), 5796-5804.
149. Reimhult, E.; Larsson, C.; Kasemo, B.; Hook, F., Simultaneous Surface Plasmon Resonance and Quartz Crystal Microbalance with Dissipation Monitoring Measurements of Biomolecular Adsorption Events Involving Structural Transformations and Variations in Coupled Water. *Analytical Chemistry* 2004, 76, (24), 7211-7220.
150. De gennes, P. G., *Scaling Concepts in Polymer Physics*. Cornell University Press: Ithica, 1979.
151. Vidyasagar, A.; Majewski, J.; Toomey, R., Temperature Induced Volume-Phase Transitions in Surface-Tethered Poly(N-isopropylacrylamide) Networks. *Macromolecules* 2008, 41, (3), 919-924.
152. Pethrick, R. A., Molecular Motion in Concentrated Systems: High Frequency Behavior. In *Polymers in Solutions*, Forsman, W. C., Ed. Plenum Press: New York, 1986; pp 239-264.
153. Annaka, M.; Amo, Y.; Sasaki, S.; Tominaga, Y.; Motokawa, K.; Nakahira, T., Salt effect on volume phase transition of a gel. *Physical Review E* 2002, 65, (3), 031805.
154. Freitag, R.; Garret-Flaudy, F., Salt effects on the thermoprecipitation of poly-(N-isopropylacrylamide) oligomers from aqueous solution. *Langmuir* 2002, 18, (9), 3434-3440.

155. Inomata, H.; Goto, S.; Otake, K.; Saito, S., Effect of Additives on Phase Transition of N-isopropylacrylamide gels. *Langmuir* 1992, 8, (2), 687-690.
156. Lopez-Leon, T.; Elaissari, A.; Ortega-Vinuesa, J. L.; Bastos-Gonzalez, D., Hofmeister effects on poly(NIPAM) microgel particles: Macroscopic evidence of ion adsorption and changes in water structure. *ChemPhysChem* 2007, 8, 148-156.
157. Park, T. G.; Hoffman, A. S., Sodium chloride-induced phase transition in nonionic poly(N-isopropylacrylamide) gel. *Macromolecules* 1993, 26, (19), 5045-5048.
158. Zhang, Y.; Furyk, S.; Bergbreiter, D. E.; Cremer, P. S., Specific Ion Effects on the Water Solubility of Macromolecules: PNIPAM and the Hofmeister Series. *Journal of the American Chemical Society* 2005, 127, (41), 14505-14510.
159. Vidyasagar, A.; Smith, H.; Majewski, J.; Toomey, R., Continuous and Discontinuous Volume-Phase Transitions in Surface-Tethered, Photo-crosslinked poly(N-isopropylacrylamide) networks. *Soft Matter* 2009.
160. Von Hippel, P. H.; Schleich, T., Ion effects on the solution structure of biological macromolecules. *Accounts of Chemical Research* 1969, 2, (9), 257-265.
161. Zhang, Y. J.; Cremer, P. S., Interactions between macromolecules and ions: the Hofmeister series. *Curr Opin Chem Biol* 2006, 10, (6), 658-663.
162. Kinsella, J. E.; Srinivasan, D., The Effects of Neutral Salts on the Stability of Macromolecules. *The Journal of Biological Chemistry* 1981, 256, (7), 3394-3398.
163. Hey, M. J.; Clough, J. M.; Taylor, D. J., Ion effects on macromolecules in aqueous solution. *Nature* 1976, 262, (5571), 807-809.
164. Zhang, Y.; Furyk, S.; Sagle, L. B.; Cho, Y.; Bergbreiter, D. E.; Cremer, P. S., Effects of Hofmeister anions on the LCST of PNIPAM as a function of molecular weight. *Journal of Physical Chemistry C* 2007, 111, (25), 8916-8924.

165. Zhang, Y. J.; Furyk, S.; Bergbreiter, D. E.; Cremer, P. S., Specific ion effects on the water solubility of macromolecules: PNIPAM and the Hofmeister series. *J Am Chem Soc* 2005, 127, (41), 14505-14510.
166. Sedláč, E.; Stagg, L.; Wittung-Stafshede, P., Effect of Hofmeister ions on protein thermal stability: Roles of ion hydration and peptide groups? *Archives of Biochemistry and Biophysics* 2008, 479, (1), 69-73.
167. Schild, H. G.; Tirrell, D. A., Microcalorimetric Detection of Lower Critical Solution Temperatures in Aqueous Polymer Solutions. *Journal of Phys. Chem* 1990, 94, (10), 4352-4356.
168. Kunz, W.; Lo Nostro, P.; Ninham, B. W., The present state of affairs with Hofmeister effects. *Current Opinion in Colloid & Interface Science* 2004, 9, (1-2), 1-18.
169. Vrbka, L.; Jungwirth, P.; Bauduin, P.; Touraud, D.; Kunz, W., Specific Ion Effects at Protein Surfaces: A Molecular Dynamics Study of Bovine Pancreatic Trypsin Inhibitor and Horseradish Peroxidase in Selected Salt Solutions. *The Journal of Physical Chemistry B* 2006, 110, (13), 7036-7043.
170. Baldwin, R. L., How Hofmeister ion interactions affect protein stability. *Biophys J* 1996, 71, (4), 2056-2063.
171. Pegram, L. M.; Record, M. T., Thermodynamic origin of Hofmeister ion effects. *Journal of Physical Chemistry B* 2008, 112, (31), 9428-9436.
172. Hofmeister, F., Zur Lehre von der Wirkung der Salze. Zweite Mittheilung. *Arch. Exp. Pathol. Pharmacol.* 1888, 24, 247-260.
173. Voet, A., Quantitative Lyotropy. *Chemical Reviews* 1936, 20, (2), 169-179.
174. Hamabata, A.; Vonhippe, Ph, Model Studies on Effects of Neutral Salts on Conformational Stability of Biological Macromolecules .2. Effects of Vicinal Hydrophobic Groups on Specificity of Binding of Ions to Amide Groups. *Biochemistry-U.S.* 1973, 12, (7), 1264-1271.

175. Pegram, L. M.; Record, M. T., Hofmeister salt effects on surface tension arise from partitioning of anions and cations between bulk water and the air-water interface. *Journal of Physical Chemistry B* 2007, 111, (19), 5411-5417.
176. Petersen, P. B.; Saykally, R. J., On the nature of ions at the liquid water surface. *Annu. Rev. Phys. Chem.* 2006, 57, 333-364.
177. Mcdevit, W. F.; Long, F. A., The Activity Coefficient of Benzene in Aqueous Salt Solutions. *J Am Chem Soc* 1952, 74, (7), 1773-1777.
178. Nandi, P. K.; Robinson, D. R., Effects of Salts on Free-Energy of Peptide Group. *J Am Chem Soc* 1972, 94, (4), 1299.
179. Lawal, O. S., Kosmotropes and chaotropes as they affect functionality of a protein isolate. *Food Chemistry* 2006, 95, (1), 101-107.
180. Plumridge, T. H.; Waigh, R. D., Water structure theory and some implications for drug design. *Journal of Pharmacy and Pharmacology* 2002, 54, (9), 1155-1179.
181. Maeda, Y.; Nakamura, T.; Ikeda, I., Changes in the hydration states of poly(N-alkylacrylamide)s during their phase transitions in water observed by FTIR spectroscopy. *Macromolecules* 2001, 34, (5), 1391.
182. Percot, A.; Zhu, X. X.; Lafleur, M., A simple FTIR spectroscopic method for the determination of the lower critical solution temperature of N-isopropylacrylamide copolymers and related hydrogels. *Journal Of Polymer Science Part B-Polymer Physics* 2000, 38, (7), 907.
183. Kesselman, E.; Ramon, O.; Berkovici, R.; Paz, Y., ATR-FTIR studies on the effect of strong salting-out salts on the phase separation scenario in aqueous solutions of poly(N-isopropylacrylamide) [PNIPA]. *Polym Advan Technol* 2002, 13, (10-12), 982-991.
184. Maeda, Y.; Nakamura, T.; Ikeda, I., Change in Solvation of Poly(N,N-diethylacrylamide) during Phase Transition in Aqueous Solutions As Observed by IR Spectroscopy. *Macromolecules* 2002, 35, (27), 10172-10177.

185. Paz, Y.; Kesselman, E.; Fahoum, L.; Portnaya, I.; Ramon, O., The interaction between poly(N-isopropylacrylamide) and salts in aqueous media: The “salting-out” phenomenon as studied by attenuated total reflection/fourier transform infrared spectroscopy. *Journal of Polymer Science Part B: Polymer Physics* 2004, 42, (1), 33-46.
186. Collins, K. D., Charge density-dependent strength of hydration and biological structure. *Biophys J* 1997, 72, (1), 65-76.
187. Von, H. P. H.; Peticolas, V.; Schack, L.; Karlson, L., Model studies on the effects of neutral salts on the conformational stability of biological macromolecules. I. Ion binding to polyacrylamide and polystyrene columns. *Biochemistry* 1973, 12, (7), 1256-64.
188. Baldwin, R. L., How Hofmeister ion interactions affect protein stability. *Biophys. J.* 1996, 71, (4), 2056-2063.
189. Hamabata, A.; Von, H. P. H., Model studies on the effects of neutral salts on the conformational stability of biological macromolecules. II. Effects of vicinal hydrophobic groups on the specificity of binding of ions to amide groups. *Biochemistry* 1973, 12, (7), 1264-71.
190. Dhara, D.; Chatterji, P. R., Phase transition in linear and cross-linked poly(N-isopropylacrylamide) in water: Effect of various types of additives. *Journal of Macromolecular Science-Reviews in Macromolecular Chemistry and Physics* 2000, C40, (1), 51-68.
191. Suzuki, A., Phase-transition in gels of submillimeter size induced by interaction with stimuli. *Advances in Polymer Science* 1993, 110, 199-240.
192. Eeckman, F.; Amighi, K.; Moes, A. J., Effect of some physiological and non-physiological compounds on the phase transition temperature of thermoresponsive polymers intended for oral controlled-drug delivery. *International Journal of Pharmaceutics* 2001, 222, (2), 259-270.
193. Eeckman, F.; Moes, A. J.; Amighi, K., Evaluation of a new controlled-drug delivery concept based on the use of thermoresponsive polymers. *International Journal of Pharmaceutics* 2002, 241, (1), 113-125.


194. Patra, L.; Vidyasagar, A.; Toomey, R., The effect of the Hofmeister series on the deswelling isotherms of poly(N-isopropylacrylamide) and poly(N,N-diethylacrylamide). *Soft Matter* 7, (13), 6061-6067.
195. Decher, G., Fuzzy nanoassemblies: toward layered polymeric multicomposites. *Science (Washington, D. C.)* 1997, 277, (5330), 1232-1237.
196. Quinn, J. F.; Caruso, F., Facile Tailoring of Film Morphology and Release Properties Using Layer-by-Layer Assembly of Thermoresponsive Materials. *Langmuir* 2004, 20, (1), 20-22.
197. Zhao, Z.; Yin, L.; Yuan, G.; Wang, L., Layer-by-Layer Assembly of Two Temperature-Responsive Homopolymers at Neutral pH and the Temperature-Dependent Solubility of the Multilayer Film. *Langmuir* 28, (5), 2704-2709.
198. Such, G. K.; Quinn, J. F.; Quinn, A.; Tjipto, E.; Caruso, F., Assembly of Ultrathin Polymer Multilayer Films by Click Chemistry. *J. Am. Chem. Soc.* 2006, 128, (29), 9318-9319.

APPENDICES

Appendix A: Publications

RightsLink® by Copyright Clearance Center

© 2010 Documents and Settings\paul\Desktop\App\Display\Server\ch...



Copyright Clearance Center

RightsLink®

[Home](#)
[Create Account](#)
[Help](#)

ACS Publications high quality - right price

Title: Viscoelastic Response of Photo-Cross-Linked Poly(N-isopropylacrylamide) Coatings by QCM-D

Author: Leena Petre et al.

Publication: Langmuir

Publisher: American Chemical Society

Date: Apr 1, 2010

Copyright © 2010, American Chemical Society

User ID: _____

Password: _____

Enable Auto Login

[Forgot Password/Username?](#)

If you're a copyright.com user, you can login to RightsLink using your copyright.com credentials. Access a RightsLink user or want to learn more?

Quick Price Estimate

Permission for this particular request is granted for print and electronic formats at no charge. Figures and tables may be modified. Appropriate credit should be given. Please print this page for your records and provide a copy to your publisher. Requests for up to 4 figures require only this record. Five or more figures will generate a printout of additional terms and conditions. Appropriate credit should read: "Reprinted with permission from {COMPLETE REFERENCE CITATION}, Copyright {YEAR} American Chemical Society." Insert appropriate information in place of the capitalized words.

I would like to...	reuse in a Thesis/Dissertation
Requestor Type	Author (original work)
Portion	make a selection
Format	Print
Select your currency	USD - \$
Quick Price	Click Quick Price

To request permission for a type of use not listed, please contact the publisher directly.

Copyright © 2010 Copyright Clearance Center, Inc. All Rights Reserved. Privacy Statement
 Comments? We would like to hear from you. E-mail us at info@copyright.com

1 of 1
3/9/2012 11:17

Appendix A: (Continued)

